

**SYNTHESIS AND TESTING OF ISOFLAGOMINE AND
DERIVATIVES AS INHIBITORS OF HUMAN
GLUCOCEREBROSIDASE**

by

TARA L. HILL

B.Sc., The University of Minnesota Duluth, 2005

A THESIS SUBMITTED IN PARTIAL FULFILLMENT OF
THE REQUIREMENTS OF THE DEGREE OF
MASTER OF SCIENCE
in
THE FACULTY OF GRADUATE STUDIES
(Chemistry)

THE UNIVERSITY OF BRITISH COLUMBIA
(Vancouver)

January 2009

© Tara L. Hill, 2009

Abstract

Gaucher disease is a lysosomal storage disorder in which the activity of the enzyme glucocerebrosidase (GCase) is deficient. As a result, the substrate of GCase, glucosylceramide, accumulates in lysosomes of Gaucher patients, causing enlargement of the spleen and liver, bone deformity and neurodegeneration. Deficient GCase activity results from point mutations in the gene encoding for GCase, which cause the protein to be misfolded. The misfolded mutant form of GCase, although catalytically competent, is identified and degraded by the endoplasmic reticulum-associated degradation (ERAD) pathway; thereby never reaching the lysosome or its substrate, resulting in accumulation. A threshold GCase activity level of 11-15% is all that is needed in order to be asymptomatic, with most Gaucher patients retaining between 5-20% of GCase activity levels. Therefore, therapeutic treatment of Gaucher disease only needs to impart modest increases in GCase activity in order to see large clinical improvements.

An emerging therapy for Gaucher disease uses competitive enzyme inhibitors as pharmacological chaperones (PCs), which act to increase GCase levels in the lysosome. The PC binds and stabilizes the native, folded form of GCase, thereby allowing the enzyme to escape ERAD and resume proper trafficking to the lysosome. Once the mutant GCase/PC complex is delivered to the lysosome, the relatively high concentration of accumulated glucosylceramide will compete for the active site of GCase, thereby displacing the PC as normal glycolipid degradation activity resumes.

Isofagomine (IFG), a known competitive inhibitor of GCase, was synthesized along with five other C6-alkyl IFG derivatives; of which four IFG derivatives were novel compounds. All six compounds were shown to be potent competitive inhibitors of GCase with measured K_i values ranging from 0.2 nM to 610 nM. As a strategy to suppress any inhibitory effects of the PCs after GCase reaches the lysosome, a potentially pH-labile acetal moiety was incorporated into IFG. Unfortunately, the synthesized acetal is very stable and unlikely to cleave under physiological conditions. All molecules synthesized,

have been, or will be, sent to our collaborators, Dr. Mike Tropak and Dr. Don Mahuran at the Hospital for Sick Children in Toronto for PC activity testing in Gaucher cell lines.

Table of Contents

Abstract	ii
Table of Contents	iv
List of Tables	vi
List of Figures	vii
List of Schemes.....	viii
List of Abbreviations	ix
Acknowledgments	xii
1. General Introduction.....	1
1.1 Glycosidases	1
1.1.1 Classification of Glycosidases	2
1.1.2 Catalytic Mechanism of Retaining β -Glycosidases	3
1.1.3 Inhibitors of Glycosidases	6
1.1.3.1 Non-covalent Imino Sugar Competitive Inhibitors	7
1.2 Lysosomal Storage Disorders	10
1.2.1 Gaucher Disease	13
1.2.1.1 Glucocerebrosidase.....	13
1.2.1.2 The Cause of Deficient GCase Activity	17
1.2.2 Therapies for Lysosomal Storage Disorders.....	18
1.2.2.1 Enzyme Replacement Therapy (ERT) and Substrate Reduction Therapy (SRT) as Applied to Gaucher Disease	18
1.2.2.2 Enzyme Enhancement Therapy (EET) using Pharmacological Chaperones (PCs) as Applied to Gaucher Disease	19
1.3 Aims of this Thesis	22
2. Synthesis of Isofagomine and Derivatives as Inhibitors of Human GCase and as PC Candidates for Gaucher Disease	23
2.1 Synthesis	23
2.1.1 Synthesis of Isofagomine.....	23
2.1.2 Synthesis of C6-Alkyl IFG Derivatives.....	31
2.1.2.1 Synthesis of C6- <i>n</i> -Nonyl IFG	31
2.1.2.2 Synthesis of C6- <i>n</i> -Propyl IFG and C6,6-Di- <i>n</i> -propyl IFG	34

2.1.2.3	Synthesis of C6-[9-Hydroxypropyl] IFG.....	37
2.1.3	Synthesis of Acetal-Containing IFG Derivatives as pH-Labile Linkers	38
2.1.3.1	Synthesis of C6-Benzyl Acetal IFG	38
2.1.3.2	Other Attempts to Synthesize Acetal-Containing IFG Derivatives	43
2.2	Inhibition Studies with Human GCase	46
2.3	Conclusions	54
3.	Materials and Methods	56
3.1	Synthesis.....	56
3.1.1	General Material and Methods	56
3.1.2	Generous Gifts.....	57
3.1.3	(3R, 4R, 5R)-5-(Hydroxymethyl)piperidine-3,4-diol [Isfagomine• HCl salt] (1.8)	57
3.1.4	(3R, 4R, 5R, 6S)-6- <i>n</i> -Nonyl-5-(hydroxymethyl)piperidine-3,4-diol [C6- <i>n</i> -Nonyl IFG•HCl salt] (1.9).....	62
3.1.5	(3R, 4R, 5R, 6S)-6- <i>n</i> -Propyl-5-(hydroxymethyl)piperidine-3,4-diol [C6- <i>n</i> -Propyl IFG• HCl salt] (2.17)	64
3.1.6	(3R, 4R, 5R)-6,6-Di- <i>n</i> -propyl-5-(hydroxymethyl)piperidine-3,4-diol [C-6,6-Di- <i>n</i> -propyl IFG• HCl salt] (2.18).....	67
3.1.7	(3R, 4R, 5R, 6S)-6-[9-Hydroxypropyl]-5-(hydroxymethyl)piperidine-3,4-diol [C6-[9-hydroxypropyl] IFG•HCl salt] (2.23)	68
3.1.8	(3R, 4R, 5R, 6S, 8S)-8-Benzyloxy[5,6- <i>b</i>]oxacyclohexane-5- piperidine-3,4-diol [C6-Benzyl acetal IFG] (2.32).....	70
3.2	Enzymology	72
3.2.1	Human Glucocerebrosidase Kinetics.....	72
3.2.2	Inhibition Studies of Human Glucocerebrosidase	73
	References	75
	Appendix	81

List of Tables

Table 2.1 Summary of inhibitors synthesized and measured K_i values towards GCase.....	55
Table 3.1 Summary of inhibitor concentrations used in the assay for each inhibitor.....	74

List of Figures

Figure 1.1 The reaction normally catalyzed by a glycosidase shown with the numbering scheme for a D-glucoside along with glycone and aglycone components	1
Figure 1.2 Stereochemical outcome of reactions catalyzed by inverting and retaining glycosidases	2
Figure 1.3 Half-chair conformation of oxocarbenium ion-like transition state with the co-planar arrangement needed for stabilization of the positive charge build up on C1	4
Figure 1.4 The ion pair intermediate proposed by Phillips	4
Figure 1.5 Examples of iminosugars that are non-covalent competitive glycosidase inhibitors	8
Figure 1.6 Surface representation of GCCase surrounding the active site.....	16
Figure 2.1a) Desired product 2.3 of the isopropylidene reaction plus all possible side-products	25
Figure 2.1b) Representation of a TLC plate obtained from the isopropylidene reaction	25
Figure 2.2 ¹ H-NMR spectra of ring protons before and after acetylation	27
Figure 2.3 Representation of a TLC plate obtained from the isopropylidene reaction with product identity assigned to each spot.....	28
Figure 2.4 Structure of the side-product identified from the IFG reaction (2.10)	31
Figure 2.5 General structure and numbering scheme for C6-alkyl IFG derivatives where R=alkyl	31
Figure 2.6 Structures of products 2.17 and 2.18	34
Figure 2.7a) Ideal structure for pH-labile linker shown here with alkyl groups.....	38
Figure 2.7b) General structure of synthetically attainable pH-labile linker	38
Figure 2.8 Undesired intra-molecular hemi-acetal formation with O4 (2.26) and O5' (2.27)	39
Figure 2.9 Structure of Grignard reagent (2.33).....	44
Figure 2.10 Compounds tested as inhibitors of GCCase	46
Figure 2.11 Dixon plot for the inhibition of GCCase by IFG (1.8).....	48
Figure 2.12 Dixon plot for the inhibition of GCCase by C6- <i>n</i> -propyl IFG (2.17).....	49
Figure 2.13 Dixon plot for the inhibition of GCCase by C6,6-di- <i>n</i> -propyl IFG (2.18).....	50
Figure 2.14 Dixon plot for the inhibition of GCCase by C6-[9-hydroxypropyl] IFG (2.23)	50
Figure 2.15 Dixon plot for the inhibition of GCCase by C6-benzyl acetal IFG (2.32).....	51
Figure 2.16 Dixon plot for the inhibition of GCCase by C6- <i>n</i> -nonyl IFG (1.9)	53
Figure 2.17 Diagram of several inhibitors of GCCase and their IC ₅₀ values	54
Figure A.1 A plot showing the typical hyperbolic nature of the Michaelis-Menten equation (Equation A.6)	83
Figure A.2 A typical Lineweaver-Burk plot for an enzymatic reaction	85

List of Schemes

Scheme 1.1	The mechanism of a retaining β -glycosidase.....	3
Scheme 1.2	Inactivation of a β -retaining glycosidase by use of 2-F 'Withers' reagent.....	5
Scheme 1.3	The degradation of acid gangliosides by enzymes in the lysosome.....	12
Scheme 1.4	The reaction catalyzed by glucocerebrosidase.....	14
Scheme 2.1	Numbering scheme and synthetic route to IFG (1.8).....	24
Scheme 2.2	Mechanisms and intermediates representing the transformations in the final step of the synthetic route to IFG (1.8).....	29
Scheme 2.3	Synthetic route to C6- <i>n</i> -alkyl IFG derivatives.....	32
Scheme 2.4	Proposed mechanisms for formation of amine 2.16.....	33
Scheme 2.5	Synthetic route to C6- <i>n</i> -propyl IFG (2.17) and C6,6-di- <i>n</i> -propyl IFG (2.18).....	33
Scheme 2.6	Synthetic route to C6-[9-hydroxypropyl] IFG (2.23).....	38
Scheme 2.7	Products of ozonolysis reaction followed by reduction with use of either PPh ₃ (2.24) or DMS (2.25).....	39
Scheme 2.8	Two possible products (2.28 and 2.29) resulting from acetal formation with 2- <i>n</i> -alkyl-1,3-propane diol derivatives and aldehyde 2.24.....	40
Scheme 2.9	Possible products (2.30 and 2.31) from hydrogenation of 2.28 resulting in complex ¹ H-NMR spectra.....	41
Scheme 2.10	Synthetic route to C6-benzyl acetal IFG (2.32).....	42
Scheme 2.11	Product resulting from dimerization of Grignard precursor (2.36).....	45
Scheme A.1	General scheme for enzyme catalyzed conversion of a single substrate into a single product.....	81
Scheme A.2	General scheme for enzyme catalyzed conversion of a single substrate into a single product in the presence of a competitive inhibitor.....	86

List of Abbreviations

Å	-	Angstrom
Abs	-	Absorbance
AcOH	-	Acetic acid
BnOH	-	Benzyl alcohol
BnCOCCl	-	Benzyl chloroformate
BCA assay	-	Bicinchoninic acid assay
C6	-	The carbon at the six position in IFG numbering
C6-benzyl acetal IFG	-	(3R, 4R, 5R, 6S, 8S)-8-Benzyloxy-[5,6-b]oxacyclohexane-5-piperidine-3,4-diol
C6,6-di- <i>n</i> -propyl IFG	-	(3R, 4R, 5R)-6,6-Di- <i>n</i> -propyl-5-(hydroxymethyl)piperidine-3,4-diol
C6-[9-hydroxypropyl] IFG	-	(3R, 4R, 5R, 6S)-6-[9-Hydroxypropyl]-5-(hydroxymethyl)piperidine-3,4-diol
C6- <i>n</i> -nonyl IFG	-	(3R, 4R, 5S, 6S)-6- <i>n</i> -Nonyl-5-(hydroxymethyl)piperidine-3,4-diol
C6- <i>n</i> -propyl IFG	-	(3R, 4R, 5R, 6S)-6- <i>n</i> -Propyl-5-(hydroxymethyl)piperidine-3,4-diol
Cbz	-	Carboxybenzyl
CHO	-	Chinese hamster ovary
CNS	-	Central Nervous System
α -D KIE	-	α -deuterium kinetic isotope effect
2,4-dNP-Glu	-	2,4-Dinitrophenyl β -D-glucopyranoside
DMAP	-	Dimethylaminopyridine
DMF	-	Dimethylformamide
DMS	-	Dimethylsulfide
DNJ	-	Deoxynojirimicin
EET	-	Enzyme enhancement therapy
ER	-	Endoplasmic reticulum
ERAD	-	Endoplasmic reticulum-associated degradation
ERT	-	Enzyme replacement therapy
ESI	-	Electrospray ionization
Et ₃ N	-	Triethylamine

EtOAc	-	Ethyl acetate
EtOH	-	Ethanol
GCase	-	Glucocerebrosidase
GlcCer	-	Glucosylceramide
HIV	-	Human immunodeficiency virus
HRMS	-	High resolution mass spectrometry
Hz	-	Hertz
I	-	Inhibitor
IC ₅₀	-	Half maximal inhibitory concentration
IFG	-	Isfagomine
<i>i</i> -PrOH	-	Isopropanol
Isfagomine	-	(3R, 4R, 5R)-5-(Hydroxymethyl)piperidine-3,4-diol
k_{cat}/k_{non}	-	Ratio of rate constants for catalyzed and non-catalyzed reactions
k_{cat}	-	Catalytic rate constant (turnover number)
kDa	-	Kilodalton
k_H/k_D	-	Ratio of catalytic rate constants for protio and deuterio substrates
K_i	-	Dissociation constant for an enzyme-inhibitor complex
K_m	-	Michaelis constant of a substrate
LC-MS/MS	-	Liquid chromatography-tandem mass spectrometry
LRMS	-	Low resolution mass spectrometry
LSDs	-	Lysosomal storage disorders
MeOH	-	Methanol
4-MU-Glu	-	4-Methylumbelliferyl β -D-glucopyranoside
m/z	-	Mass to charge ratio
NJ	-	Nojirimycin
NMR	-	Nuclear magnetic resonance
PC	-	Pharmacological chaperone
PET	-	Positron emission tomography
ppm	-	Parts per million
psi	-	Pounds per square inch (unit of pressure)
<i>p</i> -TsOH•H ₂ O	-	<i>para</i> -Toluene sulfonic acid monohydrate
py	-	Pyridine

QC	-	Quality control
R_f	-	Retention factor
RP	-	Reverse phase
S	-	Substrate
sapC	-	Sapoin C
SRT	-	Substrate reduction therapy
TBDMSCl	-	<i>tert</i> -Butylchlorodimethylsilane
TBDPMSCl	-	<i>tert</i> -Butylchlorodiphenylsilane
Tf ₂ O	-	Triflic anhydride
THF	-	Tetrahydrofuran
TLC	-	Thin layer chromatography
TMS	-	Trimethylsilane
UV-vis	-	Ultraviolet-visible
v	-	Reaction velocity
V_{\max}	-	Maximum reaction velocity

Acknowledgements

I would like to sincerely thank my supervisor, Dr. Steve Withers, for his patience, encouragement, guidance and friendly conversation over the last few years. I also want to extend much gratitude to the Withers group, past and present members, for creating a wonderful atmosphere where mentorship, friendship, laughter and smiles were in no short supply. Without the support system of the Withers group, this work would not have been possible. Special thanks go to my former lab mate, Dr. Sabrina Buchini, for her great friendship, constant advice and willingness to help. Many thanks to: Dr. Tom Morley for his clever synthetic tricks that almost always worked and for his patience with my thousands of questions; Dr. Bojana Rakic for her friendship and help with biological and synthetic work; Dr. Chris Tarling for guidance early on and for inspiring a love of the mountains; Dr. Emily Kwan for her help with Abg expression and purification; Dr. Hongming Chen for being a constant synthetic factory and providing me with substrates for kinetics; and Ms. Miranda Joyce for being our super-powered and all-knowing support. I would also like to acknowledge the NMR lab staff, especially Maria Ezhova, the MS lab staff, and all behind-the-scenes Departmental staff for their assistance.

I also owe many thanks to those working on other lysosomal storage disorder projects, Dr. Chris Phenix and soon-to-be Dr. Brian Rempel. I greatly appreciate the time they spent optimizing conditions for work with GCCase, for their technical advice and guidance with kinetics, and for their words of encouragement and understanding.

To all my friends and fellow grad students in the Department, including but not limited to; the Tanner lab members, 3rd floor A-wing residents and fellow TAs, many thanks for making the week as fun as the weekends.

Last, but certainly not least, I would like to thank my wonderful husband, Austin, for his tremendous support and patience. I feel truly lucky to have you by my side. Without you this would not have been possible!

General Introduction

1.1 Glycosidases

It has been estimated that around 60% of the carbon in the biosphere is present in the form of carbohydrates. Due to this abundance, nature has developed extensive and varied uses for these molecules. To the cell, carbohydrates represent three essential components; energy, communication and structure. Examples highlighting the role of carbohydrates in each of these include:

Energy: Glucose is at the very center of glycolysis; a process that fuels the cell.

Communication: Antigens are often composed of oligosaccharide chains that are important in self vs. non-self recognition by the immune system.

Structure: Cellulose and chitin, polymers of carbohydrates, give plants and crustaceans the structural rigidity needed for survival.

These few examples show that carbohydrates are not simply of interest to the glyco-scientist, but of central importance to the way life sustains and propagates itself.

Nature needs a way to manipulate these all-important carbohydrates and it does so with enzymes that catalyze their synthesis, transfer, modification and hydrolysis. In particular, glycosidases are the enzymes that catalyze the hydrolysis of the carbon-oxygen glycosidic bond between the glycone and aglycone components (Figure 1.1).

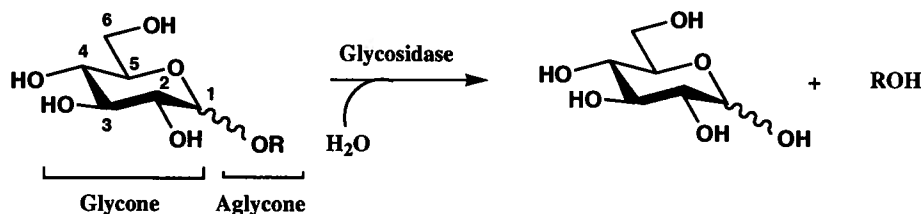


Figure 1.1 The reaction normally catalyzed by a glycosidase shown with the numbering scheme for a D-glucoside along with glycone and aglycone components.

It is important to note that glycosidases achieve extraordinary rate enhancements (k_{cat}/k_{non}) of more than 10^{17} in the reactions they catalyze.¹ In the absence of these powerful catalysts, a typical extremely stable glycosidic bond would take more than 5 million years to spontaneously hydrolyze.¹

1.1.1 Classification of Glycosidases

Glycosidases can be classified by several criteria including:

1. **The nature of the substrate/glycone.** A specific glycosidase usually exhibits maximum specificity and activity for a specific glycone. For example, a glucosidase will more readily cleave a glucoside than a mannoside or a galactoside.
2. **The anomeric configuration of the substrate.** Usually a glycosidase will catalyze exclusive cleavage of either an α or β glycosidic linkage.
3. **Stereochemical outcome of the catalyzed reaction.** A glycosidase will catalyze the cleavage of the glycosidic bond with either retention or inversion of configuration at the anomeric centre (Figure 1.2).
4. **Sequence homology.** Based on amino acid sequence similarities, glycosidases have been classified into some 113 different families. This system for classifying glycosidases is called CAZy and was developed by Henrissat.² It can be accessed at (<http://www.cazy.org/>).

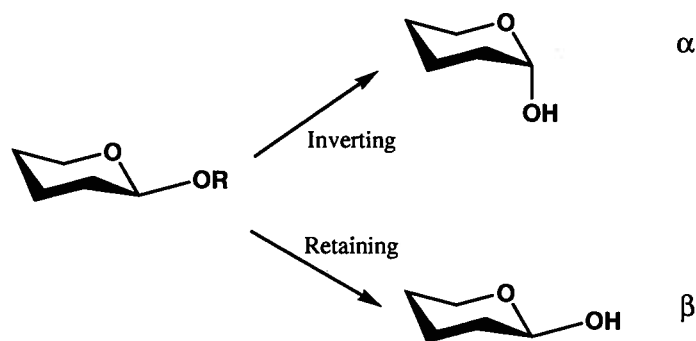
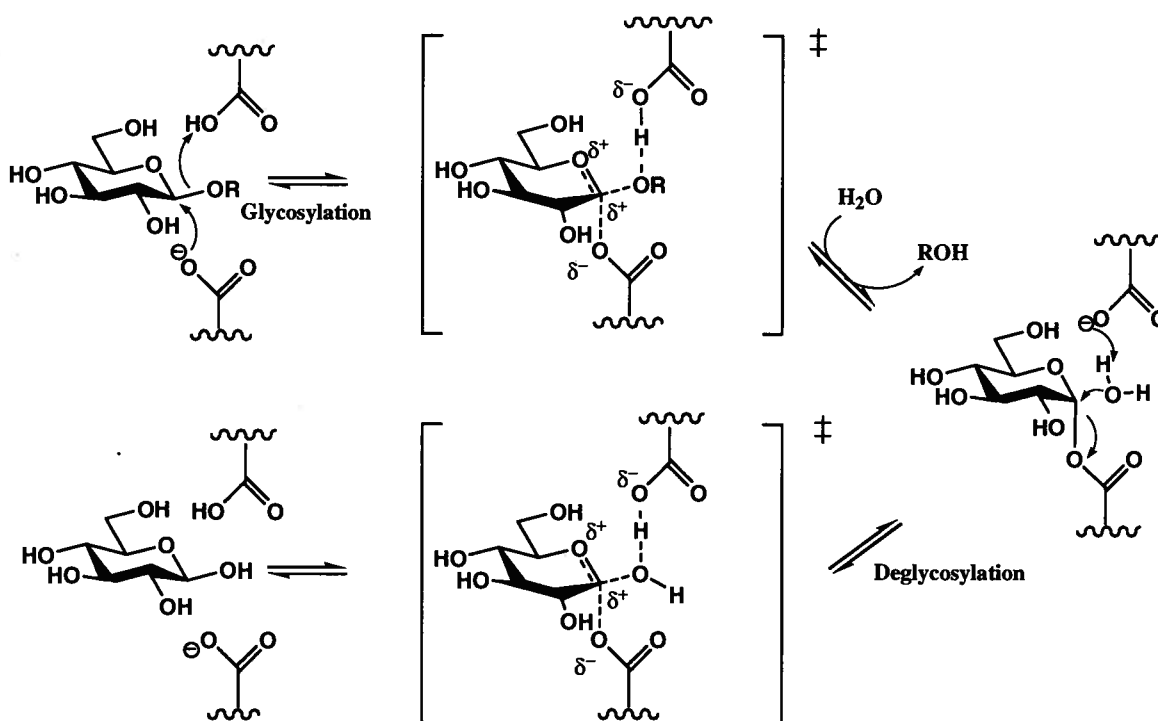


Figure 1.2 Stereochemical outcome of reactions catalyzed by inverting and retaining glycosidases.

1.1.2 The Catalytic Mechanism of Retaining β -Glycosidases

First proposed in 1953 by Koshland³ and now widely accepted, the mechanism for retaining β -glycosidases consists of two steps that each proceed with inversion of stereochemistry leading to a net retention of stereochemistry. This process is referred to as a double displacement. Typically two carboxylic acid residues in the active site are essential for this mechanism. One plays the role of the catalytic nucleophile and leaving group, while the other is the catalytic acid/base (Scheme 1.1). In the first step of the mechanism (glycosylation), the catalytic nucleophile attacks the anomeric center, and with assistance from the catalytic acid, displaces the aglycone to form a covalent glycosyl-enzyme intermediate. In the second step of the mechanism (deglycosylation), an incoming water molecule or carbohydrate (in the case of transglycosylation) is deprotonated by the catalytic base as it attacks the anomeric center and displaces the enzyme nucleophile, regenerating free enzyme and product.



Scheme 1.1 The mechanism of a retaining β -glycosidase.

Each step in this mechanism proceeds through an oxocarbenium-ion like transition state that must stabilize the developing positive charge on the anomeric carbon (C1) as the aglycone departs. This stabilization is accomplished by efficient orbital overlap and electron delocalization, hence partial double bond character, between the p-like orbitals on the endocyclic oxygen (O5) and C1 (Scheme 1.1 and Figure 1.3). A conformational change is necessary to line up the orbitals, which results in trigonal geometry at C1 and greater sp^2 hybridization. The substrate must be distorted and take on a half-chair conformation with a coplanar arrangement between C-5, O-5, C-1 and C-2 atoms (Figure 1.3).

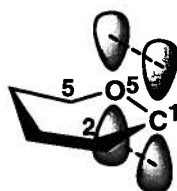


Figure 1.3 Half-chair conformation of oxocarbenium ion-like transition state with the coplanar arrangement needed for stabilization of the positive charge build up on C1.

In 1967 Phillips⁴ proposed an alternative to the glycosyl-enzyme intermediate in the double displacement mechanism. He suggested an sp^2 hybridized ion-pair intermediate (Figure 1.4). After many experiments and much debate, the double displacement mechanism with a covalently linked glycosyl-enzyme intermediate is now widely accepted.

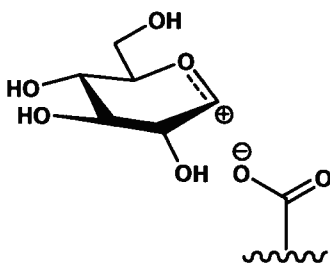
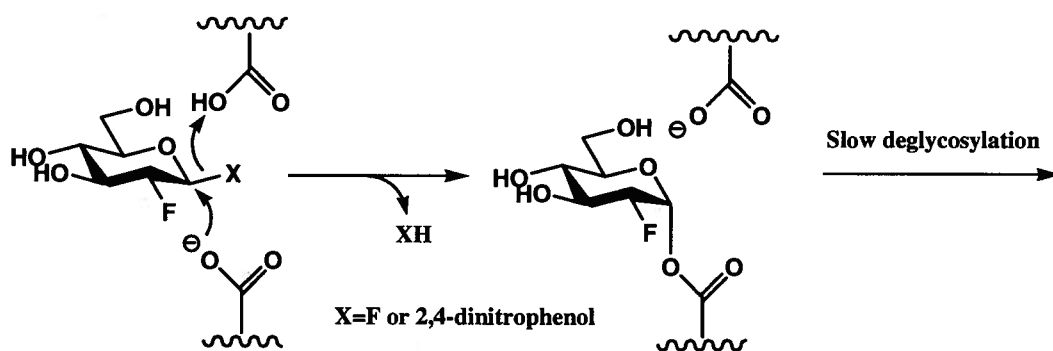


Figure 1.4 The ion pair intermediate proposed by Phillips.⁴

The first evidence against the ion-pair intermediate came with Sinnott and Souchard's α -deuterium kinetic isotope effect (α -D KIE) experiments⁵ as defined by k_H/k_D . For each of the seven substrates used in this study, it had already been demonstrated that

the second step (deglycosylation) was rate limiting.⁶ The resulting $(k_H/k_D) > 1$ indicates that the second step involves a decrease in hybridization at the anomeric centre from sp^3 to sp^2 , which is fully consistent with the double displacement mechanism and a glycosyl-enzyme intermediate. If an ion-pair intermediate did exist then an inverse KIE would be expected from the increase in hybridization (sp^2 to sp^3) needed to break down the intermediate en-route to product.⁵

More evidence in favor of the double displacement mechanism comes in the form of X-ray crystal structures that reveal the covalent intermediate. Modified substrates containing an electronegative fluorine substituent at either C2 or C5 are used to inductively destabilize the positive charge build up in the oxocarbenium-ion like transition state.⁷ These molecules are actually mechanism-based inactivators and have proven useful in many experiments – even garnering the name of ‘Withers’ reagents.⁸ The destabilizing effect of fluorine slows each step in the mechanism, but in order to accumulate the intermediate, glycosylation must proceed faster than deglycosylation. This tuning can be accomplished by using a good leaving group, typically fluoride or dinitrophenolate, as the aglycone of the substrate. A good leaving group mitigates the destabilizing effect of fluorine, speeding glycosylation while deglycosylation remains slow, thereby resulting in accumulation of the glycosyl-enzyme intermediate (Scheme 1.2).



Scheme 1.2 Inactivation of a β -retaining glycosidase by use of 2-F ‘Withers’ reagent.

The trapped species is long lived enough to obtain crystals that can be imaged using X-ray crystallography, confirming the covalent bond between the glycosyl moiety

and the enzyme.^{9,10} This trapping approach can also be used to identify the catalytic nucleophile through proteolytic digestion of the labeled enzyme and subsequent LC-MS/MS analysis¹¹ (and as reviewed by Withers and Aebersold).¹² Experimental results have also shown the active site carboxylates to be consistently positioned about 5 Å apart from one another, leaving ample room for the proposed mechanism to take place.^{13,14}

Attempts to determine which of the active site residues are responsible for general acid/base catalysis have used crystal structures along with mutagenesis and kinetic studies (as reviewed by Zechel and Withers with references therein).¹⁰ As is expected, and observed, acid/base mutants exhibit rates that vary widely with the leaving group ability of the aglycone. For substrates with poor leaving groups (disaccharides, methyl glycosides), initial cleavage of the glycoside is greatly slowed when compared to substrates with good leaving groups. On the other hand, the deglycosylation step is greatly slowed for all substrates because base catalysis is unavailable for deprotonation of the incoming water nucleophile. As a result, the covalent intermediate accumulates for substrates with good leaving groups in a pre-steady state kinetic 'burst', accompanied by unusually low K_m values. These trapped acid/base mutants can have their activity rescued by addition of nucleophilic anions such as azide, formate or acetate. These anions do not need general base assistance and turn over the glycosyl-enzyme intermediate to generate a new product with retained stereochemistry. With wild-type enzyme, the same anion rescue experiments yield normal hydrolyzed substrates. This is presumably due to charge repulsion between the general base carboxylate and the anion, making it more favorable for water to enter the active site and react.

1.1.3 Inhibitors of Glycosidases

Glycosidase inhibitors fall into several categories because they can bind enzymes reversibly, as with non-covalent inhibitors, or irreversibly, as with most covalent inhibitors. A class within the covalent category is that of the aforementioned mechanism-based inactivators (Scheme 1.2). Further classification within the non-covalent type includes competitive, non-competitive/mixed and uncompetitive inhibitors. Competitive inhibitors bind to the enzyme active site thereby competing with the natural substrate for

this space (See Appendix for theory on reversible competitive inhibition). This thesis will focus on competitive, non-covalent inhibitors of glycosidases.

Glycosidases can achieve such great rate enhancements because their active sites lower the activation energy of a particular reaction by binding the transition state much better than the ground state.¹⁵ It is not surprising then, that the best competitive glycosidase inhibitors mimic aspects of the oxocarbenium ion-like transition state such as positive charge and/or planar geometry. These competitive inhibitors can be powerful tools in kinetic assays for probing mechanistic aspects of a reaction.¹⁶ They can also be used to gain insight into important active site binding interactions through crystallographic studies with enzyme/inhibitor complexes.¹⁷ Using inhibitors to better understand substrate binding and catalysis will not only lead to better inhibitors, but possibly better enzymes with increased activities¹⁸ and/or altered specificities.¹⁹

Glycosidase inhibitors are used in a wide variety of settings, as described above, as well as in therapeutics. They are either proposed or shown to be useful in the treatment of diabetes²⁰, HIV²¹, cancer²² and influenza.²³ As the biological roles of carbohydrates and their interactions with glycosidases continue to be elucidated, inhibitors of these enzymes will enjoy much 'job' security.

1.1.3.1 Non-covalent Iminosugar Competitive Inhibitors

Although there is a good degree of ambiguity in the literature surrounding nomenclature of these compounds, in this thesis the general term iminosugar will be used for sugar-like, polyhydroxylated molecules containing at least one nitrogen, either in an endocyclic or exocyclic position (Figure 1.5). Many of these compounds are natural products that collectively have been shown to be potent competitive inhibitors of a wide range of glycosidases.^{24,25,26} At physiological pH, the nitrogen in most iminosugars is protonated and carries a positive charge, thus mimicking the oxocarbenium ion-like transition state that glycosidase active sites have evolved to stabilize.^{27,28}

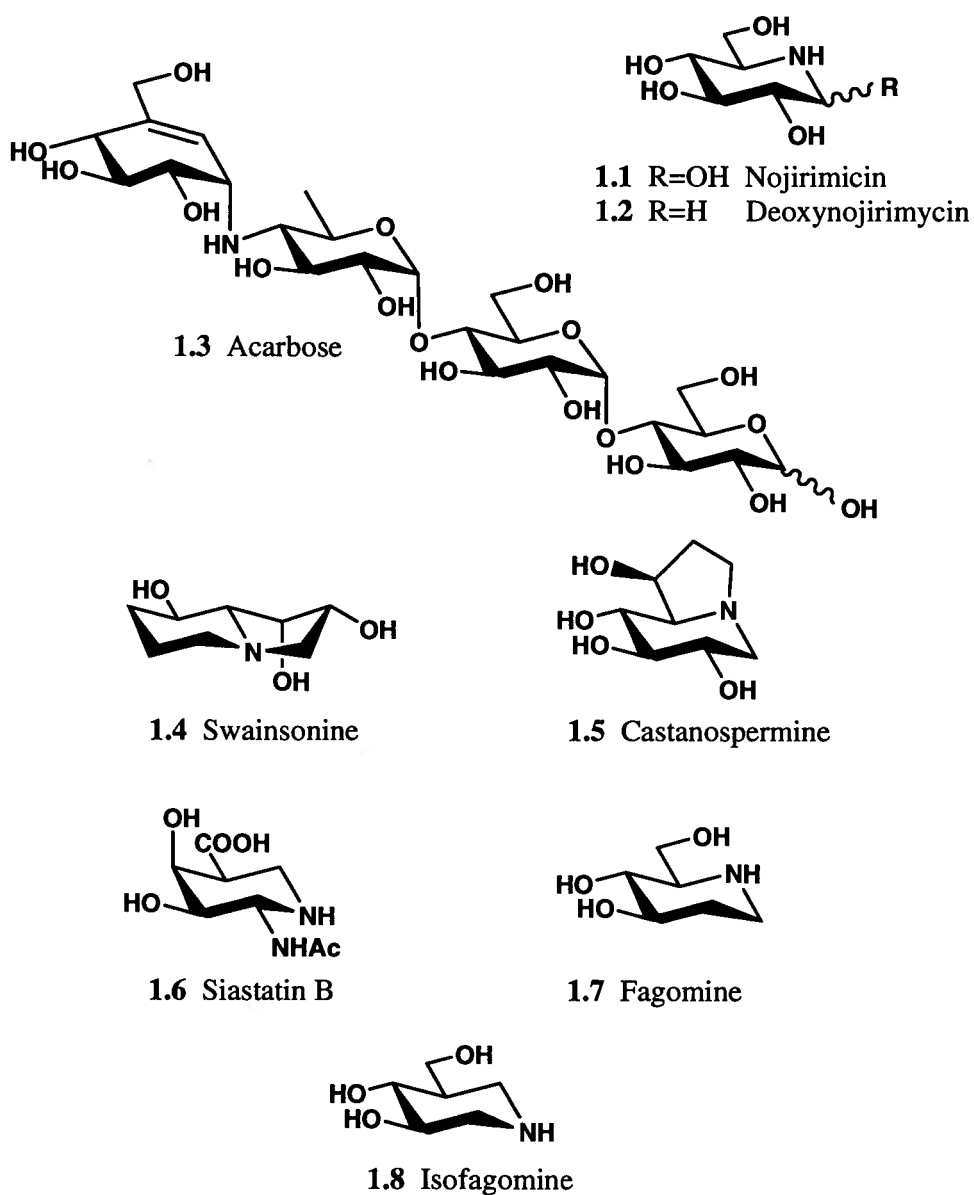


Figure 1.5 Examples of iminosugars that are non-covalent competitive glycosidase inhibitors.

Arguably the most prominent iminosugar, nojirimicin (NJ) (**1.1**) contains a nitrogen atom at the endocyclic oxygen position. Interestingly, its synthesis was accomplished ten years prior to its discovery in nature or knowledge of its powerful biological activity.²⁹ The deoxygenated version, deoxynojirimicin (DNJ) (**1.2**), also inhibits many enzymatic targets including both α and β glucosidases and has attracted the attention of synthetic chemists looking to expand the scope of this type of molecule. Nearly every possible isomer of DNJ, along with hundreds of N-substituted and C-

branched derivatives have been synthesized and tested for biological activity³⁰ (and references 6-9 therein). Of particular success is the N-hydroxyethyl version of DNJ, which acts as an α -glucosidase inhibitor for the treatment of diabetes and is marketed as miglitol (Glyset[®]).³¹ Another iminosugar natural product used for treatment of diabetes is acarbose (sold in North America as Precose[™]) (**1.3**).²⁰ The key moiety in this metabolically stable pseudo-tetrasaccharide is the valienamine unit with an exocyclic nitrogen atom. The valienamine moiety also contains a double bond, which serves to flatten the ring, thereby further mimicking the oxocarbenium ion-like transition state.

Quite a few bicyclic iminosugars have also been identified from biological sources such as swainsonine (**1.4**), an α -mannosidase inhibitor,³² and castanospermine (**1.5**), a broad spectrum glucosidase inhibitor.^{25,33} The discovery of natural products siastatin B (**1.6**),³⁴ where the nitrogen atom replaces the carbon at the anomeric centre, and fagomine (**1.7**), which is the 2-deoxy version of DNJ, spurred the synthesis of a semi-rationally designed, very potent β -glucosidase inhibitor, isofagomine (IFG) (**1.8**).^{35,36}

Placing the nitrogen at the anomeric centre leads to dramatic increases in inhibitory power towards certain glycosidases. An interesting comparison between DNJ and IFG, both inhibitors of α and β retaining glucosidases, is that DNJ is a more potent inhibitor of α glucosidases by roughly 3-fold, while IFG is more potent towards β glucosidases by nearly 500-fold.³⁶ This phenomenon can be partially explained by the different transition state charge distributions in the reactions catalyzed by α and β glucosidases³⁷ (and as reviewed by Zechel and Withers).¹⁰

Many derivatives^{38,39} and isomers^{40,41} of IFG have also been synthesized. N-alkylated derivatives of IFG generally exhibit lower levels of inhibition compared to the parent IFG nonetheless, there is still interest in these molecules.³⁹ Along with IFG, N-adamantyl and N-octyl IFGs have been investigated as potential pharmacological chaperones for treatment of the lysosomal storage disorder, Gaucher Disease,⁴²⁻⁴⁴ with IFG currently in clinical trials (<http://www.amicustherapeutics.com/clinicaltrials/at2101.asap>). Along with IFG,

structures of *N*-butyl DNJ and *N*-nonyl DNJ complexed with glucocerebrosidase, a lysosomal hydrolase, have been determined by X-ray crystallography in order to gain insights into important binding characteristics.^{17,45} One research group has taken on the synthetic challenge of making C6-branched alkyl IFG derivatives and honed in on the most potent glucocerebrosidase inhibitor to date, C6-*n*-nonyl IFG (**1.9**) with an IC₅₀ value of 0.6 nM.³⁸

1.2 Lysosomal Storage Disorders (LSDs)

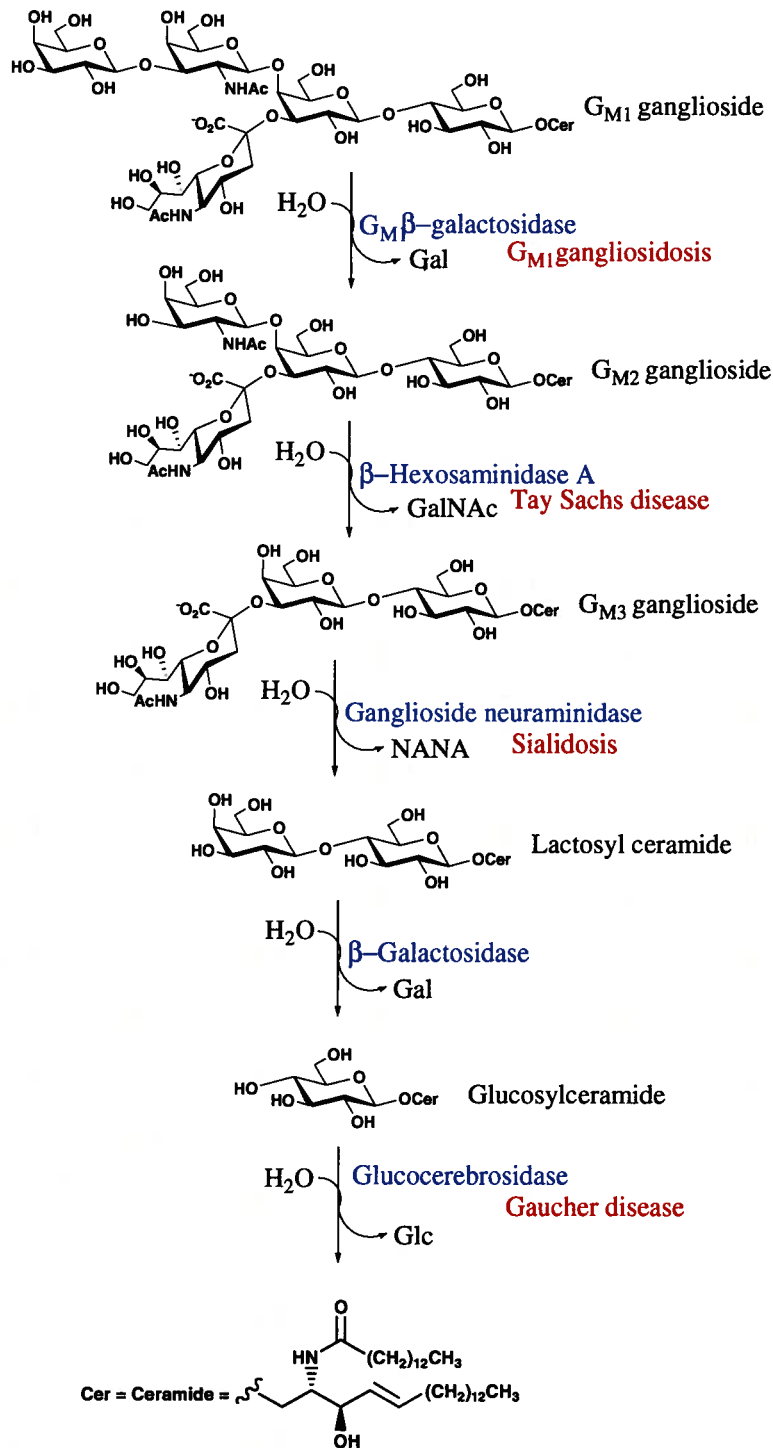
Lysosomes are organelles within the cell that are essentially the recycling depots and which operate under acidic conditions at pH 5.⁴⁶ Various enzymes within the lysosome are responsible for the proper degradation and recycling of cellular components such as glycoproteins and glycolipids.⁴⁷ If there is a deficiency in the activity of a particular degradation enzyme, that enzyme's substrate will accumulate. This physical storage, along with a perturbation of signaling pathways, leads to a disease state.⁴⁷⁻⁴⁹ So far around 40 of these disorders have been characterized, each by itself rare, but taken together there is a prevalence of 1 in 7,700 in the general population.⁵⁰ These are collectively known as lysosomal storage disorders.

Amongst the glycolipids degraded in the lysosome there is a class of molecules known as gangliosides. These are glycosphingolipids that contain a ceramide moiety attached to an oligosaccharide chain (Scheme 1.3). Ceramide is a lipid that imbeds in the membranes of animal cells in order to display the oligosaccharide chains into the extracellular space. This display allows for cell-cell interactions that mediate signaling and differentiation.⁵¹

The gangliosides are degraded in a step-wise fashion by specific enzymes in the lysosome that act on a specific glycone (Scheme 1.3). If there is a missing enzyme activity in this orderly line of degradation, an accumulation of its substrate will occur, which contributes to disease phenotypes. Each accumulation product and disease phenotype is specific to the deficient enzyme. Scheme 1.3 shows the degradation of acid

gangliosides by lysosomal enzymes as well as the diseases associated with the deficiencies.

This thesis will focus on the enzyme glucocerebrosidase and the disease associated with it, Gaucher disease.



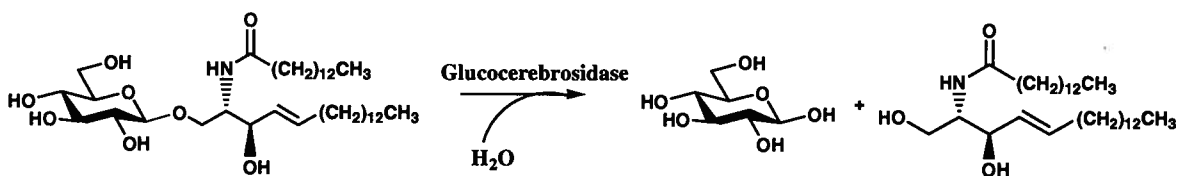
Scheme 1.3 The degradation of acid gangliosides by enzymes in the lysosome. Enzymes are written in blue and the disease associated with the enzyme deficiency is written in red.

1.2.1 Gaucher Disease

Gaucher disease is the most common of all lysosomal storage disorders with a prevalence of 1 in 40,000–60,000 in the general population and 1 in 800 among the Ashkenazi Jewish population.⁵⁰ Like all other lysosomal storage disorders, it is a heritable disease and was first described in 1882 by Phillippe Gaucher in his medical thesis.⁵² In it he described a patient with abnormal spleen cells, but it wasn't until 1907 that Aghion characterized that abnormality to be the storage of glucosylceramide.⁵² Since then, the phenotypes of Gaucher disease have been elucidated to include enlargement of the liver and spleen, bone deformity, anemia, neuronopathic/central nervous system (CNS) involvement and death.^{47,49,52} The severity of these symptoms can vary widely, as does the age of onset and degree of CNS involvement. As a result, Gaucher disease is classified into three types. The most common and mild form is type 1 where patients lack CNS involvement and have early childhood to adult onset. Type 2 patients experience infant onset with rapid and severe neuronopathic involvement often resulting in death before age 2. Type 3 patients experience a slower childhood onset with typically milder neuronopathic involvement.⁵² There is no cure for Gaucher disease but there are currently two types of therapies available to patients, with an additional therapy in clinical trials; all of which will be discussed in section 1.2.2.

1.2.1.1 Glucocerebrosidase

Glucocerebrosidase (GCase) is a membrane-associated 67 kDa protein with 497 amino acids.⁵² As a β -glucosidase from CAZy family 30,² GCase catalyzes the cleavage of the glycosidic bond between glucose and ceramide in a retaining fashion as shown in Scheme 1.4. The proposed mechanism for this transformation is that of the retaining β -glucosidases shown in Scheme 1.1 (page 3). The pH optimum for GCase is 5.5 and corresponds to the pH maintained in the lysosome.⁵³



Scheme 1.4 The reaction catalyzed by glucocerebrosidase.

The substrate, glucosylceramide (GlcCer), resides in the inner lysosomal membrane and is not water soluble. The question of how GCCase, a soluble protein, accesses GlcCer, an insoluble substrate, must be addressed.⁵⁴ For full activity *in vivo*, GCCase requires negatively charged phospholipids and the activator protein saposin C (sapC).⁵² The exact mechanisms of activation are still being elucidated but recent studies have observed conformational changes in both GCCase and sapC that must take place in order for proper catalysis to occur.^{55,56} The “liftase” model, which is most supported in the literature, suggests that sapC binds and simply perturbs the surface of the membrane thereby exposing GlcCer. GCCase recognizes this membrane-bound sapC complex and binds at its interface gaining access to the substrate.⁵⁵ An alternative “solubilizer” model suggests a more active role for sapC where it not only perturbs the membrane, but actually extracts GlcCer and presents it to GCCase as a soluble lipid-protein complex, as is seen with Saposin D.⁵⁵

X-ray crystal structures of GCCase show many hydrophobic residues in close proximity to the active site which may facilitate the membrane and sapC associations.⁵⁷ When GlcCer is modeled into GCCase using computational programs, there are ambiguous conclusions about where the hydrophobic tails reside in relation to GCCase. In one simulation the tails point away from the protein, indicating interactions with either the membrane or sap C.⁵⁷ The other simulations have modeled the tails residing in two valleys emerging from the active site.^{17,45} In the valley scenario, the hydrophobic tails can still interact with the membrane or sapC.

Extensive *in vitro* work has shown that GCCase, in the absence of negatively charged phospholipids and sapC, requires triton-X 100 and sodium taurocholate for activity.⁵⁸

Several X-ray crystal structures of wild type GCase have been solved under different conditions including: with a covalent inhibitor⁵⁹, with several non-covalent competitive inhibitors^{17,45}, without inhibitors^{45,57} as well as at neutral and acidic pH values.⁴⁵ The crystal structure solved at pH 7.5 is the first and only at that pH as well as the first truly apo-structure.⁴⁵ The findings of all these reports reveal several important dynamic loops that flank the active site (residues 311-319 : loop 1, residues 342-354 : loop 2, residues 393-396 : loop 3). These loops adopt a variety of conformations in the free enzyme at both pH values but interestingly, when a competitive inhibitor was found in the active site (only at acidic pH), the loops were always fixed in one preferred conformation with loop 1 being found in a helical conformation.^{17,45} Specific hydrogen bond networks were also observed, which stabilize these preferred conformations and allow open access to the active site (Figure 1.6b).⁴⁵ This open active site conformation was always observed in inhibitor/enzyme complexes, whereas it was only observed once at neutral pH in the structures of free enzyme (Figure 1.6c). For all other free enzyme structures, different hydrogen bond networks were observed and subsequently, the active sites in these structures were largely closed and inaccessible. (Figure 1.6a,d).

Attempts to computationally dock GlcCer into the active sites of inhibitor/enzyme versus free enzyme structures yielded good scores only for bound structures with open active sites (Figure 1.6e).⁴⁵ Movements of the loops that are needed to open or close the active site may also correspond to changes needed in order to interact with lipids, sapC and/or the membrane.

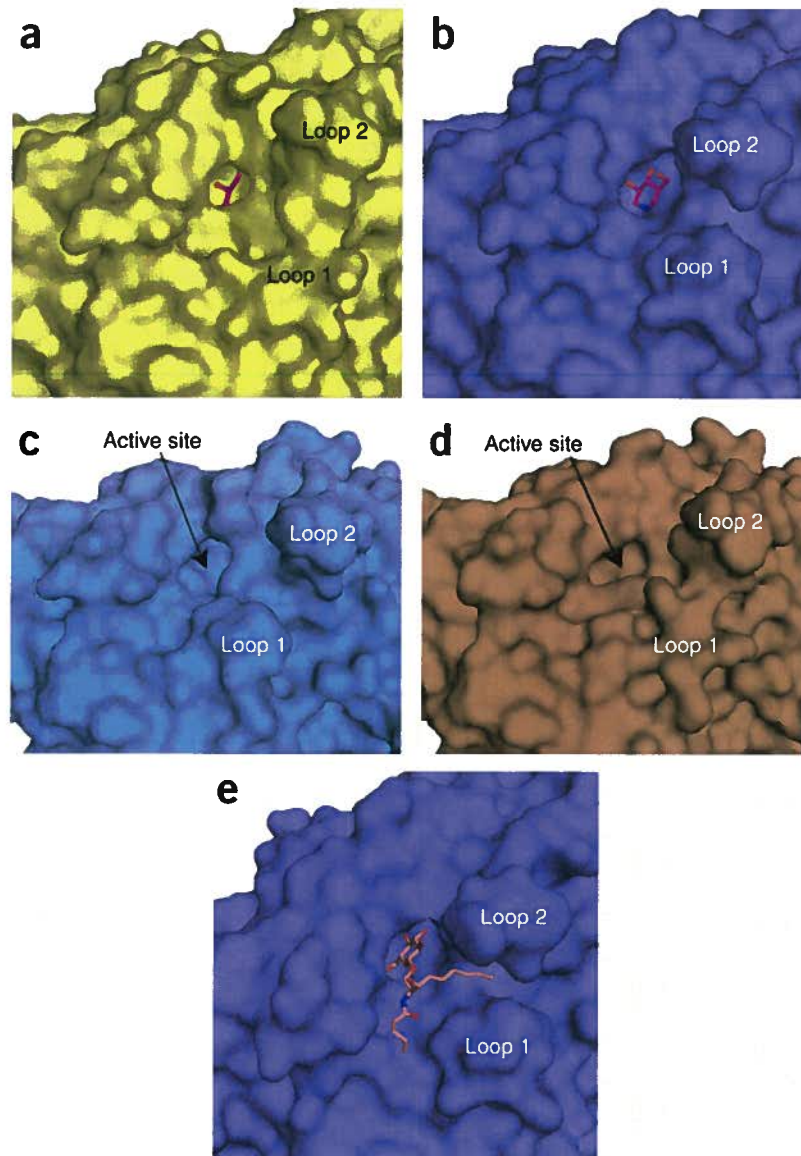


Figure 1.6 Surface representation of GCCase surrounding the active site. **a)** pH = 4.5 with glycerol bound in active site. Active site closed. **b)** pH = 7.5 with IFG bound in active site. Active site open. **c)** pH = 7.5 free enzyme. Active site open. **d)** pH = 7.5 free enzyme. Active site closed. **e)** Truncated GlcCer docked into structure **b**. Figure taken from Lieberman *et. al.*⁴⁵ Reprinted with permission from MacMillan Publishers Ltd: [Nature Chemical Biology] (Lieberman *et. al. Nat. Chem. Biol.* 2007, 3, 101-107), copyright 2007

1.2.1.2 The Cause of Deficient GCase Activity

Like many proteins, GCase is synthesized and folded in the endoplasmic reticulum (ER), which maintains neutral pH. Under normal conditions, the emerging polypeptide chain is folded properly (native form), secreted out of the ER, transported to the Golgi apparatus for further maturation, and finally trafficked to the lysosome where it degrades GlcCer. A point mutation in the gene encoding GCase can result in an unstable, slightly misfolded GCase variant (non-native form), which is subsequently identified and retained in the ER by the quality control (QC) system. QC targets the misfolded protein for degradation by ER-associated degradation (ERAD) and as a result, GCase never reaches its substrate (GlcCer) in the lysosome and GlcCer accumulates. For extensive reviews on ER QC and ERAD see Ellgaard *et al.*⁶⁰ and Yoshida.⁴⁸ One interesting feature to note is that most people suffering from this enzyme deficiency express catalytically active, yet unstable, GCase, making this mostly a problem of protein misfolding and subsequent degradation.⁶¹ If these enzymes could 'fool' the QC and ERAD mechanisms and maintain proper trafficking to reach the lysosome, they would be able to properly catalyze degradation of GlcCer.

The residues responsible for maintaining the hydrogen bond networks that surround the active site and act to stabilize the open conformation have been identified,^{17,45} and correspond to some of the GCase mutants that lead to Gaucher disease. Notably N370, the most common mutation seen in Gaucher patients (N370S), has a direct role in stabilizing the preferred helical conformation of loop 1. In the absence of inhibitor, it is known that GCase samples many conformations.⁴⁵ It is possible that when any remote residues are mutated, the resulting interactions bias closed active site conformations of GCase or allow a loop to be disordered. It is not known what exact structural features cause GCase variants to be identified by QC and degraded by ERAD. It is, however, generally understood that quaternary structure elements like hydrophobic patches, mobile loops and lack of compactness are important in the differentiation of native versus non-native proteins by cellular processes.⁶⁰

1.2.2 Therapies for Lysosomal Storage Disorders

The therapies about to be discussed are in specific reference to GCase and Gaucher Disease but there are examples of parallel therapies for many other LSDs.⁶² Each disease has its own special set of circumstances that need to be optimized for each therapeutic strategy. In theory, each strategy can be applied to any LSD, as all share common themes of misfolded proteins leading to enzymatic deficiencies.

1.2.2.1 Enzyme Replacement Therapy (ERT) and Substrate Reduction Therapy (SRT) as Applied to Gaucher Disease

A threshold GCase activity level of 11-15% is all that is needed in order for Gaucher patients to be asymptomatic, with lower levels of activity corresponding to a worsening clinical course of disease. It has also been demonstrated that many type 1 patients exhibit residual GCase activity levels that are 5-20% of normal levels.⁶³ This means that modest increases in GCase activity could prove to be life changing for some patients.

Today there are two types of therapy available for Gaucher patients, with a third on the way. The first is called enzyme replacement therapy (ERT)⁶⁴ and involves injection of the recombinant form of GCase (Cerezyme[®])⁶⁵ directly into the patient's bloodstream. ERT is only effective for type 1 patients without CNS involvement because the administered enzyme cannot cross the blood brain barrier. This treatment option, offered since 1991,⁶⁶ is very expensive with costs upwards of \$200,000 per year, per patient and even more to administer it.⁶⁷ Current research efforts surrounding this strategy focus on expression of GCase in systems other than Chinese hamster ovary (CHO) cells⁶⁸ and elucidation of GCase bio-distribution through use of PET imaging. This information should help to tune the dose to an individual in order to minimize costs.

The other therapy available to Gaucher patients is substrate reduction therapy (SRT). This involves inhibiting the enzyme responsible for GlcCer biosynthesis with N-butyl deoxynojirimycin (NB-DNJ, Miglustat, Zavesca[®]).⁶⁹ With a reduction in the

amount of GlcCer being synthesized, less is stored in the lysosome and the clinical course of the disease can be improved. However, this therapy is accompanied by some serious side-effects.⁷⁰ It is not known what long-term effects this may have on glycolipid distribution since these molecules and their roles are only partially understood. Both ERT and SRT address the GlcCer storage problem, but do not address downstream effects of the unfolded protein response in which ER stresses, such as ERAD activation by misfolded proteins, can also activate other inflammatory pathways and induce apoptosis.⁴⁸

1.2.2.2 Enzyme Enhancement Therapy (EET) using Pharmacological Chaperones (PCs) as Applied to Gaucher Disease.

As previously stated, only modest increases in GCase activity are needed to alleviate the maladies of Gaucher Disease. An upcoming and very promising therapeutic strategy called enzyme enhancement therapy (EET) seeks to use small molecule pharmacological chaperones (PCs) in order to stabilize the native conformation of misfolded GCase mutants.^{61,71,72} This PC-induced stabilization ‘fools’ the QC and ERAD mechanisms, allowing the patient’s endogenous enzyme to be trafficked to the lysosome as normal. The majority of small molecules identified thus far as PC candidates for Gaucher Disease have been competitive inhibitors of GCase.⁶¹ By definition, competitive inhibitors bind to the enzyme active site and it is through these interactions that the native conformation of GCase is stabilized.⁶¹ Also by definition, competitive inhibitors can be displaced from the active site if another inhibitor or substrate is present in high enough concentrations. Ideally, increased levels of mutant GCase reach the lysosome following PC treatment, and a high concentration of accumulated GlcCer will compete for the active site, thereby displacing the PC and allowing normal degradation to take place. This whole therapeutic strategy leads to the apparent paradox that an inhibitor will *increase* cellular enzymatic activity.

For this strategy to be viable, the PC dosing must be fine-tuned in order to maximize lysosomal GCase levels. At certain concentrations, which vary depending on

the PC and the mutation, these molecules will actually decrease mutant GCCase activity; adding insult to injury for someone already suffering because of insufficient activity.⁷³ Even with the precautions and apparent paradoxes, PC therapy is desirable because small molecules can often cross the blood-brain barrier, making this a potentially useful therapy for type 2 and 3 Gaucher patients with CNS involvement. Another benefit of small molecule therapies, as opposed to peptide and protein-based therapies, is the reduced cost for administration.⁶⁷ A third benefit is PCs allow the endogenous mutant enzyme to traffic normally. Thus, EET has the ability to relieve downstream effects from the unfolded protein response.⁴⁸

IFG is currently in clinical trials as a PC (sponsored by Amicus Therapeutics) for EET of Gaucher Disease (<http://www.amicustherapeutics.com/clinicaltrials/at2101.aspx>). The exact mode of GCCase stabilization and chaperoning by IFG has been proposed based on H/D exchange mass spectrometry⁷⁴ and crystallographic studies^{17,43,45} both with and without IFG bound. A sampling of many conformations occurs in a rugged energy landscape as the mutant protein is being folded in the ER. As previously stated in section 1.2.1.1, the native form of GCCase requires that loop 1 be in an ordered helical conformation for the active site to be open and accessible. It is this native conformation that IFG will preferentially bind, thereby stabilizing loop 1 and locking it in the preferred conformation. IFG binding is also thought to impart greater global stability to GCCase mutants as observed by a decrease in H/D exchange⁷⁴ and an increase in melting temperatures.⁷⁵ This IFG-induced, globally stable native form is no longer a marker for ERAD and normal trafficking to the lysosome will resume.

In order for IFG to function as a PC according to this mechanism an assumption must be met; that mutant GCCase can sample the native conformation during ER folding. It is possibly because of this that PCs exhibit chaperoning profiles that are highly dependent on the particular mutation. For example, IFG can act as a PC for the most common GCCase mutant N370S, but for L444P mutants it shows no efficacy.⁷³

Strategies to optimize selectivity and/or activity of Gaucher PCs include high throughput screening of large compound libraries,^{74,76} as well as rationally designed small molecules.^{38,42,77} The hopes of these efforts are to find small molecules that are either non-active site directed PCs, or active site directed PCs that exhibit differential binding profiles under different conditions, particularly different pH conditions. Strong inhibition representative of low K_i values would be ideal at neutral pH (conditions of the ER) with weaker inhibition and higher K_i values being ideal at acidic pH (conditions of the lysosome). These sorts of PCs are desirable because of the concern that when using potent *in vitro* inhibitors, they will behave as such *in vivo* as well.

One way to rationally design a molecule that has differential binding characteristics in different organelles is to build in a pH-labile, or local environment-labile linker. With the lysosome operating at pH 5 and home to many proteases, an acetal or amide linker may well be susceptible to hydrolysis under these conditions. This would allow the inclusion of a hydrophobic arm which, based on previous studies,³⁸ should impart tighter binding to GCCase. Once the linker is cleaved under the predicted conditions and the hydrophobic arm released, a less potent GCCase binder would remain and concerns for the molecule inhibiting delivered GCCase would be alleviated. The idea for this strategy came about after a surprising observation from a study that tested many different small molecules as PCs for GCCase. An adamantyl group was incorporated, into two otherwise identical molecules, via an ether or amide linkage. The amide linked version exhibited a 150% increase in GCCase activity while the ether-linked version was inhibitory at all concentrations tested.⁷³ The authors commented that the result was unexpected, but did not attribute it to cleavage of the amide. However it seemed possible to us that cleavage of the amide (but not the ether) in the lysosome could give rise to this outcome.

1.3 Aims of this Thesis

Isofagomine (IFG) has been shown to act as a pharmacological chaperone (PC) in the treatment of Gaucher Disease in which GCCase activity is deficient. It has also been shown that C6-alkyl derivatives of IFG are the most potent inhibitors of GCCase to date. The goal of my work is to develop novel GCCase inhibitors based on the C6-alkyl derivatives of IFG that also have the potential to behave as PCs for the treatment of Gaucher Disease. The specific aims of this thesis towards that goal are three-fold.

The first aim is to use synthetic organic and carbohydrate chemistry methodologies in order to synthesize novel C6-alkylated versions of IFG. In particular, it is ideal if these IFG derivatives contain a pH-labile acetal linker, and/or have the potential to exhibit differential binding profiles under the conditions encountered in the ER versus the lysosome. The second aim is to measure the GCCase inhibition constants (K_i values) of the synthesized IFG derivatives and determine what kind of inhibition they exhibit. The third aim is to provide promising PC candidates to our colleagues Dr. Don Mahuran and Dr. Mike Tropak in Toronto at the Hospital for Sick Children for PC activity testing in Gaucher cell lines.

2 Synthesis of Isofagomine and Derivatives as Inhibitors of Human GCase and as PC candidates for Gaucher Disease

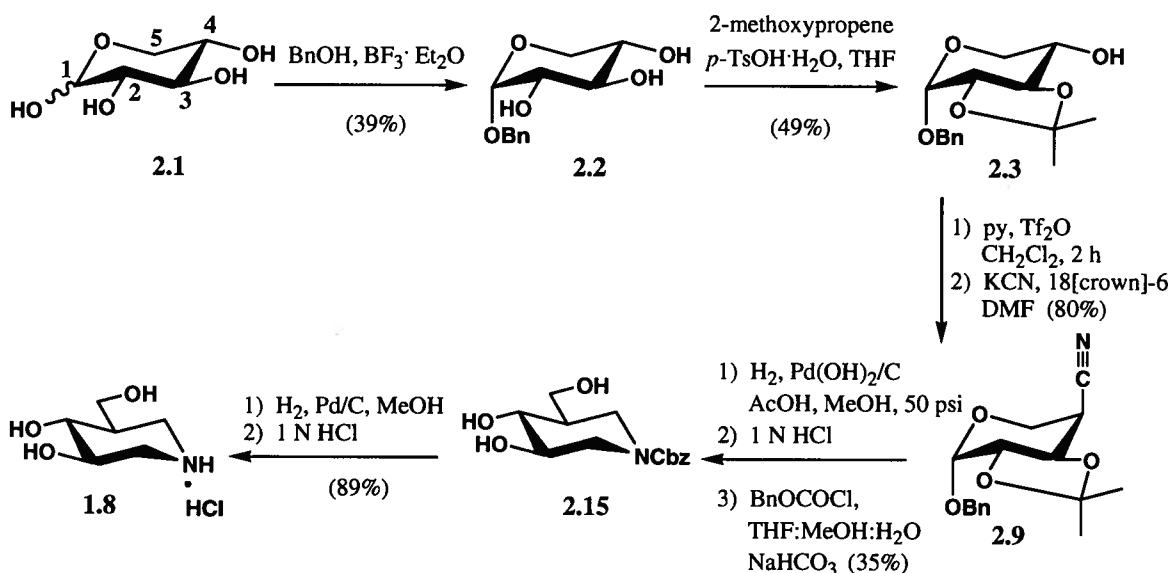
2.1 Synthesis

2.1.1 Synthesis of Isofagomine

Isofagomine (IFG) (**1.8**) is not found in nature and therefore all the material used in research and medicine must come from a synthesis. As a result several routes have been developed to access IFG and derivatives. When making this seemingly very simple molecule there are several major challenges that need to be overcome. First, it is necessary to introduce the nitrogen atom selectively, which often requires the use of complex protecting group strategies, and second, the stereochemistry at the three stereocentres must be controlled. A final consideration is choosing starting materials that can provide some of these elements but without exorbitant costs. Carbohydrates with the desired stereochemistries, or alkaloids with the nitrogen in a desirable position, are attractive options. In 1994 the first route to IFG was reported by Jespersen *et al.*,³⁵ wherein IFG was synthesized in 10 steps from levoglucosan. The stereochemistries throughout the synthesis were set within the starting material and via a selective epoxide opening with vinyl magnesium bromide. The nitrogen atom was introduced via reductive amination with NH₃. Subsequent publications describing syntheses of IFG have commented on the length and complexity of this route.³⁹

The second route to IFG was published in 1995 by Ichikawa *et al.*,⁷⁸ and started from D-Lyxose. The nitrogen was installed via an azido substitution of a tosyloxy group with inversion of stereochemistry, followed by hydrogenation to reach IFG in seven steps. Stereochemistry throughout this synthesis was largely controlled by the starting material and a partially selective deoxygenation. This synthesis also suffers from lengthy protecting group manipulation and complex purification procedures to separate diastereomers. As a brief sampling, other groups have synthesized IFG in five steps from the alkaloid arecolin,⁷⁹ in five steps from D-arabinose,⁸⁰ in seven steps from (*R*)-2,3-*O*-

cyclohexylidene-glyceraldehyde,⁴⁰ and in seven steps from L-xylose.⁸¹ Following the appearance of the L-xylose synthetic route in the literature, many of the new syntheses published have used this general methodology but either have reduced the number of steps, or reduced the use of expensive reagents.⁸² There have also been efforts towards the development of divergent syntheses that can access many different piperidine/IFG isomers.⁴¹ However, these routes are lengthy in comparison to those developed to exclusively synthesize IFG. A short four step synthesis adapted from the L-xylose synthetic route was published in 2005 by Zhu *et al.*³⁸ It seemed to provide a convenient platform for the development of C6-alkyl IFG derivatives, exactly along the lines of the project's goal. For this reason, Zhu's route and protecting groups were chosen for reproduction and exploration (Scheme 2.1). A year later in 2006, when the project was already underway, Goggard-Borger *et al.* published a modification of this method which made use of D-arabinose, a cheaper starting material than L-xylose.⁸³



Scheme 2.1 Numbering scheme and synthetic route to IFG (1.8). Adapted from Zhu *et al.*³⁸

For the portions of this thesis describing syntheses that were exact reproductions of Zhu's work, I will focus on the steps that I had difficulty reproducing, and what was done to synthesize the target molecules.

Zhu's published protocol begins with benzyl α -L-xyloside (**2.2**), so this needed to be made in large quantities from L-xylose (**2.1**) first. For initial reaction optimization, the much cheaper D-xylose was used as the starting material. Once good conditions had been established, it was reproduced with L-xylose (**2.1**). The benzyl xyloside was made under Fischer glycosylation conditions by refluxing the starting material and acid catalyst, $\text{BF}_3 \cdot \text{Et}_2\text{O}$, in benzyl alcohol. The product was isolated by precipitation in diethyl ether and purified by recrystallization from hot EtOH. The trade-off for such an easy protocol is a poor reaction yield; as demonstrated in my hands and reported as such in the literature.⁸³

After the anomeric centre was protected, hydroxyls 2 and 3 were protected by installation of an isopropylidene group (Scheme 2.1, page 24). Starting with triol **2.2**, the addition of 2-methoxypropene and *p*-TsOH in THF at 0° C resulted in the formation of the desired product (**2.3**) along with several side-products (Figure 2.1a).

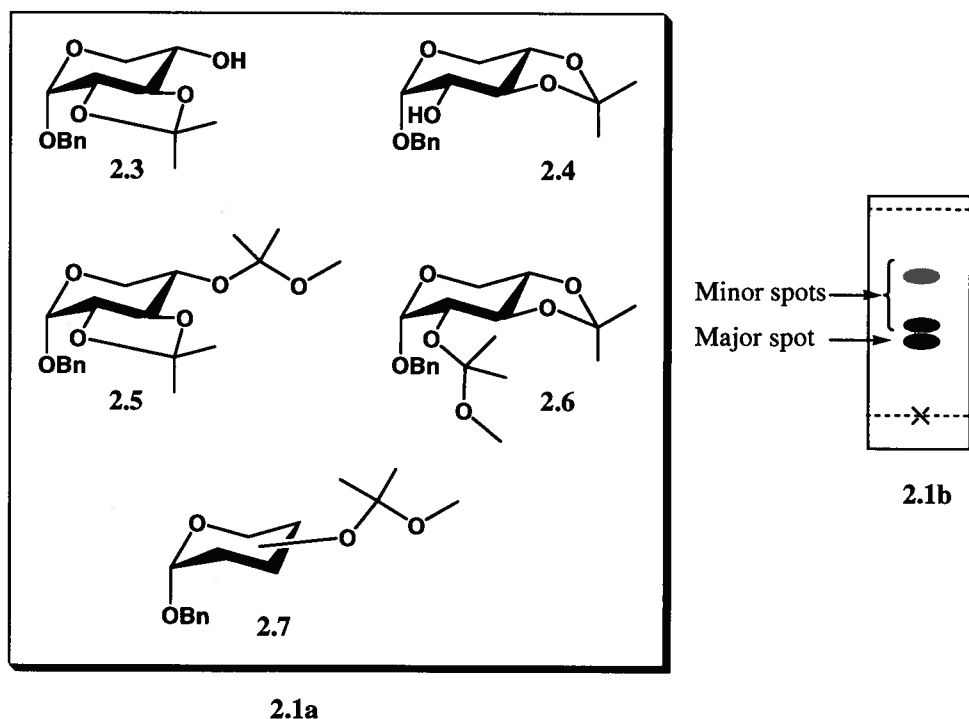


Figure 2.1 a) Desired product **2.3** of the isopropylidene reaction plus possible side-products. Structure **2.7** indicates incomplete installation of the protecting group at either the 2, 3 or 4 positions with the remaining two hydroxyls free. b) Representation of a TLC plate obtained from the isopropylidene reaction. The black spot indicates highest degree of staining by molybdate and the grey spots indicate staining to a lesser degree.

Zhu reported yields of 53% for synthesis of **2.3**, thus he was able to attain partial selectivity. In my hands, stoichiometry was important because when more or less than 2.5 equivalents of electrophile were used, the reproducibility was poor. Perhaps even more important was the amount of acid catalyst used. When the amount of *p*-TsOH was varied from 6.3 mol% to 2.5 mol%, there was an increase in selectivity for the desired product (**2.3**) from 42% in the crude mix to 66%. The TLC plate showed three spots when stained with molybdate; one major, two minor (Figure 2.1b). The separation on silica gel with 4:1 hexanes:EtOAc was difficult but eventually accomplished with the three spots isolated from one another. In Zhu's protocol, there was no mention of how the isolated products were verified to be the 2,3-O-isopropylidene (**2.3**), 3,4-O-isopropylidene (**2.4**), or any of the other possible side-products (**2.5**, **2.6** and **2.7**). More experiments were therefore needed before moving on to the next step. As identified by LRMS, the top spot contained a mix of compounds **2.5** and **2.6** and the middle and bottom spots contained **2.3**, **2.4** and a mix of **2.7** isomers (Figure 2.1b). This narrowed down the field but still did not provide any conclusive individual identifications.

In separate NMR experiments, ring protons were assigned for the middle and bottom spots based on data obtained from 2D ¹H-NMR COSY experiments; however, no distinguishing features were identified. This is because ¹H-NMR shifts of protons adjacent to unprotected hydroxyl groups are expected to fall within the same range as those adjacent to isopropylidene protecting groups (3-4 ppm). As well, spin systems of the ring protons are isolated from those of the protecting group protons, rendering COSY correlations ambiguous for the distinction between 2,3-O protection and 3,4-O protection. The coupling constants are expected to be the same for each product due to identical stereochemistry; so with this technique alone there was no unequivocal way to tell the difference between each isolated spot.

The method I used to identify each spot was as follows: A portion of each isolate was acetylated with pyridine and acetic anhydride. Without purification, ¹H-NMR and COSY data were obtained and assignments of ring protons were made. When comparing the spectra obtained before and after acetylation, one would expect to detect a proton

whose chemical shift had moved downfield following acetylation. This would correspond to the proton now adjacent to the electron-withdrawing acetyl group. The isolate which corresponded to the bottom spot showed a downfield shift for H4 after acetylation (**2.8**), indicating a free hydroxyl at that position prior to acetylation (Figure 2.2). This was the desired product and attainable in pure form (Figure 2.3). The middle spot contained more than one compound, but for the major component a downfield shift of the H2 peak was observed after acetylation, identifying it as the undesired compound **2.4**. Yields for the desired product (**2.3**) eventually reached those reported by Zhu.

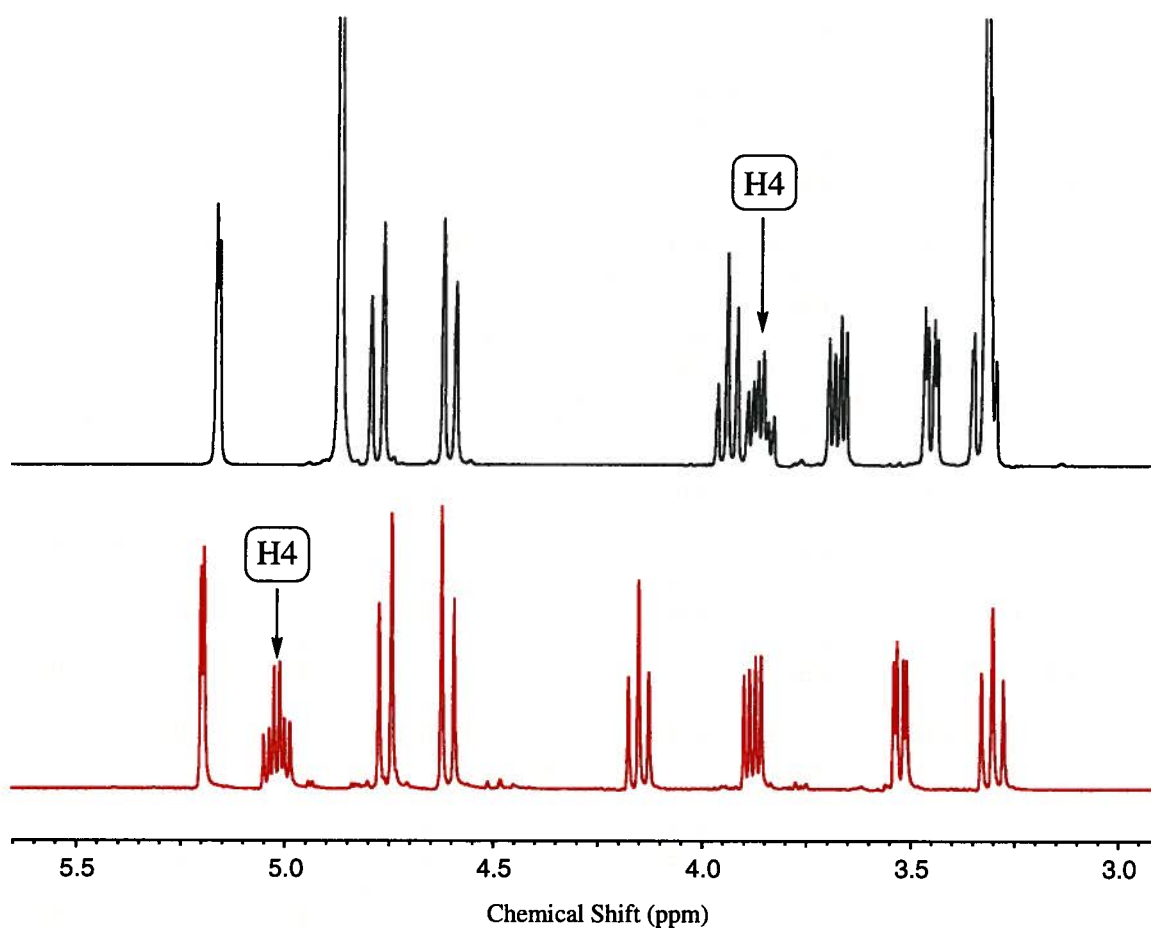


Figure 2.2 ¹H-NMR spectra of ring protons before and after acetylation. Top black spectrum was measured before acetylation (**2.3**) and bottom red spectrum was measured after acetylation (**2.8**) with H4 peak denoted by arrows.

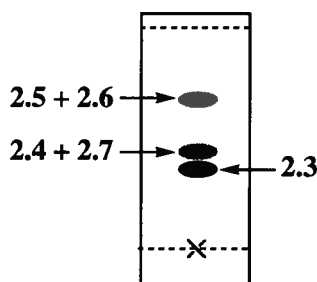
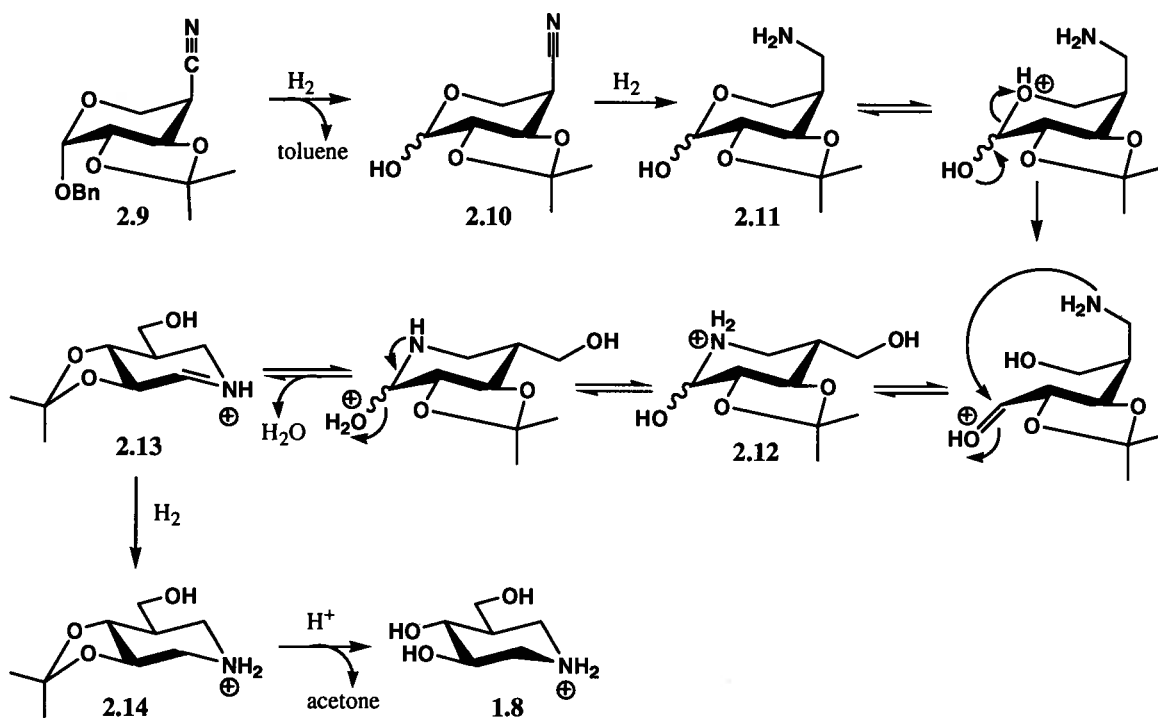


Figure 2.3 Representation of a TLC plate obtained from the isopropylidene reaction with product identity assigned to each spot.

The installation of the nitrogen was accomplished through activation of the 4-hydroxyl in **2.3** by triflation followed by S_N2 displacement with cyanide anion, inverting the stereochemistry at that centre to yield nitrile **2.9** (Scheme 2.1, page 24). Interestingly, this transformation also changes the molecule from an L-xylo configuration to a D-arabino configuration. Yields continued to go up as I became better at handling this sensitive reaction and also eventually reached the yields reported by Zhu.

The final one-pot hydrogenation under mild acidic conditions, followed by strong acid treatment, to reach IFG (**1.8**) is a very elegant reaction (Scheme 2.2). Six different transformations take place, several under reversible conditions with the reactive species being one of the tautomeric forms:

- 1) Reductive removal of benzyl glycoside reveals a hemi-acetal (**2.10**) in equilibrium with the open chain aldehyde.
- 2) Reduction of the nitrile to a primary amine (**2.11**).
- 3) Nucleophilic attack by free primary amine onto the open chain form of the aldehyde yielding a hemi-aminal (**2.12**).
- 4) Imine (**2.13**) formation by expulsion of water under acidic conditions.
- 5) Reduction of imine to form secondary amine (**2.14**).
- 6) Acidic conditions hydrolyze isopropylidene and reveal free diol (**1.8**).



Scheme 2.2 Mechanisms and intermediates representing the transformations in the final step of the synthetic route to IFG (**1.8**).

Taking clues from the literature, it was thought that purification would be difficult. Several lengthy purification protocols have been published for isolating pure **1.8** including, cation exchange chromatography (NH₄⁺ form), silica gel chromatography under conditions of 7:2:1 (*i*-PrOH:H₂O:7 M NH₄OH), as well as size exclusion chromatography plus combinations thereof.^{39,81} Zhu reported just one purification step using cation exchange chromatography (NH₄⁺ form) and this method was tried first. The basic idea behind this chromatographic method for separating amines is as follows:

The amine-containing sample is loaded under acidic aqueous conditions. This ensures the amines are positively charged and bind to the negatively charged carboxylate moieties immobilized on the resin beads that make up the stationary phase. In theory, a water wash elutes all anions and neutral compounds leaving all positively charged compounds bound to the resin. Once all undesired compounds have been eluted, an NH₄⁺-containing eluent (NH₄OH) is applied in an increasing gradient to displace the

positively charged amines according to binding affinity, with the weakest binders eluting first.

Zhu reported elution of IFG (**1.8**) upon using 0.05M NH₄OH, whereas I started with this concentration and increased it at 0.1 M intervals until the product eluted at 0.35 M NH₄OH. Unfortunately it was not in pure form. It was necessary to treat fractions that contained the desired product with benzyl chloroformate in 2:1:1 THF:H₂O:MeOH and sodium bicarbonate to install a carboxybenzyl (Cbz) group on the nitrogen atom (**2.15**) (Scheme 2.1). This allowed easier separation on silica gel with conditions of 1:1 petroleum ether:EtOAc followed by 9:1 CHCl₃:MeOH. After the pure, derivatized product (**2.15**) was in hand, a simple 2 hour hydrogenation under atmospheric pressure followed by filtration yielded pure IFG (**1.8**) (Scheme 2.1, page 24).

While Zhu reported a yield of 81% for the one-pot hydrogenation under atmospheric pressure, I was obtaining impure yields of only 30% prior to derivatization. The reaction was conducted under rigorously dry conditions, as well as with no special consideration for dryness, and at several different pH values ranging from pH 2–6, all to no avail.

In an effort to solve the problem of poor yields, the reaction mixture composition was investigated to look for side products and/or partially reacted products. A major component besides the desired product was identified as a hemi-acetal which also contained a nitrile moiety **2.10** (Figure 2.4 and Scheme 2.2). Several forms of evidence support this conclusion. The compound was eluted from a cation exchange column during the water wash; indicating the absence of an amine functionality, which is consistent with the expected elution profile of **2.10**. As well, the compound was analyzed by ¹H-NMR and two anomeric proton shifts were observed, consistent with the α- and β-anomers present when an aldose/hemi-acetal undergoes mutarotation at the anomeric centre. The compound was also acetylated and the resulting syrup was prepared as an IR sample. The peak observed at 2551 cm⁻¹ was indicative of the presence of a nitrile, further supporting the proposed structure. Finally, LRMS data were consistent with the

structure of **2.10**.

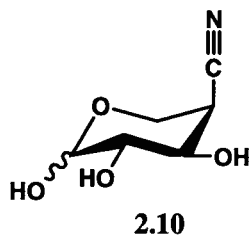


Figure 2.4 Structure of the side-product identified from the IFG reaction.

Upon realization that poor yields stemmed from incomplete reductions, 50 psi of H₂ was applied in a special apparatus for high pressure reactions. This was required in order for the hydrogenation to proceed at a decent rate. Simply using a catalyst (Pd(OH)₂/C 20%) obtained from Alfa Aesar as opposed to Sigma Aldrich also improved impure yields to 80% prior to derivatization. After the reaction was performed under high pressure, followed by cation exchange chromatography, Cbz derivatization, silica gel purification and Cbz removal, pure yields of 31% were reached for the transformation of the nitrile (**2.9**) to IFG (**1.8**) (Scheme 2.1, page 24).

2.1.2 Synthesis of C6-Alkyl IFG Derivatives

2.1.2.1 Synthesis of C6-*n*-Nonyl IFG

In the same paper that outlined a four step synthesis of IFG, Zhu *et. al.* reported the only synthetic route that accesses C6-alkyl IFG derivatives of the general structure shown in Figure 2.5.³⁸

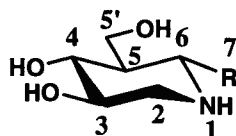
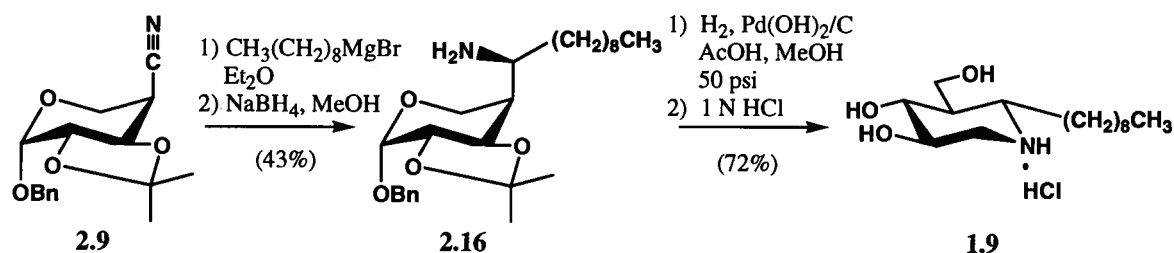


Figure 2.5 General structure and numbering scheme for C6-alkyl IFG derivatives where R=alkyl.

Zhu reported a series of C6-*n*-butyl through C6-*n*-nonyl IFG compounds synthesized via addition of the corresponding *n*-alkyl Grignard reagents to the nitrile intermediate (**2.9**) (Scheme 2.3). As the carbon atom in a nitrile moiety is electrophilic, and in **2.9** that carbon atom corresponds to the C6 position of IFG, nucleophilic addition of an alkyl grignard is a seemingly straightforward way to build up a series of C6-alkylated IFG derivatives, all of which have been shown to be strongly inhibitory towards GCCase.³⁸

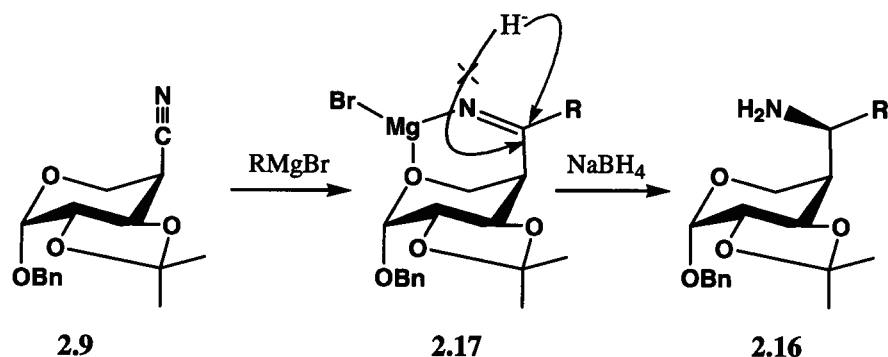


Scheme 2.3 Synthetic route to C6-*n*-alkyl IFG derivatives. Shown here with C6-*n*-nonyl IFG (**1.9**). Conditions listed are adapted from Zhu and yields shown are those obtained in my hands.

It was thought that reproducing the entire series would be unnecessary, therefore the most potent inhibitor of GCCase (**1.9**, $\text{IC}_{50} = 0.6 \text{ nM}$) was chosen for synthetic reproduction. It was also desirable to synthesize **1.9** because the only confirmation of inhibitory ability for the four longest alkylated versions of the published series were IC_{50} values.³⁸ Zhu cited mixed type inhibition as the reason why K_i values were not measured as well. We hypothesized that these compounds were indeed competitive inhibitors but that their inhibition assay was not sufficiently sensitive to handle sub-nanomolar inhibitors. It was hoped that the extensive kinetic evaluation done in our lab would allow the measurement of a true K_i value for **1.9**.

In the preparation of primary amine **2.16** (Scheme 2.3), the Grignard reaction required heating to 35°C and use of up to 5 equivalents of Grignard reagent in order to push the reaction to completion. In the second step, wherein the imino-magnesium complex (**2.17**) is reduced to the primary amine (**2.16**) by NaBH_4 , exclusive hydride

attack from behind (*Re* face) was observed (Scheme 2.4). This yielded only the *S*-configured diastereomer as confirmed with data obtained from Nuclear Overhauser Effect (NOE) NMR experiments of the final product (**1.9**). Strong correlations were observed between axial protons H4 and H2 when H6 was irradiated. This mechanism of stereoselective hydride delivery was first proposed by Zhu and the proof was in the form of NOESY NMR data from the final product.³⁸



Scheme 2.4 Proposed mechanisms for formation of amine **2.16**. Crossed out red arrow indicates the unfavoured *Si* face attack. Green arrow indicates the favoured *Re* face attack yielding amine **2.16** in a stereoselective manner. R= C₉H₁₉. Adapted from Zhu *et. al.*³⁸

Purification of the free amine (**2.16**) was accomplished on silica gel by using 20:1 CH₂Cl₂:MeOH with 0.1% Et₃N. A substantial amount of nonane was eluted from the column with **2.16** and it took two columns to obtain **2.16** in pure form. After confirmation of only single Grignard addition by ¹H-NMR and LRMS, one pot cyclization in the high pressure reactor under 50 psi of H₂ afforded the desired C6-*n*-nonyl IFG (**1.9**) (Scheme 2.3, page 32). The final product was purified via C-18 RP silica gel.

Originally I thought that the column yielded two distinct products because one compound eluted in 30% MeOH in H₂O and another in 60% MeOH in H₂O. LRMS data revealed the same masses for both compounds and ¹H-NMR and COSY data revealed the same number of protons and two very similar, yet distinct, looking spectra. The compound which eluted in 30% MeOH matched the analytical data published by Zhu, but the identity of the second compound was still unknown. At first, it was thought that the

extra compound was the result of epimerization during the Grignard reaction. The proton α to the nitrile (H4 of **2.9**) (Scheme 2.1, page 24) is slightly acidic with an estimated pK_a of 25-30, lower than the estimated pK_a of a terminal alkyl proton of nonane at 45-50. Nonyl magnesium bromide could react as a base by abstracting H4 rather than acting as a nucleophile. Upon quenching with MeOH, that centre might be reprotonated from either face yielding a mix of epimers at C4. However, when NOE experiments for both compounds were similar with respect to the stereocentre in question (C5 in IFG numbering, Figure 2.5, page 31), it was thought that the distinct $^1\text{H-NMR}$ spectra might be reflective of different protonation states of the amine. The compound which eluted in 60% MeOH was treated with 1 M HCl and concentrated several times to ensure protonation. The $^1\text{H-NMR}$ of the HCl treated version revealed an identical spectrum to that of the compound eluted in 30% MeOH, as well as to the data published by Zhu for **1.9**. The extra compound was merely the free base version of C6-*n*-nonyl IFG (**1.9**). The C-18 RP column distinguished between these protonation states with surprising clarity.

2.1.2.2 Synthesis of C6-*n*-Propyl IFG and C6,6-Di-*n*-propyl IFG

A trend was established within the K_i and/or IC_{50} values for the series of compounds synthesized by Zhu whereby an *n*-alkyl chain of longer than four carbons was needed in order to observe stronger inhibition than that afforded by IFG (unalkylated).³⁸ The planned synthetic route to establish a pH-labile linker diverged to also access C6-*n*-propyl IFG (**2.17**) and C6,6-di-*n*-propyl IFG (**2.18**) (Figure 2.6), neither of which had been published or tested by Zhu. It was desirable to see where **2.17** would fit within the trend as well as to probe the tolerance of GCase for C6 axial substituents, as in **2.18**.

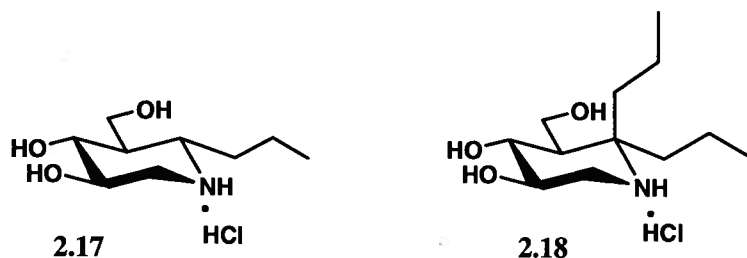
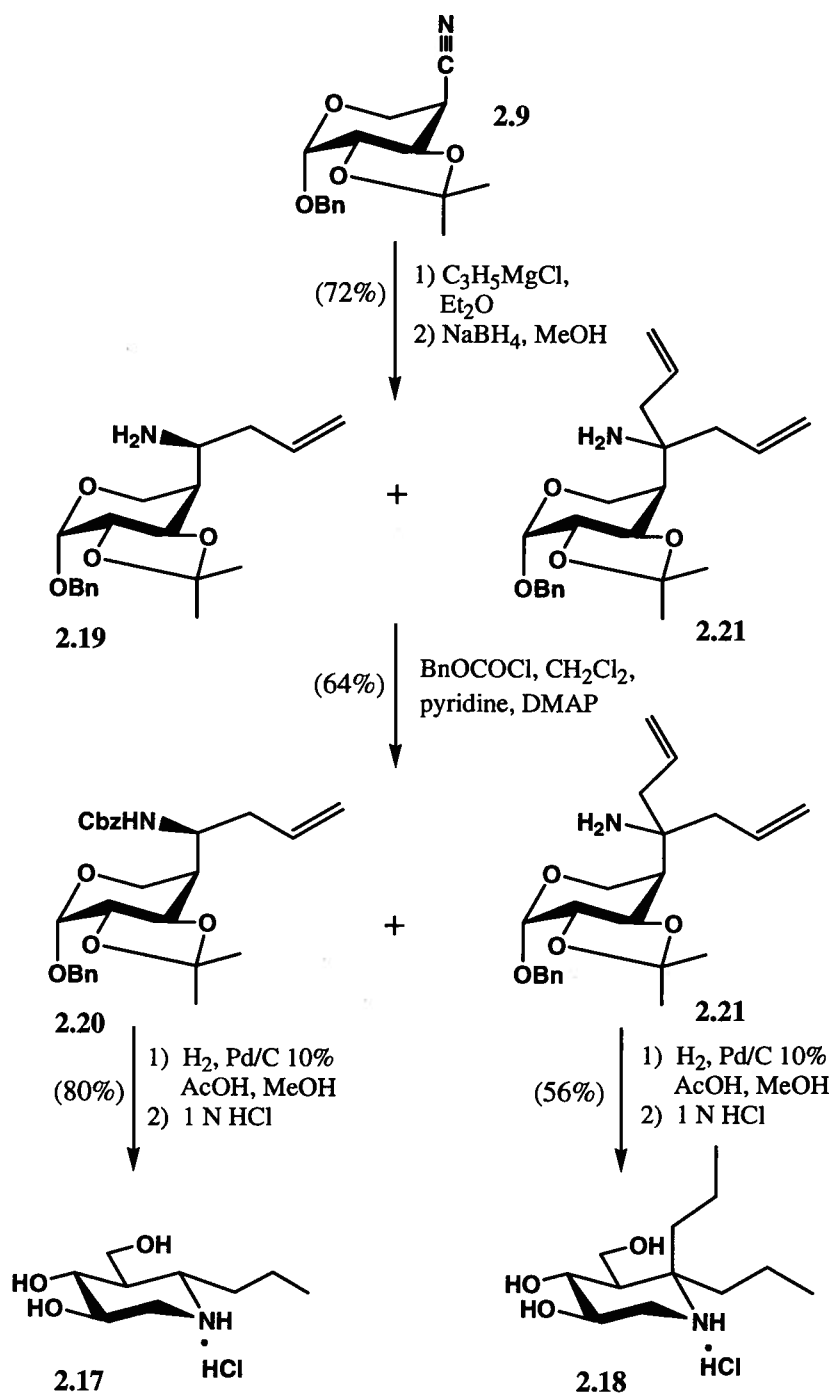


Figure 2.6 Structures of products **2.17** and **2.18**.

Starting with the nitrile intermediate (**2.9**), allyl magnesium bromide was used to make the allyl amine (**2.19**) (Scheme 2.5). It was assumed that double Grignard addition would not happen since it had not been observed in the nonyl system, thus many equivalents of allyl Grignard were added in the first attempt, only later to discover that double addition does indeed occur in this system. This reaction was much faster than the nonyl Grignard reaction and required reduced temperatures upon addition of reagent in order to minimize the double addition. Purification was simpler than with the nonyl version because the quenched Grignard reagent yielded propene, a gas at room temperature, rather than nonane, with a boiling point of 151° C. Subsequent installation of a Cbz group onto the nitrogen atom using benzyl chloroformate in pyridine, CH₂Cl₂, and DMAP served to protect the amine (Scheme 2.5) for further functional group manipulation, and simplified purification on silica gel. After the protected amine (**2.20**) was obtained in very pure form, a batch was hydrogenated in MeOH under atmospheric pressure overnight to access C6-*n*-propyl IFG (**2.17**) (Scheme 2.5). No purification was necessary as all protecting groups that were removed are volatile including; two equivalents of toluene and one equivalent of acetone, CO₂, and H₂O.



Scheme 2.5 Synthetic route to C6-*n*-propyl IFG (**2.17**) and C6,6-di-*n*-propyl IFG (**2.18**).

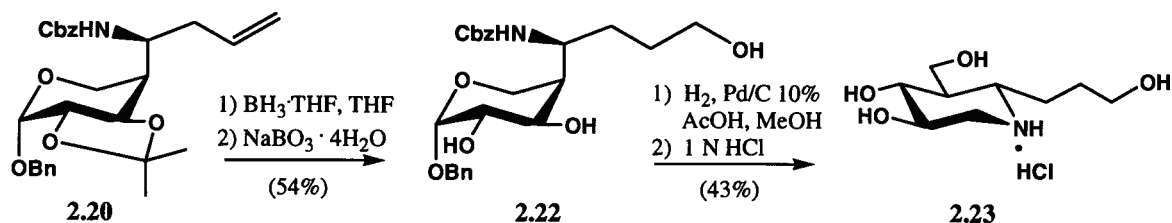
After the protected amine (**2.20**) was eluted from the column in 20:1 CH_2Cl_2 :EtOAc, the column was flushed with neat EtOAc in hopes that some unprotected amine **2.19** would be recovered for re-reaction. However the actual compound flushed from the column was unexpected and corresponded to the double Grignard addition

product, di-allyl amine (**2.21**) (Scheme 2.5) as confirmed by MS, ¹H-NMR and COSY data. Apparently **2.21** was too hindered around the nitrogen to install the bulky Cbz group. This provided a very convenient way to separate the very chromatographically similar primary amines (**2.19** and **2.21**).

Compound **2.21** was hydrogenated at atmospheric pressure overnight under acidic conditions to yield C6,6-di-*n*-propyl IFG (**2.18**) (Scheme 2.5), which was purified via C-18 RP silica gel. Access to **2.18** provided the opportunity to investigate how an axial substituent at the C6 position of IFG affects GCCase binding. It was desirable to know this in order to provide a basis for any further diversification of the C6-alkyl IFG derivatives.

2.1.2.3 Synthesis of C6-[9-Hydroxypropyl] IFG

Using protected alkene **2.20** as starting material, another IFG derivative was accessible that could be used to probe the effect on GCCase binding of a hydroxyl group within the alkyl chain. Addition of water across the double bond in an anti-Markonikov fashion under hydroboration – oxidation conditions yielded the primary alcohol **2.22** (Scheme 2.6). The other possible product, a secondary alcohol, was not observed. Upon purification on silica gel, with an increasing gradient of 10% to 25% EtOAc in CH₂Cl₂, **2.22** eluted with the isopropylidene group cleaved, presumably during the course of column purification. This protecting group was going to be removed in the next step anyway so it was unnecessary to re-install it. The next step was the final hydrogenation at atmospheric pressure overnight under acidic conditions to reach C6-[9-hydroxypropyl] IFG (**2.23**) (Scheme 2.6). This product was purified via cation exchange chromatography in the same manner as IFG (**1.8**) and eluted in 0.25 M NH₄OH. Treatment with HCl ensured that all the compound rested in one protonation state, yielding pure **2.23**.



Scheme 2.6 Synthetic route to C6-[9-hydroxypropyl] IFG (2.23).

2.1.3 Synthesis of Acetal-Containing IFG Derivatives as pH-Labile Linkers

2.1.3.1 Synthesis of C6-Benzyl acetal IFG

Many attempts were made to synthesize a C6 IFG derivative that contained an acetal moiety, which in theory would be pH labile. Ideally, the acetal would contain two alkyl or aryl arms (Figure 2.7a), which would mimic the hydrophobicity of ceramide and impart tight binding to GCCase at neutral pH values (ER) while intact. Upon hydrolytic cleavage at acidic pH values (lysosome), a weaker GCCase binder would be left, minimizing any inhibition of the delivered enzyme. After much trial and error, the only type of acetal-containing IFG derivative that could be synthesized and purified was of the general structure shown in Figure 2.7b.

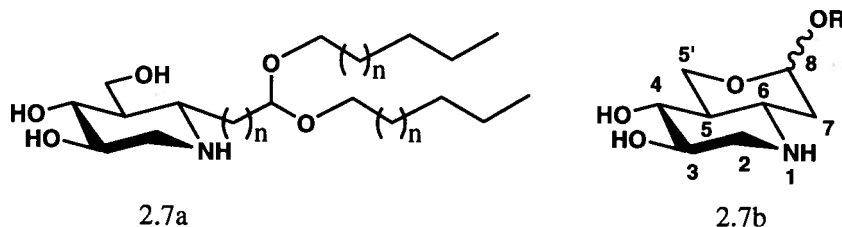
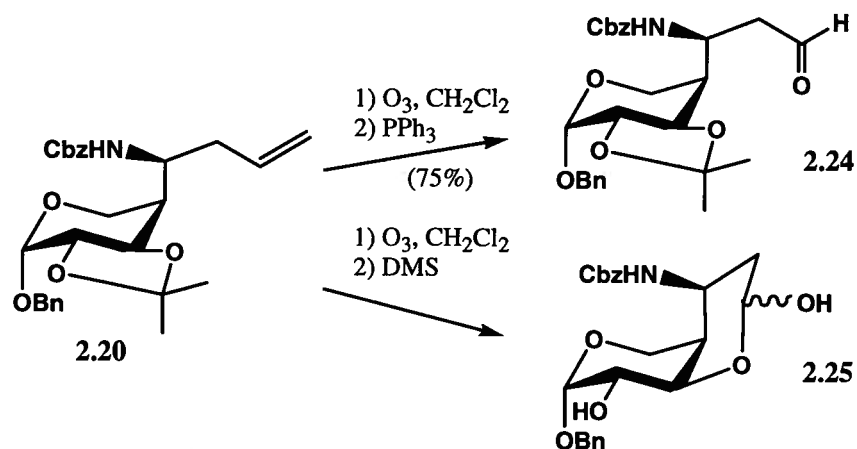


Figure 2.7 a) Ideal structure for pH-labile linker shown here with alkyl groups b) General structure of synthetically attainable pH-labile linker.

Starting again with 2.20, ozonolysis of the alkene followed by reduction of the ozonide with triphenylphosphine afforded the aldehyde 2.24 (Scheme 2.7) in good yield. Attempts to reduce the ozonide with dimethyl sulfide (DMS) resulted in cleavage of the isopropylidene group. This liberated the 3-hydroxyl group, which was situated six bonds

away from the carbonyl carbon of the aldehyde and easily formed the six-membered hemi-acetal (**2.25**) as shown in Scheme 2.7.



Scheme 2.7 Products of ozonolysis reaction followed by reduction with use of either PPh₃ (**2.24**) or DMS (**2.25**).

It was discouraging to realize so late in the project that the molecule was set up for an undesired intra-molecular hemi-acetal formation upon deprotection, not only with O4 of the final product (**2.26**), but with O5' as well (**2.27**) (Figure 2.8).

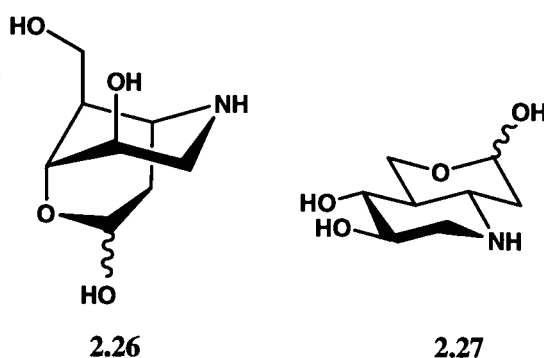
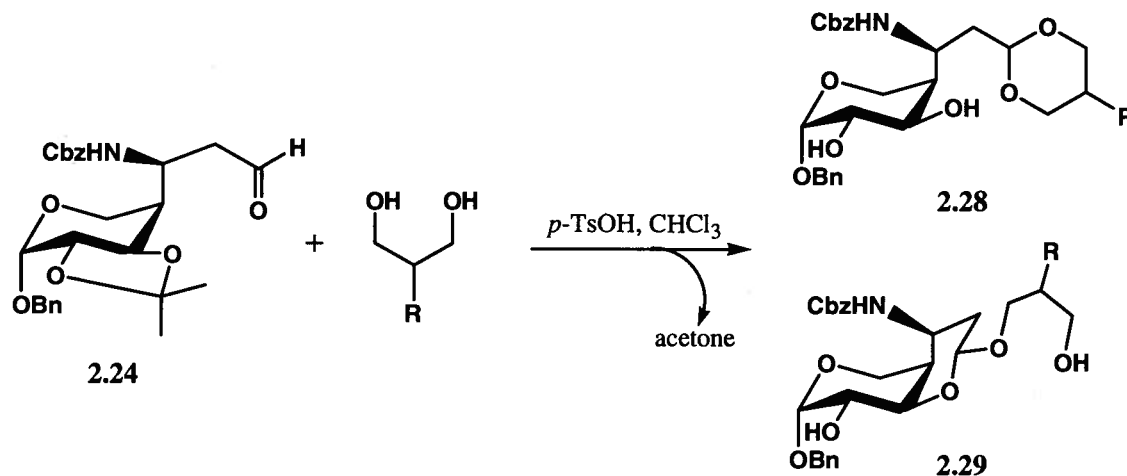


Figure 2.8 Undesired intra-molecular hemi-acetal formation with O4 (**2.26**) and O5' (**2.27**).

As was realized at the time, in order to access IFG derivatives of the general structure shown in Figure 2.7a (page 38), an inter-molecular reaction between an alcohol such as hexanol, and the aldehyde would have to proceed faster than, and be favoured over, an intra-molecular reaction. The fundamentals of reaction kinetics would suggest that this was impossible. The only hope would rest in use of a 1,3-propane diol derivative as the alcohol, which would force two intramolecular processes to compete for acetal formation (Scheme 2.8).

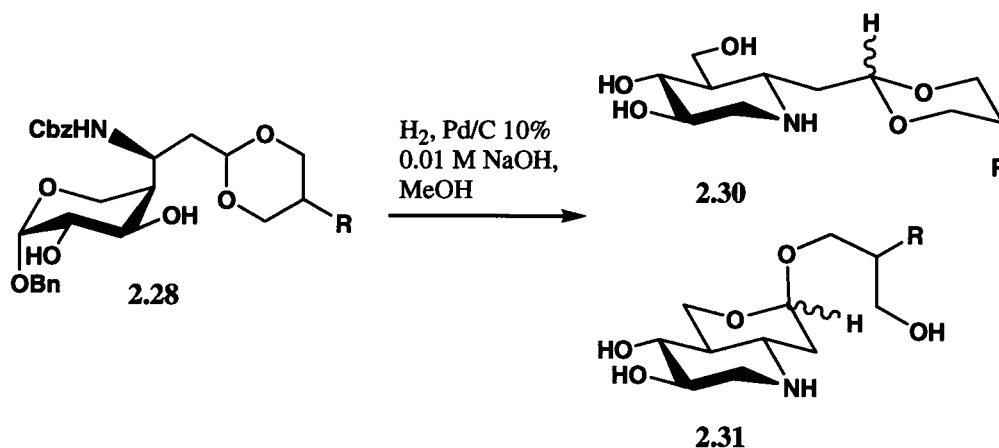


Scheme 2.8 Two possible products (**2.28** and **2.29**) resulting from acetal formation with 2-*n*-alkyl-1,3-propane diol derivatives and aldehyde **2.24**.

A pure sample of aldehyde **2.24** was reacted with 2-*n*-butyl-1,3-propane diol and *p*-TsOH in CDCl₃ and the reaction monitored by ¹H-NMR every two minutes. Two regions of the ¹H-NMR spectra were helpfully diagnostic in monitoring this reaction. First, the aldehyde proton peak at δ 9.8 ppm disappeared as the hemi-acetal and acetal formed. Second, as the isopropylidene group cleaved to yield acetone, a peak at δ 2.05 ppm was observed. Other spectral regions contained multiple overlapping peaks that could not be used diagnostically. While the ¹H-NMR spectra did not allow product identification, it was apparent that equilibrium was established quickly because the spectra stopped changing after 12 minutes and remained the same after reaction overnight in the NMR tube.

The reaction mixture was purified on silica gel with 1:1 hexanes:EtOAc, and a product with the correct mass was isolated. The $^1\text{H-NMR}$ spectrum of the isolated material was not helpful in distinguishing between the two possible products (**2.28** and **2.29**) (Scheme 2.8) so an attempt was made to chemically differentiate the products, if indeed a mixture was present in the column isolate. Only one of the two proposed products contains a primary hydroxyl group (**2.29**), which would react much faster with TBDMSCl than would the secondary hydroxyls of **2.28**. This should alter the R_f value of the undesired product (**2.29**) and allow separation. However, when I attempted to perform the reaction, no new spots appeared on the TLC plate and the MS data did not change, yet the reagent was confirmed to be active by reaction with a model compound. As a result, it was concluded that the isolate contained only the desired product **2.28**.

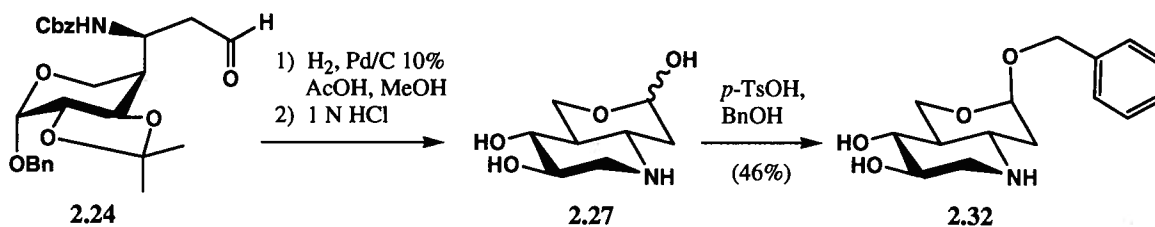
Emboldened by this finding, the product **2.28** was subjected to standard hydrogenation conditions at atmospheric pressure, but this time, the pH was adjusted to 8 with 0.01 M NaOH to minimize any new acetal formation. Unfortunately the $^1\text{H-NMR}$ spectrum of the resulting product mixture was extremely complex and contained four triplet peaks between δ 4.5 and 4.7 ppm, all of equal intensity, presumably corresponding to the different stereochemistries of the acetal proton of each possible acetal product (Scheme 2.9). Apparently my attempts to suppress new acetal formation were unsuccessful and no useful approaches were found for separation of these products.



Scheme 2.9 Possible products (**2.30** and **2.31**) from hydrogenation of **2.28** resulting in complex $^1\text{H-NMR}$ spectra. Red bond indicates acetal proton observed as triplet peaks from δ 4.5 and 4.7 ppm.

It was apparent that the goal of synthesizing molecules with the general structure shown in Figure 2.7a (page 38) was unattainable with this particular carbon skeleton. The carbon chain extending from C6 would need to be at least three carbons longer in order to suppress all undesired five and six-membered intramolecular reactions and cyclizations. Given the limited time remaining this was not feasible. Moving forward with what was available and known; it seemed that only a single hydrophobic substituent could be introduced to the acetal as shown in Figure 2.7b (page 38). After contemplation, it appeared that this type of structure might actually be beneficial for a PC. Due to the intramolecular hemi-acetal formation (Figure 2.8, page 39), liberation of a free aldehyde upon hydrolysis is avoided. This is desirable because a free aldehyde could possibly react with any lysine residues of GCase and form a Schiff base, which could have negative side-effects. The intra-molecular hemi-acetal formation (Figure 2.8) (**2.26** and **2.27**) upon acetal hydrolysis might mitigate these effects.

Aldehyde **2.24** was hydrogenated under acidic conditions at atmospheric pressure and, without purification, the residue was stirred in benzyl alcohol and *p*-TsOH (Scheme 2.10). Due to limited reactant solubility, the reaction was continued for four days. The reaction mixture was neutralized with anion exchange resin (⁻OH form) and the protonated form of product **2.32** was extracted with aqueous ammonium acetate solution at pH 7. This was washed with petroleum ether to remove the excess high-boiling benzyl alcohol. The product was purified on C-18 RP silica gel and eluted in 30% MeOH in H₂O. The trans-decalin ring system rigidifies **2.32** and, from the coupling constant of 3.1 Hz between H-7_{ax} and H-8, it appears that only one anomer was formed wherein the -OR group is axial; presumably due to the anomeric effect.



Scheme 2.10 Synthetic route to C6-benzyl acetal IFG (**2.32**).

The stability of **2.32** was tested by dissolving an aliquot of the intact acetal in water, adjusting the pH to 2, 3, 4, 5, 6, and 7 and incubating each solution at 37°C. Aliquots at time points of two hours, four hours, 24 hours, and 5 days were taken and analyzed by LRMS. The data revealed that **2.32** is a very stable acetal indeed. Hydrolytic cleavage was not observed at any of the pH values for any time aliquots. Indeed hydrolysis within 2 days at 37°C required lowering the pH to 1. One factor contributing to the unusual stability of this acetal is that it is part of a trans-decalin system. In order for acetal cleavage to occur, the hybridization of the acetal carbon atom must go from sp^3 to sp^2 , and this requires a flattening of the ring system. The rigid trans-decalin system makes this unfavourable.

This result and conclusion is also consistent with a study published which describes relative hydrolytic cleavage rates of acyclic and six-membered cyclic acetals.⁸⁴ In general, there was an increased rate with an increase in the stability of the corresponding alkoxy carbenium ion intermediate. This translates into faster rates for compounds with a higher degree of substitution at the acetal carbon, and for acyclic acetals in comparison to their cyclic counterparts. More specifically, acyclic acetals that were closest in structure to **2.32** hydrolyzed some thousand-fold faster than the corresponding cyclic acetal closest in structure to **2.32**. Therefore, it is not unreasonable to assume that if acyclic acetal-containing IFG derivatives (Figure 2.7a, page 38) were accessible, their hydrolytic cleavage profiles would be more in line with the goals of designing a pH-labile linker.

2.1.3.2 Other Attempts to Synthesize Acetal-Containing IFG Derivatives

In Zhu's work, only *n*-alkyl Grignard reagents were used and at the beginning of this project, it was not apparent if this methodology could be applied with more complex Grignard reagents. The initial attempts to synthesize a pH-labile IFG derivative centered around incorporation of a pre-formed acetal by using a Grignard reagent such as **2.33** shown in Figure 2.9. After attempts to use a commercially available Grignard reagent had failed, I tried to synthesize it in the lab. Benzaldehyde was used as a model

electrophile in order to test whether an active Grignard reagent was being made from the bromide. In the model system it was confirmed that active Grignard reagent was being made however, inseparable mixtures resulted when **2.33** was reacted with nitrile **2.9** (Scheme 2.3, page 32).

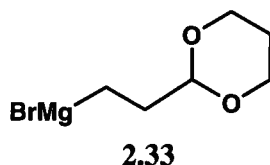
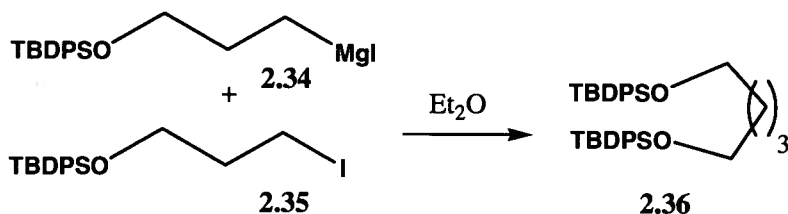


Figure 2.9 Structure of Grignard reagent (**2.33**).

In an attempt to gain insight into the problems I was having with the Grignard reaction, I searched the literature for examples of Grignard reagent addition to nitriles followed by reduction to the amine; as opposed to hydrolysis to the ketone. The literature had a very scant representation of this type of reaction. A 1986 paper described tandem alkylation-reduction of nitriles. They tested various Grignard reagent additions to nitriles followed by reduction to the primary amine with anhydrous ammonia and lithium metal. The yields for these reactions were unreliable and ranged from 32%-99%.⁸⁵ In a follow-up paper they described copper (I) activated addition of Grignard reagents to nitriles with a little more success.⁸⁶ However, when I replicated the procedure using copper (I) iodide with the cyclic acetal Grignard reagent (**2.33**) and nitrile (**2.9**), I observed no reaction. Continuing the literature search, I found another paper describing cerium (III) chloride-activated addition of Grignard reagents to various electrophiles including ketones, α , β -enones, esters, amides and nitriles.⁸⁷ Of more than 100 reactions reported, the yields for addition to nitriles came in last; ranging from no reaction at all to 28% with 72% recovered starting material. Nevertheless, the protocol with anhydrous cerium chloride was followed with the cyclic acetal Grignard reagent (**2.33**) and nitrile (**2.9**), and only about 5% reaction was observed. Side reactions that resulted in inseparable mixtures in the absence of copper or cerium salts were clearly suppressed in their presence. Unfortunately the desired reaction was suppressed as well. The cyclic acetal Grignard reagent (**2.33**) was no longer pursued after these results.

The next strategy was to make a Grignard reagent with a protected alcohol (**2.34**) which could be oxidized at a later stage (Scheme 2.11). The synthesis of the Grignard precursor (**2.35**) was straightforward starting with 1,3-propane diol followed by mono-protection with TBDPSCl. Next was de-oxygenative iodination with triphenylphosphine, imidazole and iodine. Unfortunately this route led to a dead end when the reagent simply dimerized (**2.36**) upon treatment with magnesium as shown in Scheme 2.11.



Scheme 2.11 Product resulting from dimerization of Grignard precursor (**2.36**). Active Grignard (**2.34**) reacting with iodide (**2.35**) in S_N2 fashion.

What can be taken from the literature search and the less than ideal results from the Grignard reagent additions to nitrile (**2.9**), is that this is a difficult transformation and has limited applicability. In my experience the best results were obtained when using hydrocarbon and alkenyl Grignard reagents, which is also consistent with what has been published about this reaction in the literature. It was apparent that attempts to introduce a pre-formed acetal moiety into the molecule via a Grignard reaction were futile. The best strategy seemed to require the use of a simple alkenyl Grignard reagent followed by oxidation in order to develop the acetal linker afterwards. This lengthens the synthesis considerably due to the required protecting group manipulation, but it still provides the best route of those investigated towards C6-acetal containing IFG derivatives.

2.2 Inhibition Studies with Human GCCase

After the desired compounds of IFG and derivatives thereof (Figure 2.10) had been synthesized and characterized, inhibition studies with human GCCase were performed. I started with inhibition studies because the Michaelis-Menten parameters have already been established for GCCase with the substrate that was used, 2,4-dinitrophenyl β -D-glucopyranoside (2,4-dNP-Glu).⁸⁸ Within the inhibition data collected there was always a control with no inhibitor. These uninhibited data were used to generate the K_m and V_{max} values, which always matched with what has already been published for this system.

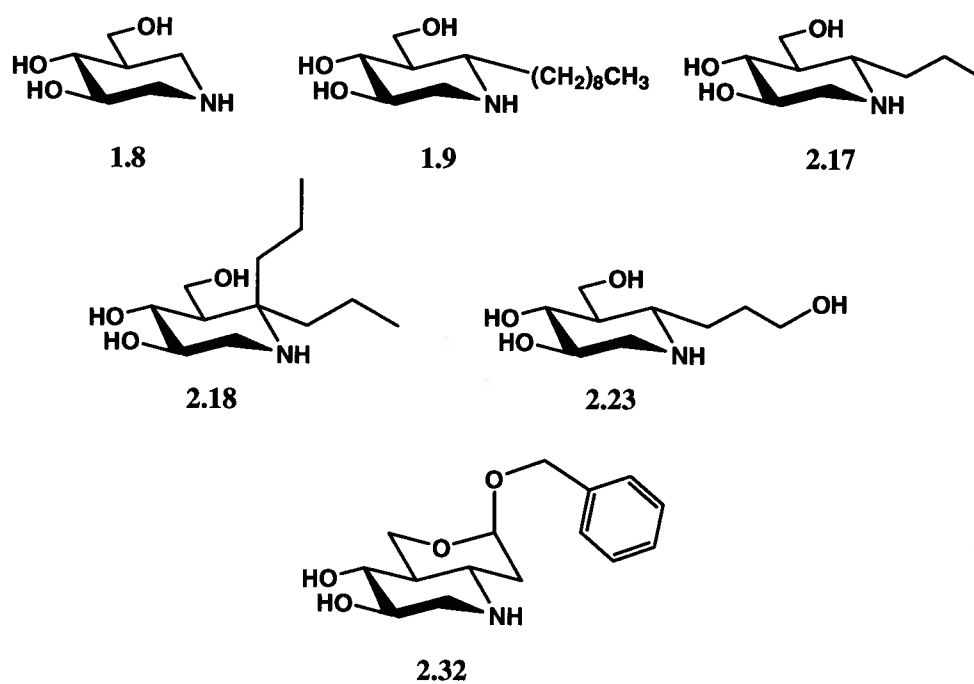


Figure 2.10 Compounds tested as inhibitors of GCCase.

For all compounds except **1.9**, a standard continuous UV-Vis spectrophotometric assay was performed in which GCCase buffer, GCCase and inhibitor were pre-incubated at 37°C for ten minutes. The reactions were initiated by addition of the substrate 2,4-dNP-Glu and the release of 2,4-dinitrophenolate was monitored at 400 nm. Steady state rates were measured in the linear region of each curve as Abs/min readings.

The concentrations of substrate that were used were 0.5 mM, 1.1 mM, 3.0 mM and 5.0 mM. Each substrate concentration was tested with five or six different inhibitor concentrations based on the inhibitor's estimated K_i value, usually $1/3 K_i$ to $3 K_i$, plus data with no inhibitor. After the first series of inhibitor and substrate concentrations were assayed, the data were fit to several nonlinear regression models for different modes of inhibition in order to calculate K_i values along with associated errors. For all inhibitors tested, the data fit best to the equation describing competitive inhibition as shown below.

$$v = \frac{V_{\max}[S]}{[S] + K_m(1 + [I]/K_i)} \quad \text{Equation 2.1}$$

The first calculated K_i value was often lower than expected from the IC_{50} runs performed at a single substrate concentration. As a result, a second series was assayed in which the same substrate concentrations were used and inhibitor concentrations shifted to sandwich the true K_i value. This also allowed duplicate measurements, and in all cases the second calculated K_i value did not change considerably from the first.

Special consideration with respect to the enzyme concentration needs to be exercised when the inhibitors assayed bind in the nanomolar and sub-nanomolar range. This is because the enzyme must be present at a concentration much less than those of substrate or inhibitor in order to fulfill all the assumptions of Michaelis-Menten kinetics and to thereby obtain useful data. In practice this means that inhibitor concentrations must be at least five times that of enzyme concentration, ideally ten times more. If very low enzyme concentrations are used, one needs to ensure that the spectrometer used is sensitive enough to measure a reliable rate. For measurements with IFG, I dropped the concentration of GCase to 0.9 nM so that this requirement was fulfilled and still managed to observe reliable rates. A GCase concentration of 2.2 nM was used for all the other inhibitors evaluated by the UV assay.

Dixon plots were used to graphically represent the data and the theory describing this method, along with reversible competitive inhibition, is outlined in the Appendix.

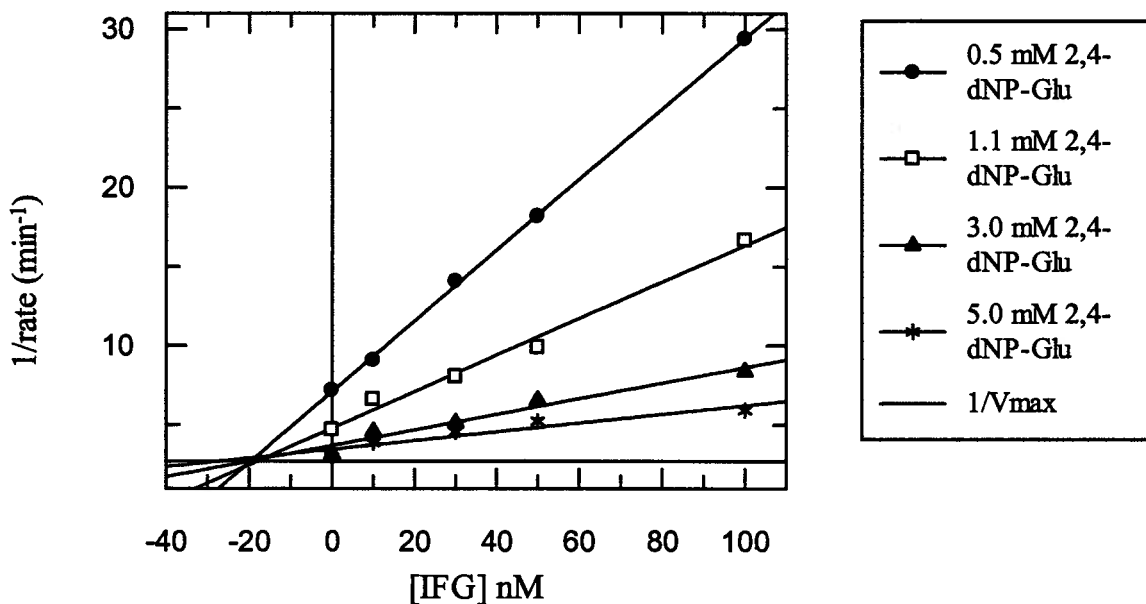


Figure 2.11 Dixon plot for the inhibition of GCCase by IFG (1.8).

Zhu reported the K_i value for IFG (1.8) with GCCase to be 25 nM whereas I measured it to be $23 \text{ nM} \pm 2$, statistically the same. It was reassuring that this value agreed with what had been published.³⁸

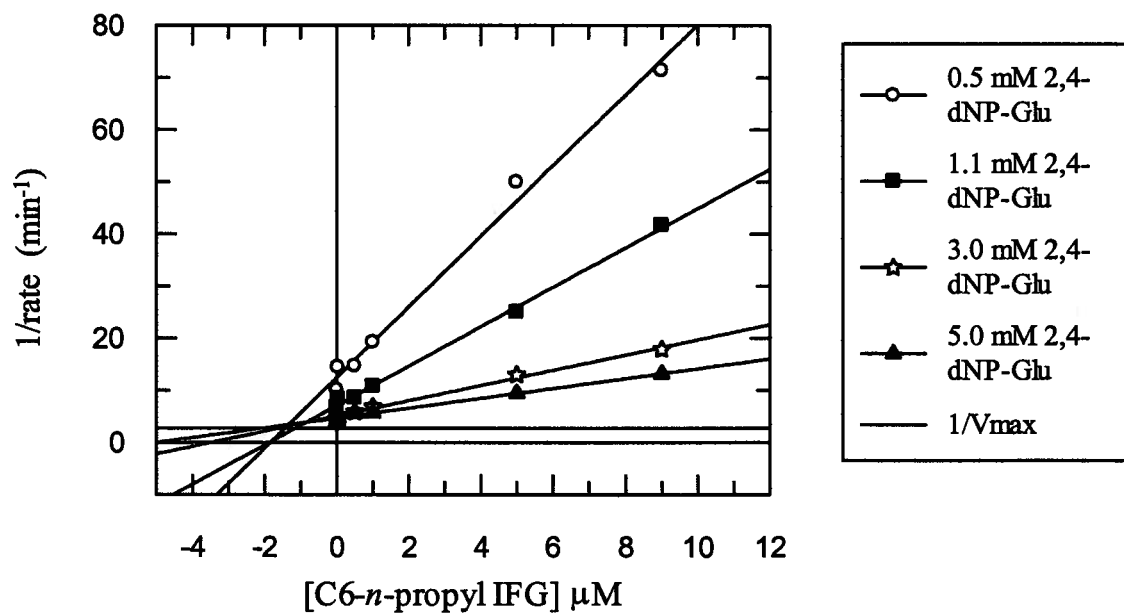


Figure 2.12 Dixon plot for the inhibition of GCCase by C6-n-propyl IFG (2.17).

Although C6-*n*-propyl IFG (**2.17**) was a C6-*n*-alkyl IFG derivative of the kind Zhu had published, this particular derivative was not synthesized or investigated. It was desirable to see where **2.17** would fit within the trend observed by Zhu whereby five carbons or more were needed at C6 in order to observe stronger inhibition than that afforded by IFG (unalkylated). Compound **2.17** did fit within the trend with a measured K_i value of $0.61 \mu\text{M} \pm 0.075$, almost six-fold higher than the butyl derivative at $0.12 \mu\text{M}$.³⁸

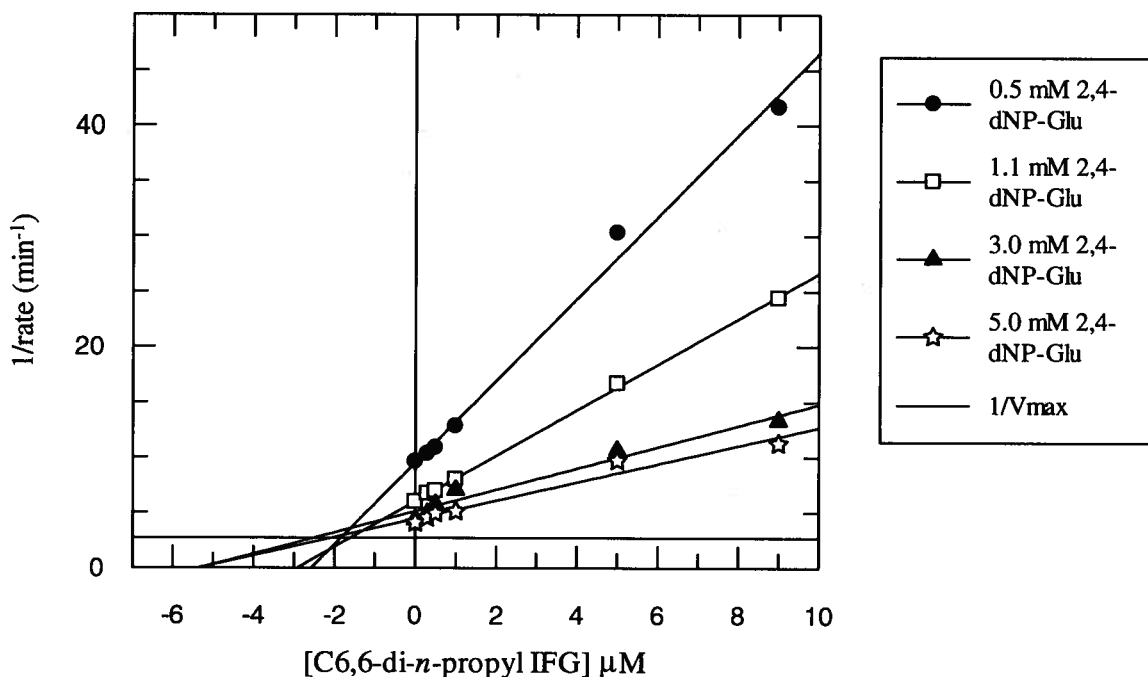


Figure 2.13 Dixon plot for the inhibition of GCCase by C6,6-di-*n*-propyl IFG (**2.18**).

It was hypothesized that the tolerance of GCCase for C6 axial substituents, such as in compound **2.18**, would be poor. Surprisingly, this was not the case; the dipropyl compound (**2.18**) exhibited the same level of inhibition as that of **2.17** with a measured K_i value of $0.61 \mu\text{M} \pm 0.10$. This result is particularly interesting because it forms the basis for any future exploration of C6-axial IFG derivatives as it seems GCCase has space in the active site to accommodate a C6-axial group of at least three carbons in length.

The natural substrate hydrolyzed by GCCase, glucosyl ceramide (GlcCer), is quite hydrophobic overall. However, it contains a secondary hydroxyl group as well as an amide bond. Amongst the inhibitors tested to date, none of the C6-alkyl IFG derivatives have contained any hydrophilic moieties within their alkyl chain, such as the hydroxyl group in **2.23**. It was not clear how this would affect GCCase binding. When this compound was assayed as an inhibitor of GCCase, the K_i value was measured to be $104 \text{ nM} \pm 19$. This was lower than we had expected and perhaps suggests that a new hydrogen bond forms between a residue in GCCase and the hydroxyl group. This certainly could account for the tighter binding of **2.23** relative to **2.17** or **2.18**.

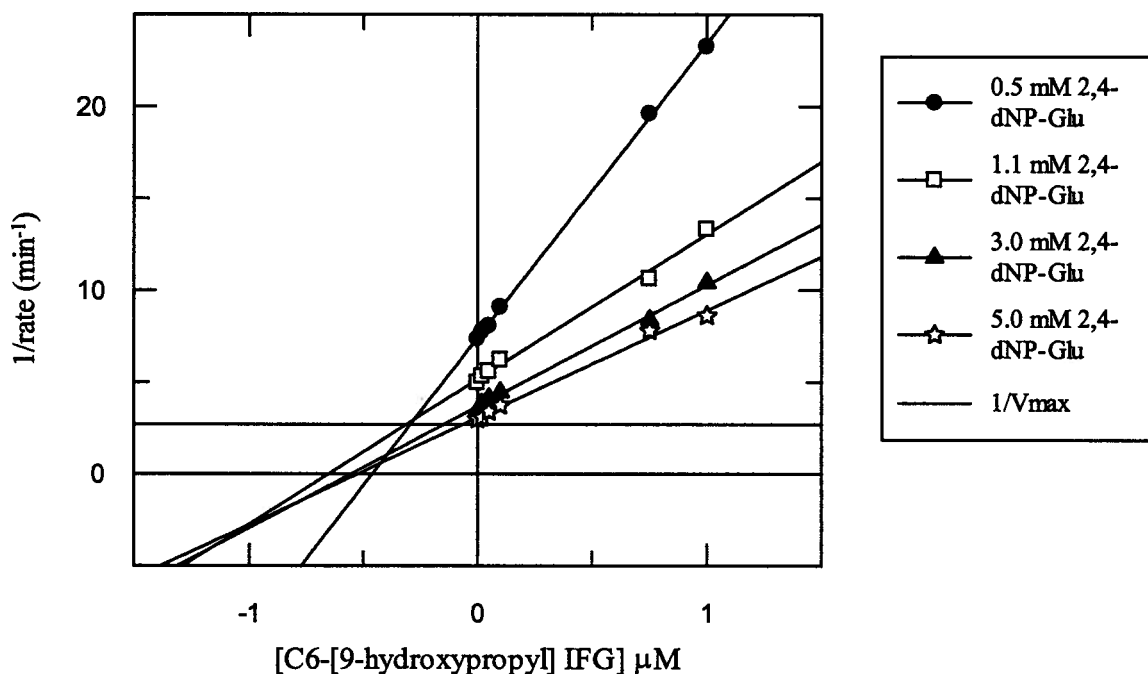


Figure 2.14 Dixon plot for the inhibition of GCCase by C6-[9-hydroxypropyl] IFG (**2.23**).

The data for the Dixon plot associated with **2.23** showed some signs of mixed-type inhibition because the lines do not all intersect at the $1/V_{\text{max}}$ line. However, when the raw data were fit to the various nonlinear regression models of inhibition including competitive, mixed type and non-competitive; the best fit was achieved with the competitive model.

Previous studies performed in our group suggested that the 5' primary hydroxyl group (equivalent to O6 in glucose) was particularly important for inhibitory power. When this hydroxyl group was replaced with a fluorine atom, there was a substantial decrease in the inhibitory ability of the compound compared to the parent compound, presumably due to the deletion of an important hydrogen bond. In compound **2.32**, the intramolecular acetal involves the 5' hydroxyl group, reducing the opportunities for hydrogen bonding. However, since the inclusion of a benzyl group might improve affinity, it was not clear what the overall effect would be. In fact, the K_i value was measured to be $160 \text{ nM} \pm 6$, still quite a good inhibitor.

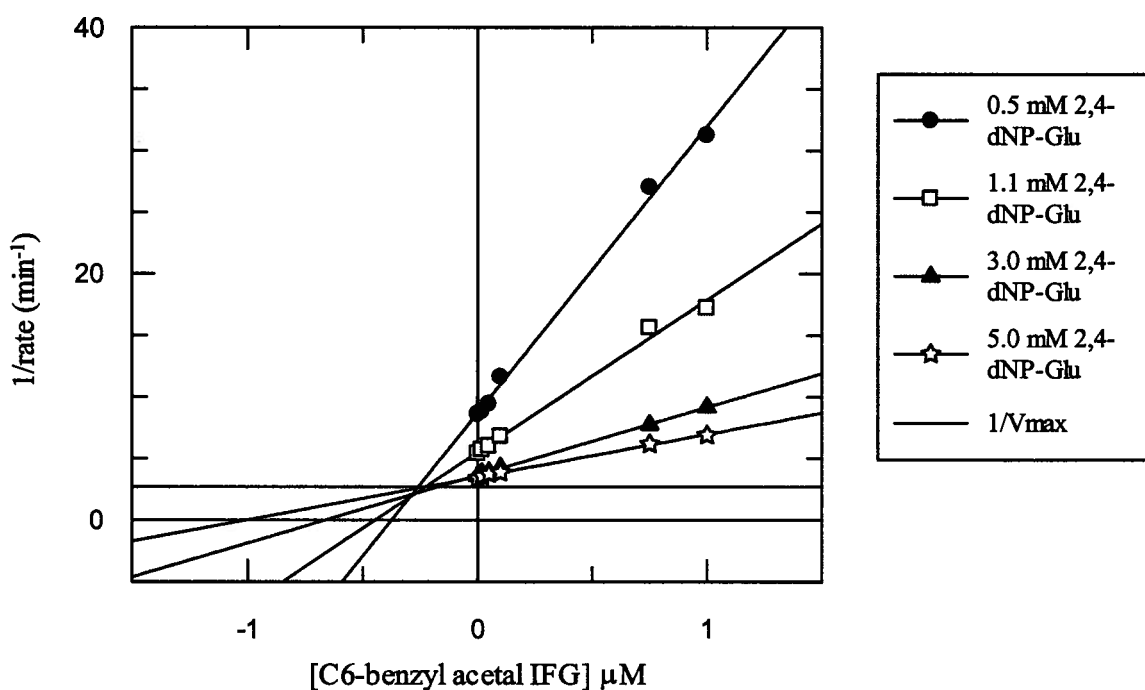


Figure 2.15 Dixon plot for the inhibition of GCCase by C6-benzyl acetal IFG (**2.32**).

Due to the limited amount of **2.32** that remained, inhibition studies could not be performed on the cleaved version of the acetal, **2.27** (Figure 2.7). As it happens, it is unlikely that this version would cleave under physiological conditions anyway. So this was not deemed to be a crucial measurement.

Measurement of the K_i value of C6-*n*-nonyl IFG (**1.9**) was rendered much more challenging by its anticipated sub nanomolar K_i value. As mentioned previously, the inhibitor concentration must be at least five times that of the enzyme concentration in order to obtain reliable data. In attempting to satisfy this requirement when assaying C6-*n*-nonyl IFG (**1.9**) with the continuous UV-Vis assay, very low enzyme concentrations had to be used and the rates observed were not reliable when substrate concentrations were low and inhibitor concentrations high. This indicated that the level of sensitivity of the UV-Vis spectrophotometer had been reached and that this assay could not be used to measure the K_i value of **1.9**.

A more sensitive instrument, a fluorimeter, was used in order to investigate the inhibitory properties of **1.9**. The idea behind a fluorescent assay is the same as with the UV assay with respect to rate measurement at various substrate and inhibitor concentrations, however, the practicalities are different. The fluorescent substrate, 4-methylumbelliferyl β -D-glucopyranoside (4-MU-Glu) was used and the rate of release of 4-methylumbelliferrone was measured; much in the same way as the UV-Vis assay measures the release of 2,4-dinitrophenolate. Since GCCase operates in the lysosome and has a pH optimum of around 5.5, this is the pH at which the inhibition is measured. The cleaved substrate however does not emit sufficient fluorescence at this pH and therefore, the pH must be raised above pH 10 in order to fully observe the fluorescence of the cleaved moiety. This requires the assay to be stopped rather than continuous.

Buffered solutions containing the substrate were pre-incubated at 37°C in Eppendorf vials in the presence or absence of inhibitor (**1.9**). The reaction was initiated by addition of GCCase to a total concentration of 5 pM, then at fixed time intervals of 3, 6 and 9 minutes, 100 μ L aliquots were removed and diluted into a cuvette containing 500 μ L of glycine buffer at pH 10.8. This both stopped the enzyme reaction and ionized the 4-methylumbelliferrone product, increasing its fluorescence to an observable intensity. Rates were calculated by linear regression of the fluorescence intensity measured at each time point with each fluorescence value being an average of 15 individual readings. The data were fit to the inhibition models in the same manner as with the other compounds,

and the K_i value of **1.9** was measured to be $0.2 \text{ nM} \pm 0.01$. This is a remarkably potent inhibitor and the strongest towards GCCase measured to date. It also clearly exhibits competitive inhibition, laying to rest the claims made by Zhu that this is a mixed-type inhibitor.³⁸

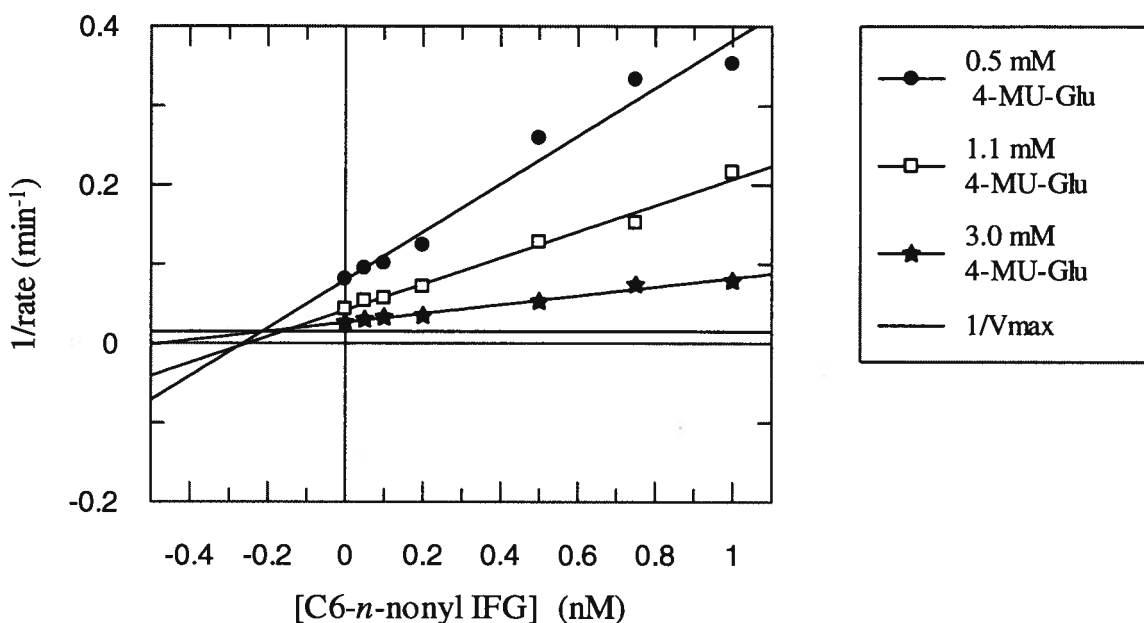


Figure 2.16 Dixon plot for the inhibition of GCCase by C6-*n*-nonyl IFG (**1.9**).

Putting all the K_i values that I measured into context with what has been published in the literature suggests that C6-alkyl IFG derivatives are among the most potent inhibitors of GCCase. Many of the compounds assayed thus far as inhibitors of GCCase have had their inhibitory power evaluated by IC_{50} values, which are not directly comparable to K_i values, but can offer a rough comparison. Figure 2.17 shows several different iminosugars as well as nitrogen-containing heterocycles and their respective IC_{50} values towards GCCase. Most of these previously published inhibitors are in the mid to low micromolar range whereas all the compounds I tested are in the sub micromolar to sub nanomolar range.

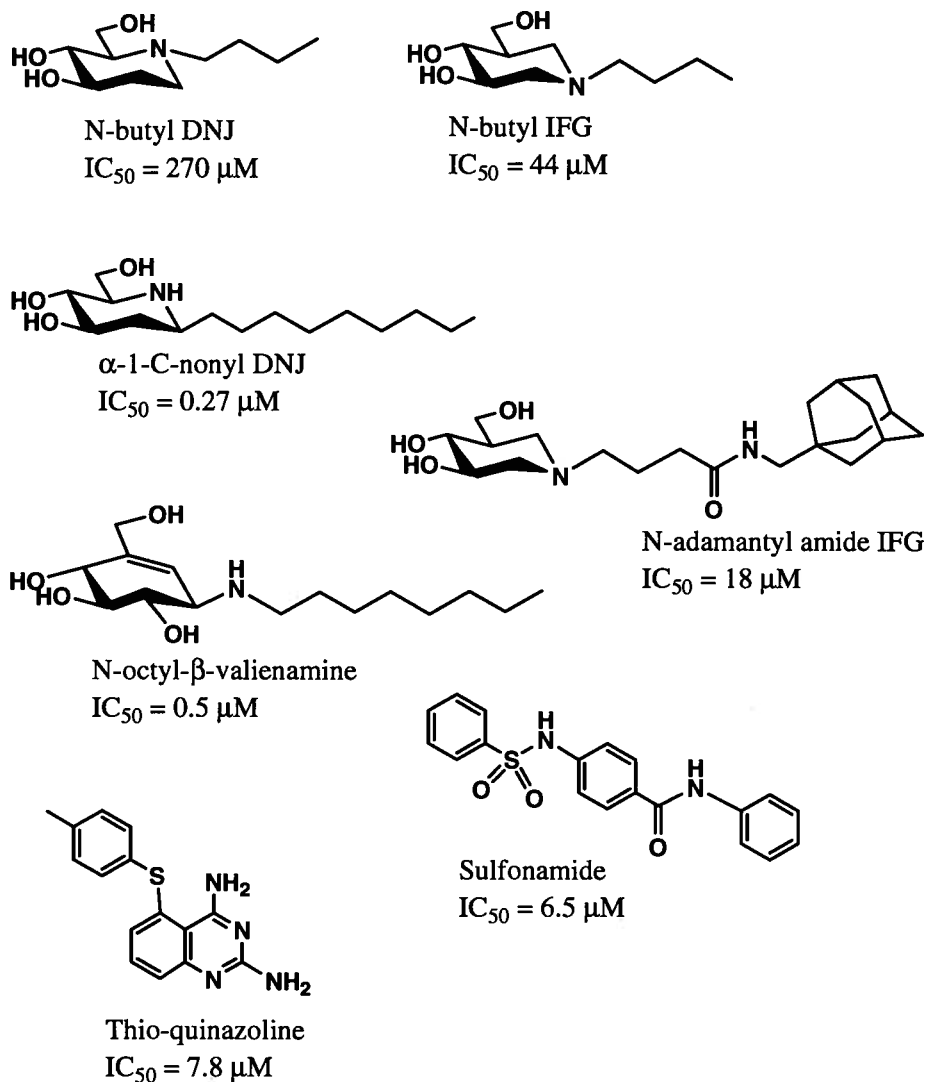


Figure 2.17 Diagram of several inhibitors of GCase and their IC_{50} values. Sulfonamide value obtained from Zheng *et. al.*,⁷⁶ thio-quinazoline value obtained from Tropak *et. al.*,⁷⁴ and all other values obtained from Butters.⁷²

2.3 Conclusions

In summary, I was successful in synthesizing five IFG derivatives in addition to IFG. Four of these derivatives were novel compounds (2.17, 2.18, 2.23 and 2.32). All the synthesized compounds were evaluated for their inhibitory ability towards

human GCase by measuring their K_i values, which are summarized in Table 2.1 below. Some compounds have been sent, with the remainder to be sent shortly, to our collaborators Dr. Don Mahuran and Dr. Mike Tropak (Hospital for Sick Children, Toronto) in order to test their ability to behave as PCs in Gaucher cell lines.

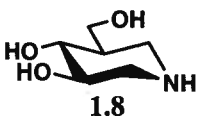
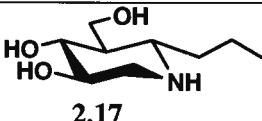
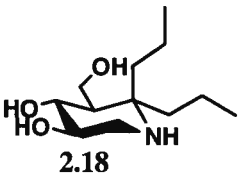
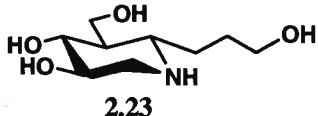
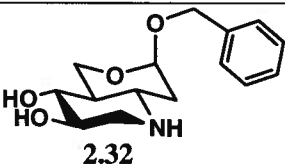
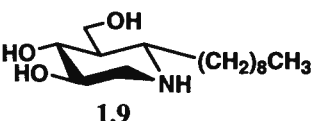
Inhibitor	K_i
 1.8	23 nM \pm 2
 2.17	610 nM \pm 75
 2.18	610 nM \pm 100
 2.23	104 nM \pm 19
 2.32	160 nM \pm 6
 1.9	0.2 nM \pm 0.01

Table 2.1 Summary of inhibitors synthesized and measured K_i values towards GCase.

3 Materials and Methods

3.1 Synthesis

3.1.1 General materials and methods

All reagents were purchased from commercial suppliers (Sigma, Aldrich, Fluka, Alfa Aesar and Reike Metals) and were used without further purification, unless otherwise stated. Solvents used were either reagent, certified or spectral grade. Anhydrous/dry solvents were prepared as follows: CH_2Cl_2 and pyridine were distilled over CaH_2 ; THF and diethyl ether were distilled over sodium and benzophenone; methanol was distilled over magnesium and iodine; DMF was dried over 4 Å molecular sieves for 2 days prior to use. Deionized water, purified with a Millipore Direct-Q™ 5 Ultrapure Water system, was used for all aqueous solutions. Melting points were determined using a Laboratory Devices Mel-Temp II melting point apparatus and are uncorrected.

Thin layer chromatography (TLC) was used to follow all reactions. TLC separations were performed using Merck Kieselgel silica gel 60 F₂₅₄ aluminum-backed analytical plates. Compounds were detected using ultra violet light (where applicable) and/or stained with 10 % ammonium molybdate in 2 M H_2SO_4 (polyhydroxylated compounds), silica gel impregnated with iodine (general use), or 0.3 % ninhydrin and 3% acetic acid in ethanol (amines). All flash column chromatography was performed under elevated pressure on Sili-Cycle silica gel, 230-400 mesh. All reverse phase (RP) column chromatography was performed under elevated pressure using 2 g Waters Sep-Pak C-18 RP cartridges.

All ^1H nuclear magnetic resonance (NMR) spectra were either recorded on a Bruker AV-400 (400 MHz) or a Bruker WH-400 (400 MHz) spectrometer and chemical shifts are given in parts per million (ppm) as referenced from tetramethylsilane (TMS). Samples were referenced internally to CD_3OD at 3.31 ppm, CDCl_3 at 7.27 ppm, D_2O at

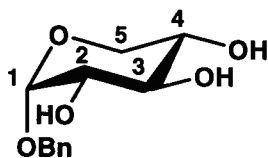
4.78 ppm and acetone-d₆ at 2.05 ppm. Abbreviations describing the multiplicity of signals are: s-singlet, bs-broad singlet, d-doublet, t-triplet and m-multiplet. All ¹³C NMR spectra are proton decoupled and were recorded on either a Bruker AV-400 (100 MHz) or a Bruker WH-400 (100 MHz) spectrometer. Samples were referenced internally to CD₃OD at 49.15 ppm, CDCl₃ at 77.16 ppm, acetone-d₆ at 29.8 ppm, and when D₂O was used, CD₃OD was added as an external reference. Low resolution mass spectra (LRMS) were acquired on an electrospray ionization (ESI) Waters liquid chromatography – mass spectrometer (LC-MS) and high resolution mass spectra (HRMS) were acquired on an ESI Micromass LCT spectrometer by the mass spectrometry laboratory at the University of British Columbia. In cases where the desired compound has already been reported, all analytical data were identical to that already reported and referenced as such.

3.1.2 Generous Gifts

Dr. Hong-Ming Chen in the Withers laboratory synthesized 2,4-dinitrophenyl β-D-glucopyranoside.

3.1.3 (3R, 4R, 5R)-5-(Hydroxymethyl)piperidine-3,4-diol [Isfagomine• HCl salt] (1.8)

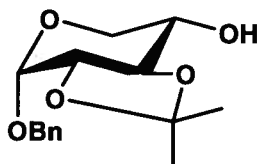
Benzyl α-L-xylopyranoside (2.2)³⁸



Boron trifluoride etherate (1.5 mL, 11.8 mmol) was added to a suspension of L-xylose (2.1) (17.9 g, 119 mmol) in benzyl alcohol (90 mL). The reaction mixture was stirred at 105 °C for 3 hours and at room temperature for 16 hours. All contents of the reaction flask were poured into an Erlenmeyer flask of cold diethyl ether (1.5 L) where a white precipitate formed immediately. Crystallization at 0 °C took 72 hours to complete. Crystals were harvested by suction filtration and re-crystallized from hot ethanol to yield

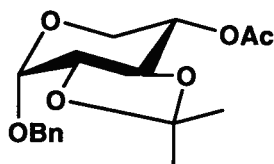
2.2 as white prisms (11.3 g, 47 mmol, 39%). ^1H NMR (acetone – d_6) δ 7.28-7.43 (m, 5 H, (Ph)), 4.83 (d, $J_{1,2} = 3.6$ Hz, 1 H, H(1)), 4.75 (d, $J_{\text{PhCH}_2} = 12.1$ Hz, 1 H, (PhCH₂)), 4.50 (d, $J_{\text{PhCH}_2} = 12.1$ Hz, 1 H, (PhCH₂)), 4.05 (dd, $J_{5_{\text{ax}},5_{\text{eq}}} = 12.6$ Hz, $J_{5_{\text{eq}},4} = 3.4$ Hz, 1 H, H(5eq)), 3.48-3.66 (m, 3 H, H(3), H(5ax), H(4)), 3.39 (m, 1 H, H(2)). ^{13}C NMR (acetone – d_6) δ 128.8, 129.0, 129.6, 99.9 (C(1)), 75.9, 74.1, 71.8, 70.2, 63.7. ESI MS m/z 263.2 [M + Na]⁺. Calculated for C₁₂H₁₆NaO₅ 263.1.

Benzyl 2,3-O-isopropylidene- α -L-xylopyranoside (2.3)³⁸



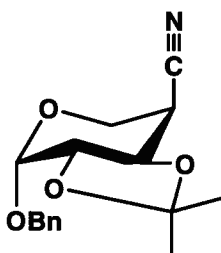
A solution of *p*-toluenesulfonic acid monohydrate (210 mg, 1.22 mmol) and THF (3 mL) was added by syringe to a solution of the benzyl xyloside (**2.2**) (10.5 g, 43.7 mmol) and 2-methoxypropene (10.5 mL, 110 mmol) in anhydrous THF (100 mL) at 0 °C. The reaction mixture was quenched with triethylamine (0.7 mL) after 1.5 hours, then diluted with EtOAc (280 mL) and washed with ice water (2 x 200 mL) and saturated aqueous NaCl (200 mL). The organic portion was dried over anhydrous MgSO₄, filtered and concentrated *in vacuo*. The residue was purified by flash column chromatography on silica gel (3.5:1 hexanes : EtOAc with 0.1% Et₃N) to yield **2.3** as a clear syrup (5.99 g, 21.4 mmol, 49%). ^1H NMR (CD₃OD) δ 7.27-7.39 (m, 5 H, (Ph)), 5.16 (d, $J_{1,2} = 3.0$ Hz, 1 H, H(1)), 4.78 (d, $J_{\text{PhCH}_2} = 12.0$ Hz, 1 H, (PhCH₂)), 4.60 (d, $J_{\text{PhCH}_2} = 12.0$ Hz, 1 H, (PhCH₂)), 3.94 (dd, $J_{3,2} = J_{3,4} = 9.5$ Hz, 1 H, H(3)), 3.86 (ddd, $J_{4,3} = J_{4,5_{\text{ax}}} = 9.5$ Hz, $J_{4,5_{\text{eq}}} = 5.2$ Hz, 1 H, H(4)), 3.58 (dd, $J_{5_{\text{eq}},5_{\text{ax}}} = 11.2$ Hz, $J_{5_{\text{eq}},4} = 5.2$ Hz, 1 H, H(5eq)), 3.36 (dd, $J_{2,3} = 9.5$ Hz, $J_{2,1} = 3.0$ Hz, 1 H, H(2)), 3.31 (masked by MeOD, H(5ax)), 1.33 (s, 3 H, (CH₃)), 1.32 (s, 3 H, (CH₃)). ^{13}C NMR (CD₃OD) δ 129.5, 128.9, 111.6, 97.6 (C(1)), 81.7, 78.4 (C(3)), 77.4 (C(2)), 71.1 (C(4)), 70.7, 64.4 (C(5)), 27.3, 26.9. ESI MS m/z 303.3 [M + Na]⁺. Calculated for C₁₅H₂₀NaO₅ 303.1.

Benzyl 4-O-acetyl-2,3-O-isopropylidene- α -L-xylopyranoside (2.8)



Acetic anhydride (3 mL) was added by syringe to a solution of the alcohol (**2.3**) (40 mg, 0.14 mmol) and pyridine (3 mL) at 0 °C. The reaction mixture was quenched with cold water (8 mL) after 6 hours, extracted with CH₂Cl₂ (2 x 20 mL) and washed with saturated aqueous NaHCO₃ (2 x 15 mL), water (20 mL) and saturated aqueous NaCl (20 mL). The organic portion was dried over anhydrous MgSO₄, filtered and concentrated *in vacuo* to yield **2.8** as a clear syrup. ¹H NMR (CDCl₃) δ 7.37-7.38 (m, 5 H, (Ph)), 5.24 (d, $J_{1,2} = 3.1$ Hz, 1 H, H(1)), 5.06 (ddd, $J_{4,3} = J_{4,5ax} = 9.6$ Hz, $J_{4,5eq} = 5.5$ Hz, 1 H, H(4)), 4.80 (d, $J_{PhCH_2} = 12.1$ Hz, 1 H, (PhCH₂)), 4.65 (d, $J_{PhCH_2} = 12.1$ Hz, 1 H, (PhCH₂)), 4.19 (t, $J_{3,2} = J_{3,4} = 9.6$ Hz, 1 H, H(3)), 3.92 (dd, $J_{5eq,5ax} = 10.8$ Hz, $J_{5eq,4} = 5.5$ Hz, 1 H, H(5eq)), 3.56 (dd, $J_{2,3} = 9.6$ Hz, $J_{2,1} = 3.1$ Hz, 1 H, H(2)), 3.34 (dd, $J_{5ax,5eq} = 10.8$ Hz, $J_{5ax,4} = 9.6$ Hz, 1 H, H(5ax)), 2.09 (s, 3 H), 1.50 (s, 3 H, (CH₃)), 1.47 (s, 3 H, (CH₃)).

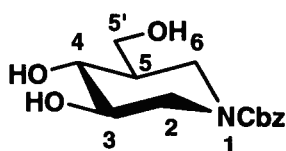
Benzyl 4-cyano-4-deoxy-2,3-O-isopropylidene- β -D-arabinopyranoside (2.9)³⁸



Tf₂O (1.3 mL, 7.7 mmol) was added dropwise by syringe to a solution of the alcohol (**2.3**) (1.44 g, 5.14 mmol) and dry pyridine (2 mL) in anhydrous CH₂Cl₂ (20 mL) at -78 °C under an inert atmosphere. The reaction mixture was warmed to 0 °C after addition was complete and stirred for an additional 2 hours. Upon warming, a dark red color persisted. The reaction mixture was then diluted with EtOAc (140 mL), washed with ice water (2 x 120 mL), saturated aqueous NaCl (1 x 120 mL) and re-extracted with EtOAc (100 mL). The organic layer was dried over anhydrous MgSO₄, filtered and concentrated *in vacuo* to yield a dark red syrup that was used immediately without further

purification. The mixture of the crude triflate, KCN (3.3 g, 50.8 mmol), 18-crown-6 (1.5 g) and 3 Å MS (3 g) in dry DMF (110 mL) was stirred at room temperature for 16 hours. The reaction mixture was diluted with EtOAc (160 mL), washed with water (2 x 160 mL), saturated aqueous NaCl (1 x 160 mL) and re-extracted with EtOAc (100 mL). The organic portions were dried over anhydrous MgSO₄, filtered and concentrated *in vacuo*. The resulting residue was purified by flash column chromatography on silica gel (CH₂Cl₂ with 0.1 % Et₃N) to yield **2.9** as a pale yellow syrup (1.18 g, 4.08 mmol, 80%). ¹H NMR (CDCl₃) δ 7.31-7.37 (m, 5 H, (Ph)), 5.37 (d, *J*_{1,2} = 2.7 Hz, 1 H, H(1)), 4.78 (d, *J*_{PhCH₂} = 12.0 Hz, 1 H, (PhCH₂)), 4.68 (d, *J*_{PhCH₂} = 12.0 Hz, 1 H, (PhCH₂)), 4.13 (dd, *J*_{3,2} = 9.6 Hz, *J*_{3,4} = 4.7 Hz, 1 H, H(3)), 3.89-3.96 (m, 2 H, H(2), H(5a)), 3.79 (dd, *J*_{5b,5a} = 12.1 Hz, *J*_{5b,4} = 2.6 Hz, 1 H, H(5b)), 3.28-3.35 (m, 1 H, H(4)), 1.51 (s, 3 H, (CH₃)), 1.50 (s, 3 H, (CH₃)). ¹³C NMR (CDCl₃) δ 136.8, 128.3, 127.8, 127.5, 116.9 (C(CN)), 110.8, 97.5 (C(1)), 74.4 (C(2)), 70.0, 69.3 (C(3)), 59.1 (C(5)), 34.0 (C(4)), 26.5, 26.4. ESI MS *m/z* 312.2 [M + Na]⁺. Calculated for C₁₆H₁₉NNaO₄ 312.1.

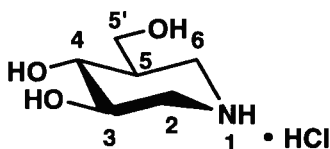
(3R, 4R, 5R)-N-Benzoyloxycarbonyl-5-(hydroxymethyl)piperidine-3,4-diol (2.15)



Pd(OH)₂/C (20% , 60 mg) was added to a solution of the nitrile (**2.9**) (150 mg, 0.52 mmol) and glacial acetic acid (8 μL) in dry methanol (6 mL) and the mixture was hydrogenated in a high pressure reactor at 50 psi for 72 hours. The catalyst was removed by suction filtration through Celite then the filter cake was washed with methanol (30 mL) and acetone (30 mL). The filtrates were concentrated *in vacuo*, dissolved in 1 M HCl (20 mL) and stirred for 12 hours. The solution was concentrated *in vacuo* and partially purified by ion exchange chromatography (Amberlite CG-50 type I, NH₄⁺ form) using aqueous 0.35 M NH₄OH as an eluent after the water wash. The fractions containing the desired product were concentrated *in vacuo* to yield impure isofagomine (**1.8**) as a pale yellow crystalline solid (68 mg, 0.46 mmol, 89%). Benzyl chloroformate (0.12 mL, 0.84 mmol) was then added to a solution of isofagomine (**1.8**) (90 mg, 0.61

mmol) and NaHCO₃ (156 mg, 1.86 mmol) in H₂O/MeOH/THF (2:1:1, 10 mL) and the mixture was stirred at room temperature for 20 hours. The reaction was quenched by adding 1 M HCl (1 mL), concentrated *in vacuo*, co-evaporating with toluene. The residue was then purified by flash column chromatography on silica gel (petroleum ether:EtOAc 1:1 then MeOH:CHCl₃ 1:9) to yield (**2.15**) as a clear oil (59 mg, 0.21 mmol, 35%). ¹H NMR (MeOD) δ 7.28-7.39 (m, 5 H, (Ph)), 5.12 (s, 2 H, (COOCH₂Ph)), 4.13-4.31 (m, 2 H, H(6a), H(2a)), 3.82 (dd, *J* = 10.9 Hz, *J* = 3.5 Hz, 1 H, H(5'a)), 3.46-3.64 (m, 1 H, H(5'b)), 3.32-3.38 (m, 1 H, H(3)), 3.25 (dd, *J* = 11.0 Hz, *J* = 9.0 Hz, 1 H, H(4)), 2.50-2.79 (m, 2 H, H(6b), H(2b)), 1.55-1.67 (m, 1 H, H(5)). ¹³C NMR (MeOD) δ 157.2, 138.4, 129.9, 129.5, 129.2, 75.9, 72.9, 68.8, 62.3, 49.8, 46.9, 46.2, 46.0. HRMS (ESI) *m/z* 304.1167 [M + Na]⁺. Calculated for C₁₄H₁₉NNaO₅ 304.1161.

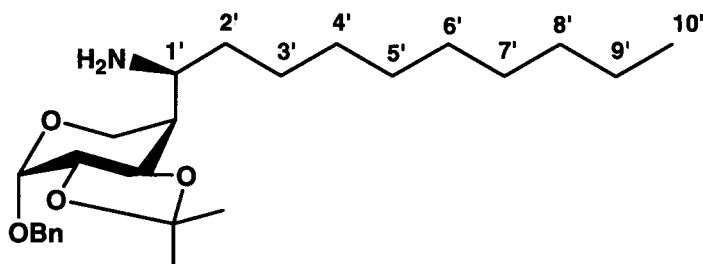
(3R, 4R, 5R)-5-(Hydroxymethyl)piperidine-3,4-diol [Isfagomine•HCl salt] (1.8)



Pd/C (10%, 10 mg) was added to a solution of IFG-Cbz (**2.15**) (28 mg, 0.10 mmol) and glacial acetic acid (8 μL) in dry methanol (6 mL) and the mixture was hydrogenated at atmospheric pressure for 10 hours. The catalyst was removed by suction filtration through Celite then the filter cake was washed with methanol (30 mL) and water (30 mL). The filtrates were concentrated *in vacuo*, dissolved in 1 M HCl (5 mL) and stirred for 12 hours. The solution was concentrated *in vacuo* and then lyophilized from water (2 mL) to yield **1.8** as a pale yellow solid (13 mg, 0.46 mmol, 89%). Analytical data matches that reported in Zhu *et. al.*³⁸ ¹H NMR (D₂O) δ 3.85 (dd, *J*_{5'a, 5'b} = 11.7 Hz, *J*_{5'a, 5} = 3.5 Hz, 1 H, H(5'a)), 3.73-3.82 (m, 2 H, H(5'b), H(3)), 3.50-3.59 (m, 3 H, H(2eq), H(4), H(6eq)), 2.85-3.04 (m, 2 H, H(6ax), H(2ax)), 1.92-2.04 (m, 1 H, H(5)). ¹³C NMR (MeOD) δ 72.3 (C(4)), 69.7 (C(3)), 60.1 (C(5')), 47.8, 46.0 (C(2), C(6)), 42.3 (C(5)). HRMS (ESI) *m/z* 148.0972 [M + H]⁺. Calculated for C₆H₁₄NO₃ 148.0974.

3.1.4 (3R, 4R, 5R, 6S)-6-*n*-Nonyl-5-(hydroxymethyl)piperidine-3,4-diol [C6-*n*-Nonyl IFG•HCl salt] (1.9)

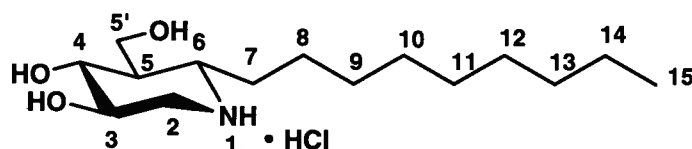
Benzyl 4-[(S)-1'-aminodecyl]-4-deoxy-2,3-O-isopropylidene-β-D-arabinopyranoside (2.16)³⁸



n-C₉H₁₉MgBr (3.4 mL of 1.0 M solution in diethyl ether) was added dropwise by syringe to a solution of the nitrile (2.9) (260 mg, 0.9 mmol) in dry diethyl ether (35 mL) at -78°C under an inert atmosphere and then slowly warmed to room temperature and stirred for 4 hours. The reaction mixture was heated at 35°C for 1.5 hours then cooled to room temperature before NaBH₄ (200 mg, 5.3 mmol) was added in one portion. The reaction mixture was then cooled to 0°C and dry methanol (13 mL) was added by syringe for 5 minutes, then allowed to warm to room temperature and stirred overnight. Water (20 mL) and diethyl ether (20 mL) were added to the reaction mixture and the solids removed by suction filtration then washed with diethyl ether (15 mL). The filtrate was washed with water (2 x 20 mL), saturated aqueous NaCl (20 mL) and re-extracted from the aqueous portion with diethyl ether (20 mL). The organic portions were dried over anhydrous MgSO₄, filtered and concentrated *in vacuo*. The resulting residue was purified by flash column chromatography on silica gel (20:1 CH₂Cl₂: MeOH with 0.1% Et₃N) to yield 2.16 as a pale yellow syrup (163 mg, 0.39 mmol, 43%). ¹H NMR (CDCl₃) δ 7.19-7.29 (m, 5 H, (Ph)), 5.17 (d, *J*_{1,2} = 2.8 Hz, 1 H, H(1)), 4.68 (d, *J*_{PhCH₂} = 12.2 Hz, 1 H, (PhCH₂)), 4.54 (d, *J*_{PhCH₂} = 12.2 Hz, 1 H, (PhCH₂)), 4.25 (dd, *J*_{3,2} = 9.9 Hz, *J*_{3,4} = 4.6 Hz, 1 H, H(3)), 3.79 (dd, *J*_{2,3} = 9.9 Hz, *J*_{2,1} = 2.8 Hz, 1 H, H(2)), 3.57-3.67 (m, 2 H, H(5a), H(5b)), 3.13-3.22 (m, 1 H, H(1')), 2.25-2.45 (bs, 2 H, (NH₂)), 1.95-2.05 (m, 1 H, H(4)), 1.54-1.57 (m, 1 H, H(2'a)), 1.39 (s, 6 H, (2 x CH₃)), 1.10-1.27 (m, 15 H, H(2'b-9')), 0.81 (t, *J*_{10',9'a} = *J*_{10',9'b} = 6.3 Hz, 3 H, H(10')). ¹³C NMR (CDCl₃) δ 137.2, 128.0, 127.3, 127.2,

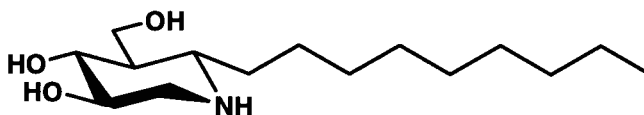
108.8, 97.2 (C(1)), 74.0 (C(3)), 72.4 (C(2)), 69.2, 59.5 (C(5)), 47.9 (C(1')), 46.7 (C(4)), 34.7, 31.6, 29.5, 29.3, 29.2, 29.0, 26.7, 26.0, 25.0, 22.3, 13.8 (C(10')). ESI MS m/z 420.3 [M + H]⁺. Calculated for C₂₅H₄₂NO₄ 420.3.

(3R, 4R, 5R, 6S)-6-*n*-Nonyl-5-(hydroxymethyl)piperidine-3,4-diol [C6-*n*-Nonyl IFG•HCl salt] (1.9•HCl)³⁸



Pd(OH)₂/C (20%, 80 mg) was added to a solution of amine (**2.16**) (160 mg, 0.38 mmol) and glacial acetic acid (8 μL) in dry methanol (20 mL) and the mixture was hydrogenated in a high pressure reactor at 50 psi for 20 hours. The catalyst was removed by suction filtration through Celite and the filter cake washed with methanol (30 mL). The filtrate was concentrated *in vacuo*, dissolved in 1 M HCl (25 mL), and stirred at room temperature for 12 hours. The solution was then concentrated *in vacuo* and purified by column chromatography using C-18 RP silica gel, eluted with 30 % methanol in water for the HCl salt product and 60 % methanol in water for the neutral product. Each set of fractions was then lyophilized from water (15 mL) to yield a white foam of **1.9•HCl** (40 mg, 0.15 mmol) and **1.9** (35 mg, 0.13 mmol) with a combined yield of 72 %. ¹H NMR (CD₃OD) δ 4.02 (dd, $J_{5'a,5'b} = 11.4$ Hz, $J_{5'a,5} = 2.4$ Hz, 1 H, H(5'a)), 3.64-3.70 (m, 2 H, H(5'b), H(3)), 3.54 (t, $J_{4,3} = J_{4,5} = 9.6$ Hz, 1 H, H(4)), 3.35 (dd, $J_{2eq,2ax} = 12.2$ Hz, $J_{2eq,3} = 4.9$ Hz, 1 H, H(2eq)), 3.25 (ddd, $J = 11.0$ Hz, $J = 7.6$ Hz, $J = 3.4$ Hz, 1 H, H(6)), 2.79 (t, $J_{2ax,2eq} = J_{2ax,3} = 12.2$ Hz, 1 H, H(2ax)), 1.88-1.98 (m, 1 H, H(7a)), 1.59-1.70 (m, 1 H, H(7b)), 1.20-1.59 (m, 15 H, H(5), H(8a/b), H(9-14)), 0.90 (t, $J_{15,14a} = J_{15,14b} = 6.9$ Hz, 3 H, H(15)). ¹³C NMR (CD₃OD) δ 72.2 (C(4)), 70.3 (C(3)), 58.2 (C(6)), 57.5 (C(2)), 48.1 (C(5')), 47.1 (C(5)), 33.2, 31.4, 30.8, 30.7, 30.6, 30.5, 25.8, 23.9, 14.6 (C(15)). HRMS (ESI) m/z 274.2389 [M + H]⁺. Calculated for C₁₅H₃₂NO₃ 274.2382.

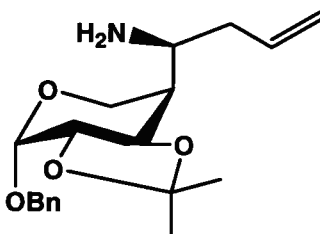
**(3R, 4R, 5S, 6S)-6-*n*-Nonyl-5-(hydroxymethyl)piperidine-3,4-diol [C6-*n*-Nonyl IFG]
(1.9)**



$^1\text{H NMR}$ (CD_3OD) δ 3.93 (dd, $J_{5'a,5} = 2.7$ Hz, $J_{5'a,5'b} = 11.2$ Hz, 1H, H(5'a)), 3.69 (dd, $J_{5'b,5'a} = 11.2$ Hz, $J_{5'b,5} = 3.3$ Hz 1H, H(5'b)), 3.36-3.46 (m, 2 H, H(4), H(3)), 3.09 (dd, $J_{2\text{eq},2\text{ax}} = 11.3$ Hz, $J_{2\text{eq},3} = 4.0$ Hz 1 H, H(2eq)), 2.56-2.64 (m, 1 H, H(6)), 2.40 (t, $J_{2\text{ax},2\text{eq}} = J_{2\text{ax},3} = 11.3$ Hz, 1 H, H(2ax)), 1.69-1.8 (m, 1 H, H(7)), 1.10-1.52 (m, 16 H, H(5), H(7), H(8-14)), 0.90 (t, $J_{15,14a} = J_{15,14b} = 6.8$ Hz, 3 H, H(15)). $^{13}\text{C NMR}$ (CD_3OD) δ 75.2 (C(4)), 74.0 (C(3)), 59.4 (C(5')), 57.1 (C(6)), 51.5 (C(2)), 50.3 (C(5)), 34.1, 33.4, 31.5, 31.0, 30.8, 30.6, 26.7, 24.1, 14.8 (C(15)).

3.1.5 (3R, 4R, 5R, 6S)-6-*n*-Propyl-5-(hydroxymethyl)piperidine-3,4-diol [C6-*n*-Propyl IFG•HCl salt] (2.17)

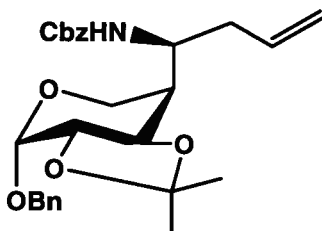
Benzyl 4-[(S)-1'-amino-3'-butenyl]-4-deoxy-2,3-O-isopropylidene- β -D-arabinopyranoside (2.19)



Allyl magnesium chloride (0.63 mL of 2.0 M solution in THF) was added dropwise by syringe to a solution of the nitrile (**2.9**) (221 mg, 0.76 mmol) in dry diethyl ether (15 mL) at 0°C under an inert atmosphere and then slowly warmed to room temperature and stirred for 3 hours. The reaction mixture was cooled to 0°C, NaBH_4 (140 mg, 3.6 mmol) was added in one portion and then dry methanol (4 mL) was added by syringe over 5 minutes. The reaction mixture was warmed to room temperature after the addition was complete and allowed to stir overnight. Water (8 mL) and diethyl ether (8 mL) were added to the reaction mixture, and then the solids were removed by suction

filtration and washed with diethyl ether (10 mL). The filtrate was washed with saturated aqueous NaHCO₃ (15 mL) then extracted with diethyl ether (2 x 20 mL) and EtOAc (20 mL). The organic portions were dried over anhydrous MgSO₄, filtered and concentrated *in vacuo*. The residue was purified by flash column chromatography on silica gel (gradient of 5% to 8% to 10% EtOAc in CH₂Cl₂ with constant 0.1% Et₃N) to yield **2.19** as a pale yellow oil (193 mg, 0.58 mmol, 72 %). ¹H NMR (CDCl₃) δ 7.28-7.39 (m, 5 H, (Ph)), 5.78-5.91 (m, 1 H, H(3')), 5.26 (d, *J*_{1,2} = 3.1 Hz, 1 H, H(1)), 5.07-5.20 (m, 2 H, H(4' a/b)), 4.76 (d, *J*_{PhCH₂} = 12.1 Hz, 1 H, (PhCH₂)), 4.62 (d, *J*_{PhCH₂} = 12.1 Hz, 1 H, H(PhCH₂)), 4.33 (dd, *J*_{3,2} = 9.9 Hz, *J*_{3,4} = 4.8 Hz, 1 H, H(3)), 3.88 (d, *J*_{2,3} = 9.9 Hz, *J*_{2,1} = 3.1 Hz, 1 H, H(2)), 3.76 (dd, *J*_{5a,5b} = 12.4 Hz, *J*_{5a,4} = 1.0 Hz, 1 H, H(5a)), 3.69 (dd, *J*_{5b,5a} = 12.4 Hz, *J*_{5b,4} = 3.0 Hz, 1 H, H(5b)), 3.35 (ddd, *J*_{1',2'a} = *J*_{1',2'b} = 9.1 Hz, *J*_{1',4} = 3.0 Hz, 1 H, H(1')), 2.44-2.53 (m, 1 H, H(2' a)), 1.84-2.16 (m, 4 H, H(2' b), H(4), (NH₂)), 1.47 (s, 6 H, (2 x CH₃)). ¹³C NMR (CDCl₃) δ 137.4, 134.7 (C3'), 128.3, 127.6, 127.4, 118.0 (C(4')), 109.0, 97.5 (C(1)), 74.1 (C(3)), 72.7 (C(2)), 69.4 (C(PhCH₂)), 59.7 (C(5)), 47.4 (C(1')), 46.5 (C(4)), 39.5 (C(2')), 26.8 (C(CH₃)), 26.3 (C(CH₃)). HRMS (ESI) *m/z* 334.2014 [M + H]⁺. Calculated for C₁₉H₂₈NO₄ 334.2018.

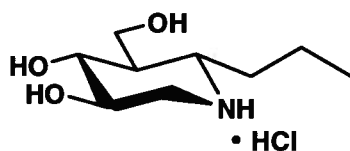
Benzyl 4-[[*(S)*-1'-N-Benzylloxycarbonyl]-3'-butenyl]-4-deoxy-2,3-O-isopropylidene-β-D-arabinopyranoside (2.20)



Benzyl chloroformate (121 μL, 0.86 mmol) was added to a solution of the amino olefin (**2.19**) (150 mg, 0.45 mmol) in pyridine (2.5 mL), CH₂Cl₂ (2.5 mL) and DMAP (6 mg, 45 μmol) at room temperature and allowed to stir for 60 hours. The reaction mixture was concentrated *in vacuo*, dissolved in CH₂Cl₂ (20 mL), washed with water (20 mL), and re-extracted with CH₂Cl₂ (2 x 20 mL). The organic portions were combined and washed with saturated aqueous NaCl (20 mL), dried over anhydrous MgSO₄ and concentrated *in vacuo*. The residue was purified by flash column chromatography on

silica gel (20:1 CH₂Cl₂:EtOAc with 0.1% Et₃N) to yield **2.20** as a white crystalline solid (m.p. 115-117°C) (134 mg, 0.28 mmol, 64%). ¹H NMR (CDCl₃) δ 7.27-7.40 (m, 5 H, (Ph)), 5.72-5.87 (m, 1 H, H(3')), 5.45-5.59 (bs, 1 H, (NH)), 5.26 (d, *J*_{1,2} = 2.9 Hz, 1 H, H(1)), 5.03-5.17 (m, 4 H, H(4'a), H(4'b), (COOCH₂Ph)), 4.76 (d, *J*_{PhCH₂} = 12.1 Hz, 1 H, (PhCH₂)), 4.63 (d, *J*_{PhCH₂} = 12.1 Hz, 1 H, (PhCH₂)), 4.27 (dd, *J*_{3,2} = 10.0 Hz, *J*_{3,4} = 4.3 Hz, 1 H, H(3)), 4.11-4.23 (m, 1 H, H(1')), 3.88 (dd, *J*_{2,3} = 10.0 Hz, *J*_{2,1} = 2.9 Hz, 1 H, H(2)), 3.71 (dd, *J*_{5a,5b} = 12.3 Hz, *J*_{5a,4} = 2.7 Hz, 1 H, H(5a)), 3.63 (d, *J*_{5b,5a} = 12.3 Hz, 1 H, H(5b)), 2.61-2.70 (m, 1 H, H(2'a)), 2.19-2.36 (m, 2 H, H(4), H(2'b)), 1.42 (s, 3 H, (CH₃)), 1.32 (s, 3 H, (CH₃)). ¹³C NMR (CDCl₃) δ 133.5 (C(3')), 128.6, 128.5, 128.2, 128.1, 127.8, 127.6, 118.6 (C(4')), 114.6, 109.7, 97.9 (C(1)), 74.1 (C(3)), 72.6 C(2)), 69.8, 66.6, 60.4 (C(5)), 47.8 (C(1')), 42.0 (C(4)), 36.1 (C(2')), 26.7 (C(CH₃)), 26.5 (C(CH₃)). HRMS (ESI) *m/z* 490.2205 [M + Na]⁺. Calculated for C₂₇H₃₃NNaO₆ 490.2206

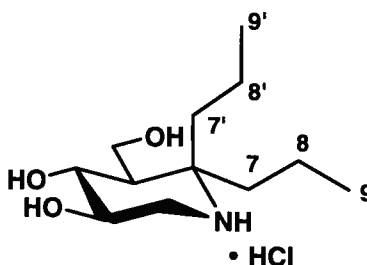
(3R, 4R, 5R, 6S)-6-*n*-Propyl-5-(hydroxymethyl)piperidine-3,4-diol [C6-*n*-Propyl IFG•HCl salt] (2.17)



Pd/C (10%, 20 mg) was added to a solution of the terminal olefin (**2.20**) (50 mg, 0.15 mmol) and glacial acetic acid (8 μL) in dry methanol (3 mL) and the mixture was hydrogenated at atmospheric pressure for 16 hours. The catalyst was removed by suction filtration through Celite and the filter cake washed with methanol (30 mL). The filtrate was concentrated *in vacuo*, dissolved in 1 M HCl (8 mL), and stirred at room temperature for 12 hours. The solution was concentrated *in vacuo* and then lyophilized from water (2 mL) to yield **2.17**•HCl as a pale yellow foam (26 mg, 0.12 mmol, 80%). ¹H NMR (D₂O) δ 3.98 (dd, *J*_{5'a,5'b} = 12.3 Hz, *J*_{5'a,5} = 2.3 Hz, 1 H, H(5'a)), 3.70-3.80 (m, 2H, H(5'b), H(3)), 3.59 (t, *J*_{4,5} = *J*_{4,3} = 10.0 Hz, 1 H, H(4)), 3.46 (dd, *J*_{2eq,2ax} = 12.0 Hz, *J*_{2eq,3} = 5.1 Hz, 1 H, H(2eq)), 3.27 (ddd, *J* = 11.3 Hz, *J* = 8.0 Hz, *J*_{6,7a} = 3.3 Hz, 1 H, H(6)), 2.86 (t, *J*_{2ax,3} = *J*_{2ax,2eq} = 12.0 Hz, 1 H, H(2eq)), 1.89 (dddd, *J*_{7a,7b} = 15.5 Hz, *J*_{7a,8a} = 10.7 Hz, *J*_{7a,}

$J_{7a,6} = 3.3$ Hz, 1 H, H(7a)), 1.58-1.69 (m, 2 H, H(7b), H(5)), 1.28-1.51 (m, 2 H, H(8a/b)), 0.93 (t, $J_{9,8a} = J_{9,8b} = 7.4$ Hz, 3 H, H(9)). ^{13}C NMR (D_2O) 71.5 (C(4)), 69.5 (C(3)), 57.4 (C(6)), 57.1 (C(5')), 47.1 (C(2)), 46.0 (C(5)), 32.6 (C(7)), 18.3 (C(8)), 14.1 (C(9)). HRMS (ESI) m/z 190.1441 $[\text{M} + \text{H}]^+$. Calculated for $\text{C}_9\text{H}_{20}\text{NO}_3$ 190.1443.

3.1.6 (3R, 4R, 5R)-6,6-Di-*n*-propyl-5-(hydroxymethyl)piperidine-3,4-diol [C6,6-Di-*n*-propyl IFG•HCl salt] (2.18)

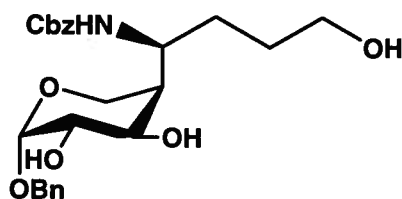


During the preparation of Cbz-protected terminal olefin (**2.20**), an additional product was accessed in the purification. After the desired single addition product (**2.19**) was eluted in 20:1 CH_2Cl_2 : EtOAc, the polarity of the eluent was increased to neat EtOAc, then the unprotected di-allyl amine (**2.21**) was eluted. Without further purification, Pd/C (10%, 20 mg) was added to a solution of the di-allyl amine (**2.21**) (40 mg, 0.11 mmol) and glacial acetic acid (8 μL) in dry methanol (3 mL) and the mixture was hydrogenated at atmospheric pressure for 16 hours. The catalyst was removed by suction filtration through Celite and the filter cake washed with methanol (30 mL). The filtrate was concentrated *in vacuo*, dissolved in 1 M HCl (25 mL), and stirred at room temperature for 12 hours. The solution was then concentrated *in vacuo* and purified by column chromatography using C-18 RP silica gel, eluted with 5 % methanol in water. The fractions containing the desired product were pooled and lyophilized from water (3 mL) to yield **2.18**•HCl as a pale yellow syrup (16 mg, 0.06 mmol, 56%). ^1H NMR (D_2O) 3.8-3.95 (m, 3 H, H(4), H(5'a), H(5'b)), 3.73-3.79 (m, 1 H, H(3)), 3.36 (dd, $J_{2\text{eq},2\text{ax}} = 12.3$ Hz, $J_{2\text{eq},3} = 5.4$ Hz, 1 H, H(2eq)), 3.02 (t, $J_{2\text{ax},2\text{eq}} = J_{2\text{ax},3} = 12.3$ Hz, 1 H, H(2ax)), 1.64-1.97 (m, 5 H, H(5), H(7a/b), H(7'a/b)), 1.18-1.49 (m, 4 H, H(8a/b), H(8'a/b)), 0.95 (t, $J = 7.1$ Hz, 2 x CH_3 , H(9), H(9')). ^{13}C NMR (D_2O) 71.4 (C(4)), 69.86 (C(3)), 64.8 (C(6)), 59.5 (C(5')), 48.2 (C(5)), 43.0 (C(2)), 38.2 (C(7)), 34.0 (C(7')), 16.2 (C(8)), 16.0 (C(8')),

14.5 (C(9)), 14.4 (C(9')). HRMS (ESI) m/z 254.1738 $[M + H]^+$. Calculated for $C_{12}H_{25}NO_3$ 254.1732.

3.1.7 (3R, 4R, 5R, 6S)-6-[9-Hydroxypropyl]-5-(hydroxymethyl)piperidine-3,4-diol [C6-[9-hydroxypropyl] IFG•HCl salt] (2.23)

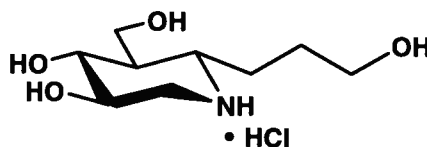
Benzyl 4-[[*(S)*-1'-N-Benzoyloxycarbonyl]-butan-4'-ol]-4-deoxy-2,3-O-isopropylidene- β -D-arabinopyranoside (2.22)



BH_3 ·THF (130 μ L of a 1.0 M solution in THF) was added to a solution of the terminal olefin (2.20) (27 mg, 57.8 μ mol) in dry THF (2.5 mL) at 0 °C under an inert atmosphere. After the addition was complete the reaction mixture was allowed to warm to room temperature and stir for 3 hours or until the starting material disappeared (by TLC). Keeping the reaction mixture at 25 °C, water (1.5 mL) was added dropwise. Once the hydrogen stopped evolving, $NaBO_3 \cdot 4H_2O$ (15 mg, 97.4 μ mol) was added in one portion and the reaction mixture stirred overnight at room temperature. The mixture was concentrated *in vacuo*, dissolved in diethyl ether (15 mL), washed with water (15 mL), re-extracted with diethyl ether (3 x 15 mL) and finally washed with saturated aqueous NaCl (15 mL). The organic portions were dried over anhydrous $MgSO_4$ and concentrated *in vacuo*. The residue was purified by flash column chromatography on silica gel (gradient of 10% to 25% to 50% EtOAc in CH_2Cl_2 with constant 0.1% Et_3N) to yield 2.22 as a clear syrup (15 mg, 31 μ mol, 54%). 1H NMR ($CDCl_3$) δ 7.27-7.41 (m, 5 H, (Ph)), 5.29 (bs, 1 H, (NH)), 5.27 (d, $J_{1,2} = 3.0$ Hz, 1 H, H(1)), 5.01-5.15 (m, 2 H, (COOCH₂Ph)), 4.76 (d, $J_{PhCH_2} = 11.8$ Hz, 1 H, (PhCH₂)), 4.64 (d, $J_{PhCH_2} = 11.8$ Hz, 1 H, (PhCH₂)), 4.27 (dd, $J_{3,2} = 10.1$ Hz, $J_{3,4} = 4.2$ Hz, 1 H, H(3)), 4.06-4.17 (m, 1 H, H(1')), 3.82-3.91 (m, 1 H, H(2)), 3.56-3.76 (m, 4 H, H(5a), H(5b), H(4'a), H(4'b)), 2.16-2.25 (m,

1 H, H(4)), 1.81-1.92 (m, 1 H, H(2'a)), 1.52-1.70 (m, 3 H, H(3'a), H(3'b), H(2'b)).
HRMS (ESI) m/z 468.2000 $[M + Na]^+$. Calculated for $C_{24}H_{31}NNaO_7$ 468.1998.

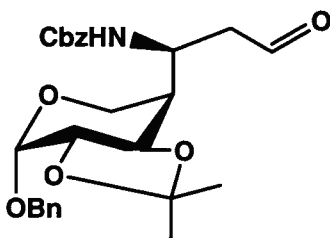
(3R, 4R, 5R, 6S)-6-[9-Hydroxypropyl]-5-(hydroxymethyl)piperidine-3,4-diol [C6-[9-hydroxypropyl] IFG · HCl salt] (2.23)



Pd/C (10%, 10 mg) was added to a solution of the terminal alcohol (**2.22**) (33 mg, 0.07 mmol) and glacial acetic acid (8 μ L) in methanol (3 mL) and the mixture was hydrogenated at atmospheric pressure for 16 hours. The catalyst was removed by suction filtration through Celite and the filter cake washed with methanol (30 mL). The filtrate was concentrated *in vacuo*, dissolved in 1 M HCl (25 mL), and stirred at room temperature for 12 hours. The solution was then concentrated *in vacuo* and purified by ion exchange chromatography (Amberlite CG-50 type I, NH_4^+ form) using aqueous 0.3 M NH_4OH as an eluent after the water wash. The fractions containing the desired product were concentrated *in vacuo*, treated with 0.01 M HCl (3 mL) and lyophilized to yield **2.23**·HCl as a pale yellow syrup (7 mg, 0.03 mmol, 43%). 1H NMR (D_2O) 4.01 (dd, $J_{5'a, 5'b} = 12.1$ Hz, $J_{5'a, 5} = 2.5$ Hz, 1 H, H(5'a)), 3.74-3.80 (m, 2 H, H(5'b), H(3)), 3.62-3.67 (m, 3 H, H(9a/b), H(4)), 3.50 (dd, $J_{2eq, 2ax} = 12.3$ Hz, $J_{2eq, 3} = 5.2$ Hz, 1 H, H(2eq)), 3.33 (ddd, $J = 11.2$ Hz, $J = 7.4$ Hz, $J = 3.7$ Hz, 1 H, H(6)), 2.89 (t, $J_{2ax, 2eq} = J_{2ax, 3} = 12.3$ Hz, 1 H, H(2ax)), 1.97-2.06 (m, 1 H, H(7a)), 1.57-1.80 (m, 4 H, H(5), H(7b), H(8a/b)). ^{13}C NMR (D_2O) δ 70.1 (C(4)), 68.5 (C(3)), 61.1 (C(9)), 56.5 (C(6)), 56.1 (C(5')), 46.2 (C(2)), 45.0 (C(5)), 26.6 (C(7)), 26.3 (C(8)). HRMS (ESI) m/z 206.1392 $[M + H]^+$. Calculated for $C_9H_{20}NO_4$ 206.1392.

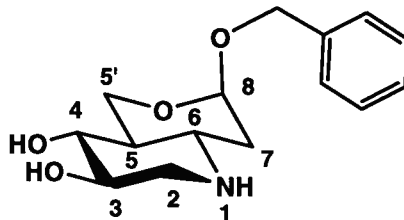
3.1.8 (3R, 4R, 5R, 6S, 8S)-8-Benzyloxy[5,6-*b*]oxacyclohexane-5-piperidine -3,4-diol [C6-Benzyl acetal IFG] (2.32)

Benzyl 4-[[*(S)*-1'-N-Benzyloxycarbonyl]-propan-3'-al]-4-deoxy-2,3-O-isopropylidene- β -D-arabinopyranoside (2.24)



Ozone was bubbled through a solution of the terminal olefin (**2.20**) (73 mg, 0.16 mmol) in CH_2Cl_2 (10 mL) at -78°C until it turned deep blue. The excess ozone was purged from the resulting solution with argon gas until the solution became clear again. Triphenylphosphine (164 mg, 0.63 mmol) was then added in one portion and the solution was allowed to warm to room temperature and stir overnight. The reaction solution was concentrated *in vacuo* and purified by flash column chromatography on silica gel (5.5:4.5 hexanes:EtOAc, 0.1% Et_3N) to yield **2.24** as a white solid (55 mg, 0.12 mmol, 75%). ^1H NMR (CDCl_3) δ 9.82 (s, 1 H, H(3')), 7.28-7.42 (m, 5 H, (Ph)), 5.76-5.96 (bs, 1 H, (NH)), 5.27 (d, $J_{1,2} = 3.1$ Hz, 1 H, H(1)), 5.08 (s, 2 H, (COOCH_2Ph)), 4.76 (d, $J_{\text{PhCH}_2} = 12.2$ Hz, 1 H, (PhCH_2)), 4.64 (d, $J_{\text{PhCH}_2} = 12.2$ Hz, 1 H, (PhCH_2)), 4.45 (ddd, $J = 10.5$ Hz, $J = 10.5$ Hz, $J = 6.0$ Hz, 1 H, H(1')), 4.29 (dd, $J_{3,2} = 10.0$ Hz, $J_{3,4} = 4.6$ Hz, 1 H, H(3)), 3.86 (d, $J_{2,3} = 10.0$ Hz, $J_{2,1} = 3.1$ Hz, 1 H, H(2)), 3.74 (dd, $J_{5a,5b} = 12.8$ Hz, $J_{5a,4} = 2.4$ Hz, 1 H, H(5a)), 3.50 (d, $J_{5b,5a} = 12.8$ Hz, 1 H, H(5b)), 2.90 (dd, $J_{2'a,2'b} = 16.9$ Hz, $J = 3.1$ Hz, 1 H, H(2'a)), 2.71 (ddd, $J_{2'b,2'a} = 16.9$ Hz, $J = 6.0$ Hz, $J = 3.1$ Hz, 1 H, H(2'b)), 2.44-2.53 (m, 1 H, H(4)), 1.44 (s, 3 H, (CH_3)), 1.34 (s, 3 H, (CH_3)). ^{13}C NMR (CDCl_3) δ 200.9 (C(3')), 137.5, 136.5, 128.6, 128.55, 128.54, 128.24, 128.2, 127.9, 127.8, 127.7, 109.9, 97.9 (C(1)), 73.9 (C(3)), 72.4 (C(2)), 70.0, 66.9, 60.2 (C(5)), 47.9 (C(2')), 45.7 (C(1')), 42.9 (C(4)), 26.7, 26.5 2x(C(CH_3)). HRMS (ESI) m/z 492.2006 [$\text{M} + \text{Na}$] $^+$. Calculated for $\text{C}_{26}\text{H}_{28}\text{NNaO}_6$ 492.1998.

(3R, 4R, 5R, 6S, 8S)-8-Benzyloxy[5,6-*b*]oxacyclohexane-5-piperidine-3,4-diol (2.32)



Pd/C (10%, 20 mg) was added to a solution of aldehyde (2.24) (60 mg, 0.13 mmol) and concentrated HCl (8 μ L) in dry MeOH and the mixture was hydrogenated at atmospheric pressure for 16 hours. The catalyst was removed by suction filtration through Celite and the filter cake washed with methanol (30 mL). *p*-Toluenesulfonic acid monohydrate (70 mg, 0.37 mmol) was added to a solution of the impure syrup (31 mg) in benzyl alcohol (1.5 mL) and CHCl₃ (1.5 mL) and stirred for 96 hours. As the reaction mixture was stirring, Amberlite IR410 strongly basic (\bar{C} OH form) resin was added until the pH of the reaction was neutral. The resin was removed by suction filtration and the filtrate was evaporated *in vacuo* until the residue was a thick syrup that was washed with petroleum ether (5 mL) and extracted with 0.8 M aqueous ammonium acetate (2 x 8 mL, pH 7). The aqueous portions were concentrated *in vacuo* and purified by column chromatography using C-18 RP silica gel, eluted with 40% methanol in water. The fractions containing the desired product were pooled and lyophilized from 0.01 M aqueous ammonium acetate (2 mL) to yield 2.32 as a clear syrup (16 mg, 0.06 mmol, 46%). ¹H NMR (CD₃OD) δ 7.28-7.38 (m, 5 H, H(Ph)), 5.03 (d, $J_{8,7ax} = 3.1$ Hz, 1 H, H(8)), 4.69 (d, $J_{PhCH_2} = 11.8$ Hz, 1 H, (PhCH₂)), 4.48 (d, $J_{PhCH_2} = 11.8$ Hz, 1 H, (PhCH₂)), 3.96 (dd, $J_{5'eq, 5'ax} = 11.3$ Hz, $J_{5'eq, 5} = 4.3$ Hz, 1 H, H(5'eq)), 3.59 (t, $J_{5'ax, 5'eq} = J_{5'ax, 5} = 11.3$ Hz, 1 H, H(5'ax)), 3.46-3.52 (m, 1 H, H(3)), 3.20 (dd, $J_{2eq, 2ax} = 11.7$ Hz, $J_{2eq, 3} = 5.1$ Hz, 1 H, H(2eq)), 3.13 (dd, $J = 10.4$ Hz, $J = 8.8$ Hz, 1 H, H(4)), 2.96 (ddd, $J_{6,5} = J_{6,7ax} = 12.3$ Hz, $J_{6, 7eq} = 4.3$ Hz, 1 H, H(6)), 2.58 (t, $J_{2ax, 2eq} = J_{2ax, 3} = 11.7$ Hz, 1 H, H(2ax)), 2.02 (dd, $J_{7eq, 7ax} = 12.3$ Hz, $J_{7eq, 6} = 4.3$ Hz, 1 H, H(7eq)), 1.63 (ddd, $J_{7ax, 7eq} = J_{7ax, 6} = 12.3$ Hz, $J_{7ax, 8} = 3.1$ Hz, 1 H, H(7ax)), 1.51-1.58 (m, 1 H, H(5)). ¹³C NMR (MeOD) δ 129.3, 128.9, 128.7, 97.3 (C(8)), 74.8 (C(4)), 72.7 (C(3)), 69.8 (C(PhCH₂)), 61.9 (C(5')), 52.9 (C(6)), 50.35 (C(2)), 46.7 (C(5)), 36.1 (C(7)). HRMS (ESI) m/z 280.1550 [M + H]⁺. Calculated for C₁₅H₂₂NO₄ 280.1549.

3.2 Enzymology

3.2.1 Glucocerebrosidase Kinetics

Pure human glucocerebrosidase was obtained from previously used vials of Cerezyme[®] (produced by Genzyme Inc.) donated from patients currently undergoing enzyme replacement therapy. The buffer used for kinetics was pH 5.5, 20 mM citric acid, 50 mM Na₂HPO₄, 1 mM tetrasodium EDTA, 0.25% v/v Triton-X-100[®] and 0.25% w/v taurocholic acid.

2,4-Dinitrophenyl β-D-glucopyranoside was used as the substrate for continuous UV spectrophotometric assays performed at 37°C on a Varian Cary 4000 or Varian Cary 300 UV-Vis spectrophotometer. The concentration of enzyme used, as determined by BCA assay,⁸⁹ was 2.2 nM for all assays except for compound **1.8** (IFG), for which 0.9 nM enzyme was used. Upon initiation with substrate, the release of 2,4-dinitrophenolate was measured at 400 nm and rates calculated using an extinction coefficient of 10.7 mM⁻¹cm⁻¹.⁹⁰

4-Methylumbelliferyl β-D-glucopyranoside was used as the substrate for all stopped fluorescent assays. Buffered solutions containing substrate were pre-incubated in Eppendorf tubes at 37°C in the presence or absence of an inhibitor. The reaction was initiated by addition of enzyme to a total concentration of 5 pM, then at fixed time intervals of 3, 6 and 9 minutes 100 μL aliquots were removed and diluted into a cuvette containing 500 μL of glycine buffer (pH 10.8). Dilution into pH 10.8 buffer both stopped the enzyme reaction as well as ionized the cleaved 4-methylumbelliferrone product, increasing the fluorescence signal. The resulting fluorescence from the release of methylumbelliferone was measured on a Varian Cary Eclipse fluorimeter. The instrument parameters were set as :

Excitation Wavelength (nm)	355.00
Emission Wavelength (nm)	460.00
Excitation Slit (nm)	5
Emission Slit (nm)	5
Ave Time (sec)	0.1000
Excitation filter	Auto
Emission filter	Open
PMT Voltage (V)	High

Michaelis-Menten parameters for both assays were determined by direct fit to the Michaelis-Menten expression using GraFit version 5.0.13.⁹¹

3.2.2 Inhibition Studies

All inhibition kinetics were performed by measuring the rate of reaction at fixed concentrations of artificial substrate and enzyme while varying the inhibitor concentration. K_i values were determined by directly fitting the data to various inhibition models using GraFit version 5.0.13. Best fits in each case were to the equation for competitive inhibition (Equation 2.1) as shown below.

$$v = \frac{V_{\max}[S]}{[S] + K_m(1 + [I]/K_i)} \quad \text{Equation 2.1}$$

In order to graphically represent K_i values, the inverse of the reaction rate was plotted against the concentration of inhibitor in what is known as a Dixon plot. The line for $1/V_{\max}$ will intersect the lines for varying substrate concentrations at $K_i = -[I]$ if the inhibitor is a competitive inhibitor. The theory describing this method of data representation is explained in the Appendix. The linear graphs, along with inhibition constants are presented in Section 2.2. The inhibitor concentrations used in all assays are listed in Table 3.1 below.

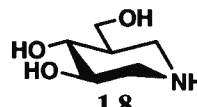
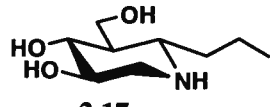
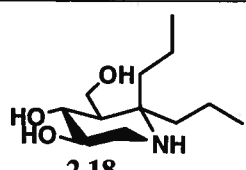
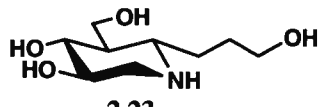
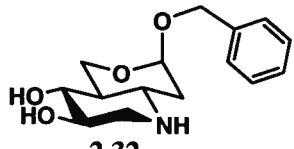
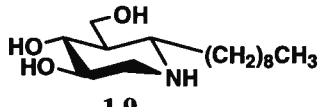
Inhibitor	[I]
 <p>1.8</p>	0, 10, 30, 50, 100 (nM)
 <p>2.17</p>	0, 300, 500, 1000, 5000, 9000 (nM)
 <p>2.18</p>	0, 300, 500, 1000, 5000, 9000 (nM)
 <p>2.23</p>	0, 20, 50, 100, 750, 1000 (nM)
 <p>2.32</p>	0, 20, 50, 100, 750, 1000 (nM)
 <p>1.9</p>	0, 0.05, 0.1, 0.2, 0.5, 0.75 (nM)

Table 3.1 Summary of inhibitor concentrations used in the assay of each inhibitor.

References

- (1) Wolfenden, R.; Lu, X. D.; Young, G. *J. Am. Chem. Soc.* **1998**, *120*, 6814-6815.
- (2) Henrissat, B.; Bairoch, A. *Biochem. J* **1996**, *316*, 695-696.
- (3) Koshland, D. E. *Biol. Rev.* **1953**, *28*, 416-436.
- (4) Phillips, D. C. *Proc. Natl. Acad. Sci. U. S. A.* **1967**, *57*, 484-&.
- (5) Sinnott, M. L.; Souchard, I. J. L. *Biochem. J* **1973**, *133*, 89-98.
- (6) Sinnott, M. L.; Viratell, O. M. *Biochem. J* **1973**, *133*, 81-87.
- (7) Withers, S. G.; Street, I. P.; Bird, P.; Dolphin, D. H. *J. Am. Chem. Soc.* **1987**, *109*, 7530-7531.
- (8) Davies, G. J.; Ducros, V. M. A.; Varrot, A.; Zechel, D. L. *Biochem. Soc. Trans.* **2003**, *31*, 523-527.
- (9) White, A.; Tull, D.; Johns, K.; Withers, S. G.; Rose, D. R. *Nat. Struct. Biol.* **1996**, *3*, 149-154.
- (10) Zechel, D. L.; Withers, S. G. *Acc. Chem. Res.* **2000**, *33*, 11-18.
- (11) Withers, S. G.; Warren, R. A. J.; Street, I. P.; Rupitz, K.; Kempton, J. B.; Aebersold, R. *J. Am. Chem. Soc.* **1990**, *112*, 5887-5889.
- (12) Withers, S. G.; Aebersold, R. *Protein Sci.* **1995**, *4*, 361-372.
- (13) McCarter, J. D.; Withers, S. G. *Curr. Opin. Struct. Biol.* **1994**, *4*, 885-892.
- (14) Wang, Q. P.; Graham, R. W.; Trimbur, D.; Warren, R. A. J.; Withers, S. G. *J. Am. Chem. Soc.* **1994**, *116*, 11594-11595.
- (15) Wolfenden, R. *Acc. Chem. Res.* **1972**, *5*, 10-18.
- (16) Vasella, A.; Davies, G. J.; Bohm, M. *Curr. Opin. Chem. Biol.* **2002**, *6*, 619-629.
- (17) Brumshtein, B.; Greenblatt, H. M.; Butters, T. D.; Shaaltiel, Y.; Aviezer, D.; Silman, I.; Futerman, A. H.; Sussman, J. L. *J. Biol. Chem.* **2007**, *282*, 29052-29058.
- (18) Kim, Y. W.; Lee, S. S.; Warren, R. A. J.; Withers, S. G. *J. Biol. Chem.* **2004**, *279*, 42787-42793.

- (19) Lairson, L. L.; Watts, A. G.; Wakarchuk, W. W.; Withers, S. G. *Nat. Chem. Biol.* **2006**, *2*, 724-728.
- (20) Truscheit, E.; Frommer, W.; Junge, B.; Muller, L.; Schmidt, D. D.; Wingender, W. *Angew. Chem. Int. Ed.* **1981**, *20*, 744-761.
- (21) Gruters, R. A.; Neefjes, J. J.; Tersmette, M.; Degoede, R. E. Y.; Tulp, A.; Huisman, H. G.; Miedema, F.; Ploegh, H. L. *Nature* **1987**, *330*, 74-77.
- (22) Goss, P. E.; Baker, M. A.; Carver, J. P.; Dennis, J. W. *Clin. Cancer Res.* **1995**, *1*, 935-44.
- (23) Gubareva, L. V.; Kaiser, L.; Hayden, F. G. *Lancet* **2000**, *355*, 827-835.
- (24) Ganem, B. *Acc. Chem. Res.* **1996**, *29*, 340-347.
- (25) Stutz, A. E. *Iminosugars as glycosidase inhibitors : Nojirimycin and beyond*; Wiley-VCH: Weinheim ; New York, 1999.
- (26) Look, G. C.; Fotsch, C. H.; Wong, C. H. *Acc. Chem. Res.* **1993**, *26*, 182-190.
- (27) Jensen, H. H.; Lyngbye, L.; Bols, M. *Angew. Chem. Int. Ed.* **2001**, *40*, 3447-3449.
- (28) Varrot, A.; Tarling, C. A.; Macdonald, J. M.; Stick, R. V.; Zechel, D. L.; Withers, S. G.; Davies, G. J. *J. Am. Chem. Soc.* **2003**, *125*, 7496-7497.
- (29) Paulsen, H. I. *Iminosugars as glycosidase inhibitors : Nojirimycin and beyond*; Stutz, A. E., Ed.; Wiley-VCH: Weinheim ; New York, 1999, pp.1-7.
- (30) Baxter, E. W.; Reitz, A. B. *J. Org. Chem.* **1994**, *59*, 3175-3185.
- (31) Scott, L. J.; Spencer, C. M. *Drugs* **2000**, *59*, 521-549.
- (32) Molyneux, R. J.; James, L. F. *Science* **1982**, *216*, 190-191.
- (33) Hohenschutz, L. D.; Bell, E. A.; Jewess, P. J.; Leworthy, D. P.; Pryce, R. J.; Arnold, E.; Clardy, J. *Phytochemistry* **1981**, *20*, 811-814.
- (34) Umezawa, H.; Aoyagi, T.; Komiyama, T.; Morishim.H; Hamada, M.; Takeuchi, T. *J. Antibiot.* **1974**, *27*, 963-969.
- (35) Jespersen, T. M.; Dong, W. L.; Sierks, M. R.; Skrydstrup, T.; Lundt, I.; Bols, M. *Angew. Chem. Int. Ed.* **1994**, *33*, 1778-1779.

- (36) Dong, W. L.; Jespersen, T.; Bols, M.; Skrydstrup, T.; Sierks, M. R. *Biochemistry* **1996**, *35*, 2788-2795.
- (37) Bols, M. *Acc. Chem. Res.* **1998**, *31*, 1-8.
- (38) Zhu, X. X.; Sheth, K. A.; Li, S. H.; Chang, H. H.; Fan, J. Q. *Angew. Chem. Int. Ed.* **2005**, *44*, 7450-7453.
- (39) Ichikawa, Y.; Igarashi, Y.; Ichikawa, M.; Suhara, Y. *J. Am. Chem. Soc.* **1998**, *120*, 3007-3018.
- (40) Kim, Y. J.; Ichikawa, M.; Ichikawa, Y. *J. Org. Chem.* **2000**, *65*, 2599-2602.
- (41) Pandey, G.; Bharadwaj, K. C.; Khan, M. I.; Shashidhara, K. S.; Puranik, V. G. *Org. Biomol. Chem.* **2008**, *6*, 2587-2595.
- (42) Chang, H. H.; Asano, N.; Ishii, S.; Ichikawa, Y.; Fan, J. Q. *FEBS J.* **2006**, *273*, 4082-4092.
- (43) Steet, R. A.; Chung, S.; Wustman, B.; Powe, A.; Do, H.; Kornfeld, S. A. *Proc. Natl. Acad. Sci. U. S. A.* **2006**, *103*, 13813-13818.
- (44) Yu, Z. Q.; Sawkar, A. R.; Whalen, L. J.; Wong, C. H.; Kelly, J. W. *J. Med. Chem.* **2007**, *50*, 94-100.
- (45) Lieberman, R. L.; Wustman, B. A.; Huertas, P.; Powe, A. C.; Pine, C. W.; Khanna, R.; Schlossmacher, M. G.; Ringe, D.; Petsko, G. A. *Nat. Chem. Biol.* **2007**, *3*, 101-107.
- (46) Alberts, B. *Essential Cell Biology : An Introduction to the Molecular Biology of the Cell*; Garland: New York, 1998, pp. 476-477.
- (47) Futerman, A. H.; van Meer, G. *Nature Rev. Mol. Cell Bio.* **2004**, *5*, 554-565.
- (48) Yoshida, H. *FEBS J.* **2007**, *274*, 630-658.
- (49) Wong, K. D.; Sidransky, E.; Verma, A.; Mixon, T. H.; Sandberg, G. D.; Wakefield, L. K.; Morrison, A.; Lwin, A.; Colegial, C.; Allman, J. M.; Schiffmann, R. *Mol. Genet. Metab.* **2004**, *82*, 192-207.
- (50) Meikle, P. J.; Hopwood, J. J.; Clague, A. E.; Carey, W. F. *J. Am. Med. Assoc.* **1999**, *281*, 249-254.

- (51) Varki, A. *Essentials of Glycobiology*; 2nd ed.; Cold Spring Harbor Laboratory Press: Cold Spring Harbor, N.Y., 2009, pp.136-141.
- (52) Zhao, H.; Grabowski, G. A. *Cell. Mol. Life Sci.* **2002**, *59*, 694-707.
- (53) Pentchev, P. G.; Brady, R. O.; Hibbert, S. R.; Gal, A. E.; Shapiro, D. J. *Biol. Chem.* **1973**, *248*, 5256-5261.
- (54) Forneris, F.; Mattevi, A. *Science* **2008**, *321*, 213-216.
- (55) Alattia, J.-R.; Shaw, J. E.; Yip, C. M.; Prive, G. G. *Proc. Natl. Acad. Sci. U. S. A.* **2007**, *104*, 17394-17399.
- (56) Rossmann, M.; Schultz-Heienbrok, R.; Behlke, J.; Rimmel, N.; Alings, C.; Sandhoff, K.; Saenger, W.; Maier, T. *Structure* **2008**, *16*, 809-817.
- (57) Dvir, H.; Harel, M.; McCarthy, A. A.; Toker, L.; Silman, I.; Futerman, A. H.; Sussman, J. L. *EMBO Reports* **2003**, *4*, 704-709.
- (58) Blonder, E.; Klibansky, C.; Devries, A. *Biochim. Biophys. Acta* **1976**, *431*, 45-53.
- (59) Premkumar, L.; Sawkar, A. R.; Boldin-Adamsky, S.; Toker, L.; Silman, I.; Kelly, J. W.; Futerman, A. H.; Sussman, J. L. *J. Biol. Chem.* **2005**, *280*, 23815-23819.
- (60) Ellgaard, L.; Molinari, M.; Helenius, A. *Science* **1999**, *286*, 1882-1888.
- (61) Fan, J. Q. *Biol. Chem.* **2008**, *389*, 1-11.
- (62) Beck, M. *Hum. Genet.* **2007**, *121*, 1-22.
- (63) Schueler, U. H.; Kolter, T.; Kaneski, C. R.; Zirzow, G. C.; Sandhoff, K.; Brady, R. O. *J. Inherited Metab. Dis.* **2004**, *27*, 649-658.
- (64) Sawkar, A. R.; D'Haese, W.; Kelly, J. W. *Cell. Mol. Life Sci.* **2006**, *63*, 1179-1192.
- (65) Grabowski, G. A.; Barton, N. W.; Pastores, G.; Dambrosia, J. M.; Banerjee, T. K.; Mckee, M. A.; Parker, C.; Schiffmann, R.; Hill, S. C.; Brady, R. O. *Ann. Intern. Med.* **1995**, *122*, 33-39.
- (66) Barton, N. W.; Brady, R. O.; Dambrosia, J. M.; Dibisceglie, A. M.; Doppelt, S. H.; Hill, S. C.; Mankin, H. J.; Murray, G. J.; Parker, R. I.; Argoff, C. E.; Grewal, R. P.; Yu, K. T. *New Engl. J. Med.* **1991**, *324*, 1464-1470.

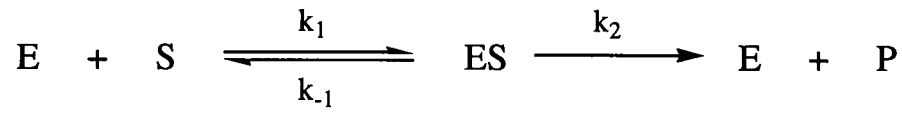
- (67) Beutler, E. *Mol. Genet. Metab.* **2006**, *88*, 208-215.
- (68) Shaaltiel, Y.; Bartfeld, D.; Hashmueli, S.; Baum, G.; Brill-Almon, E.; Galili, G.; Dym, O.; Boldin-Adamsky, S. A.; Silman, I.; Sussman, J. L.; Futerman, A. H.; Aviezer, D. *Plant Biotechnol. J.* **2007**, *5*, 579-590.
- (69) Cox, T.; Lachmann, R.; Hollak, C.; Aerts, J.; van Weely, S.; Hrebicek, M.; Platt, F.; Butters, T.; Dwek, R.; Moyses, C.; Gow, I.; Elstein, D.; Zimran, A. *Lancet* **2000**, *355*, 1481-1485.
- (70) Futerman, A. H.; Sussman, J. L.; Horowitz, M.; Silman, I.; Zimran, A. *Trends Pharmacol. Sci.* **2004**, *25*, 147-151.
- (71) Butters, T. D.; Dwek, R. A.; Platt, F. M. *Glycobiology* **2005**, *15*, R43-R52.
- (72) Butters, T. D. *Curr. Opin. Chem. Biol.* **2007**, *11*, 412-418.
- (73) Sawkar, A. R.; Adamski-Werner, S. L.; Cheng, W. C.; Wong, C. H.; Beutler, E.; Zimmer, K. P.; Kelly, J. W. *Chem. Biol.* **2005**, *12*, 1235-1244.
- (74) Tropak, M. B.; Kornhaber, G. J.; Rigat, B. A.; Maegawa, G. H.; Buttner, J. D.; Blanchard, J. E.; Murphy, C.; Tuske, S. J.; Coales, S. J.; Hamuro, Y.; Brown, E. D.; Mahuran, D. J. *ChemBioChem* **2008**, *9*, 2650-62.
- (75) Kornhaber, G. J.; Tropak, M. B.; Maegawa, G. H.; Tuske, S. J.; Coales, S. J.; Mahuran, D. J.; Hamuro, Y. *ChemBioChem* **2008**, *9*, 2643-9.
- (76) Zheng, W.; Padia, J.; Urban, D. J.; Jadhav, A.; Goker-Alpan, O.; Simeonov, A.; Goldin, E.; Auld, D.; LaMarca, M. E.; Inglese, J.; Austin, C. P.; Sidransky, E. *Proc. Natl. Acad. Sci. U. S. A.* **2007**, *104*, 13192-13197.
- (77) Compain, P.; Martin, O. R.; Boucheron, C.; Godin, G.; Yu, L.; Ikeda, K.; Asano, N. *ChemBioChem* **2006**, *7*, 1356-1359.
- (78) Ichikawa, M.; Igarashi, Y.; Ichikawa, Y. *Tetrahedron Lett.* **1995**, *36*, 1767-1770.
- (79) Jakobsen, P.; Lundbeck, J. M.; Kristiansen, M.; Breinholt, J.; Demuth, H.; Pawlas, J.; Candela, M. P. T.; Andersen, B.; Westergaard, N.; Lundgren, K.; Asano, N. *Biorg. Med. Chem.* **2001**, *9*, 733-744.
- (80) Andersch, J.; Bols, M. *Chem. Eur. J.* **2001**, *7*, 3744-3747.

- (81) Best, W. M.; Macdonald, J. M.; Skelton, B. W.; Stick, R. V.; Matthew, D.; Tilbrook, G.; White, A. H. *Can. J. Chem.* **2002**, *80*, 857-865.
- (82) Meloncelli, P. J.; Stick, R. V. *Aust. J. Chem.* **2006**, *59*, 827-833.
- (83) Goddard-Borger, E. D.; Stick, R. V. *Aust. J. Chem.* **2007**, *60*, 211-213.
- (84) Deslongchamps, P.; Dory, Y. L.; Li, S. G. *Tetrahedron* **2000**, *56*, 3533-3537.
- (85) Weiberth, F. J.; Hall, S. S. *J. Org. Chem.* **1986**, *51*, 5338-5341.
- (86) Weiberth, F. J.; Hall, S. S. *J. Org. Chem.* **1987**, *52*, 3901-3904.
- (87) Imamoto, T.; Takiyama, N.; Nakamura, K.; Hatajima, T.; Kamiya, Y. *J. Am. Chem. Soc.* **1989**, *111*, 4392-4398.
- (88) Paal, K.; Ito, M.; Withers, S. G. *Biochem. J* **2004**, *378*, 141-149.
- (89) Wiechelman, K. J.; Braun, R. D.; Fitzpatrick, J. D. *Anal. Biochem.* **1988**, *175*, 231-237.
- (90) Wong, A. W., *Ph.D. Thesis*; The University of British Columbia, 2001.
- (91) Leatherbarrow, R. J. *GraFit*; Version 5.0.13, Erithacus Software Ltd., 2006.
- (92) Segel, I. H. *Enzyme Kinetics : Behavior and Analysis of Rapid Equilibrium and Steady-State Enzyme Systems*; Wiley: New York, 1993.

Appendix

A-1 Fundamental Equations of Enzyme Kinetics

The Michaelis-Menten treatment of enzyme kinetics, where a single substrate is converted to a single product, is based on the following reaction scheme (Scheme A.1) where E represents enzyme, S the substrate and P the product.



Scheme A.1 General scheme for enzyme-catalyzed conversion of a single substrate into a single product.

In the first step of the reaction, the enzyme and substrate combine in a rapid, reversible process to produce an enzyme-substrate complex (ES). In the second step, the bound substrate is converted to product and subsequently released from the enzyme. Under steady state conditions, the rate of change of the concentration of ES complex is zero, as described in Equation A.1.

$$\frac{\partial[ES]}{\partial t} = k_1[E][S] - k_{-1}[ES] - k_2[ES] = 0 \quad \text{Equation A.1}$$

As the total amount of enzyme $[E]_0$ added to the reaction is quantifiable and is equal to the sum of the concentrations of both free enzyme $[E]$ and bound enzyme $[ES]$, $[E]_0$ can be represented by Equation A.2.

$$[E]_0 = [E] + [ES] \quad \text{Equation A.2}$$

Solving for [ES] in Equations A.1 and A.2,

$$[\text{ES}] = \frac{[\text{E}]_0[\text{S}]}{[\text{S}] + \left(\frac{k_{-1} + k_2}{k_1}\right)} \quad \text{Equation A.3}$$

Assuming that the rate limiting step is breakdown of the ES complex to yield P, then the rate of the reaction (v) can be described by Equation A.4

$$v = \frac{\partial[\text{P}]}{\partial t} = k_2[\text{ES}] \quad \text{Equation A.4}$$

By substituting the expression for [ES] from Equation A.3 into Equation A.4, the result is Equation A.5

$$v = \frac{k_2[\text{E}]_0[\text{S}]}{[\text{S}] + \left(\frac{k_{-1} + k_2}{k_1}\right)} \quad \text{Equation A.5}$$

Defining the ratio of the rate constants $(k_{-1} + k_2)/k_1$ as the Michaelis constant (K_m), and the rate constant k_2 as the turnover number (k_{cat}), then Equation A.5 can be simplified to the more general form known as the Michaelis-Menten equation (Equation A.6), where the product of k_{cat} and $[\text{E}]_0$ is also referred to as V_{max} .

$$v = \frac{k_{cat}[\text{E}]_0[\text{S}]}{[\text{S}] + K_m} \quad \text{Equation A.6}$$

Equation A.6 describes a rectangular hyperbola such as is shown in Figure A.1.

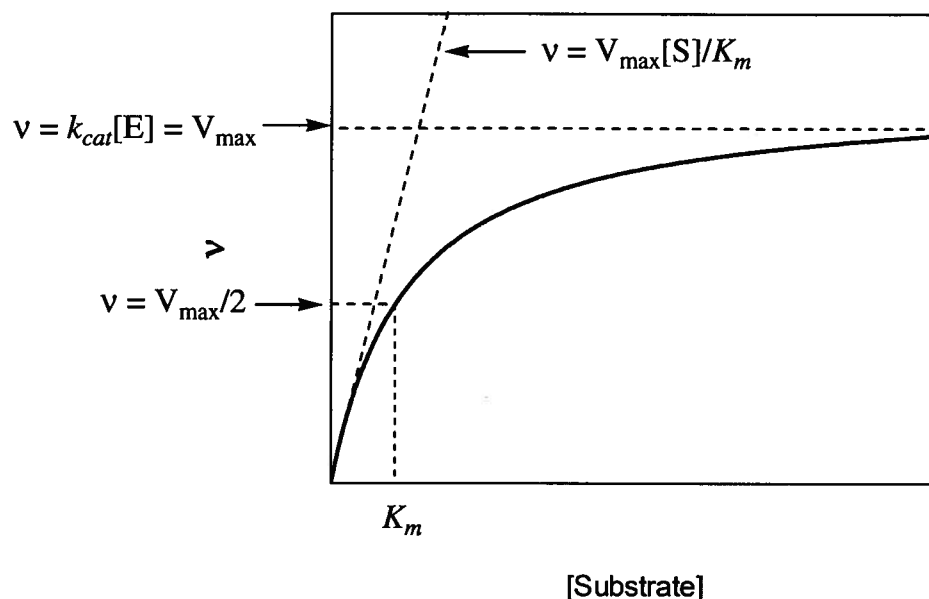


Figure A.1 A plot showing the typical hyperbolic nature of the Michaelis-Menten equation (Equation A.6)

The Michaelis constant (K_m) is defined as the substrate concentration at which the reaction rate (v) is half-maximal ($v = V_{\max}/2$). It may be treated as an apparent dissociation constant of all the enzyme bound species and is expressed in Equation A.7

$$K_m = \frac{[E][S]}{\Sigma [ES]} \quad \text{Equation A.7}$$

Therefore, the K_m value reflects the stability of the bound enzyme-substrate complex. Lower values of K_m indicate tighter binding of the substrate to the enzyme. At low $[S]$ ($[S] \ll K_m$), the Michaelis-Menten equation reduces to Equation A.8 and v is linearly dependent upon substrate concentration (also refer to Figure A.1). Since most of

$$v = \frac{k_{cat}[E]_0[S]}{K_m} \quad \text{Equation A.8}$$

the enzyme is unbound, the total enzyme concentration $[E]_0$ can be approximated to the concentration of the free enzyme $[E]$. Under these conditions, the Michaelis-Menten equation can now be expressed as Equation A.9

$$v = \frac{k_{cat}}{K_m} [E][S] \quad \text{Equation A.9}$$

In Equation A.9, k_{cat}/K_m is an apparent second-order rate constant for the reaction of the free enzyme with free substrate. This kinetic parameter is also a measure of the overall efficiency of the enzyme. At high $[S]$ ($[S] \gg K_m$), v approaches a limiting value, V_{max} , and the Michaelis-Menten equation can now be expressed as Equation A.10 (also refer to Figure A.1)

$$V_{max} = k_{cat}[E]_0 \quad \text{Equation A.10}$$

Prior to the advent of computers and for the purpose of graphical representation of the enzymatic rate data, the Michaelis-Menten equation was often rearranged into the linear form of Equation A.11

$$\frac{1}{v} = \frac{K_m}{V_{max}} \cdot \frac{1}{[S]} + \frac{1}{V_{max}} \quad \text{Equation A.11}$$

As shown in Figure A.2, plotting $1/v$ versus $1/[S]$ (also known as a Lineweaver-Burk plot) yields a straight line with a slope of K_m/V_{max} , and a y-intercept of $1/V_{max}$, and a x-intercept of $-1/K_m$.

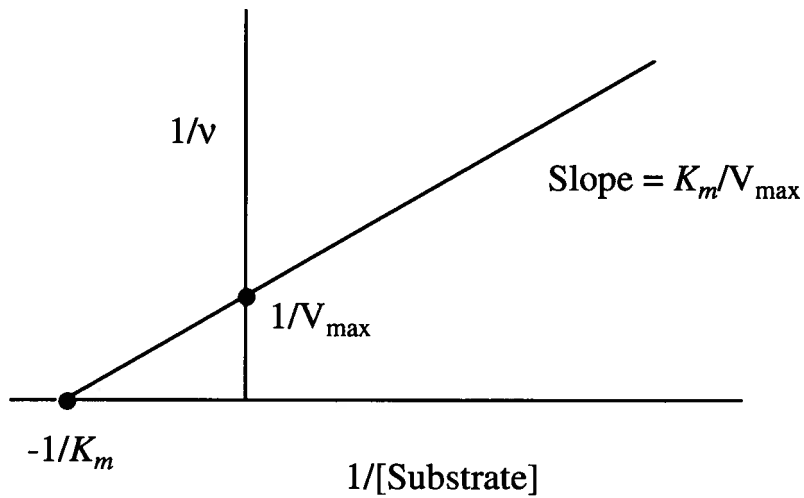
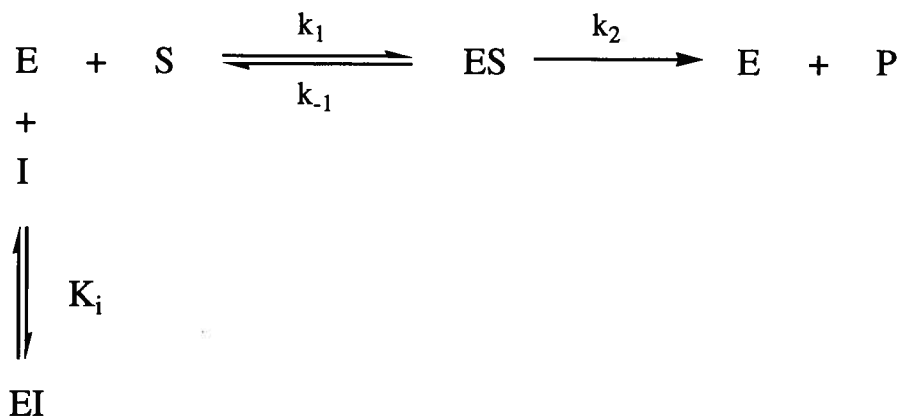


Figure A.2 A typical Lineweaver-Burk plot for an enzymatic reaction.

A-2 Reversible Competitive Inhibition

Substances that combine with an enzyme in a reversible manner to decrease the activity of that enzyme are referred to as inhibitors. A competitive inhibitor is a compound that competes directly with a normal substrate for binding to the enzyme active site. These compounds often resemble the substrate but are unreactive towards the enzyme. In the presence of such a compound, the equations for the simple enzyme-catalyzed reaction must be expanded to include a second equilibrium, K_i , which describes the dissociation of the inhibitor from the enzyme-inhibitor complex ($K_i = [E][I]/[EI]$) (Scheme A.2).



Scheme A.2 General scheme for enzyme-catalyzed conversion of a single substrate into a single product in the presence of a competitive inhibitor.

The total concentration of enzyme is now given by Equation A.12

$$[\text{E}]_0 = [\text{E}] + [\text{ES}] + [\text{EI}] \quad \text{Equation A.12}$$

Applying the steady state approach (Equation A.1) and substituting into Equation A.6 gives Equation 2.1.

$$v = \frac{V_{\max}[\text{S}]}{[\text{S}] + K_m(1 + [\text{I}]/K_i)} \quad \text{Equation 2.1}$$

As can be seen from Equation 2.1, a competitive inhibitor only affects the K_m term of the Michaelis-Menten equation, increasing it by a factor of $(1 + [\text{I}]/K_i)$. The value of V_{\max} is unaffected since at high concentrations of substrate, the inhibitor is displaced from the enzyme active site. Just as a linear transformation of the data can elucidate uninhibited kinetic parameters (Figure A.2), a similar linear plot can be used to graphically represent K_i values. By plotting $1/v$ versus $[\text{I}]$ (Dixon plot), the line for $1/V_{\max}$ intersects the lines for different substrate concentrations at $K_i = -[\text{I}]$ if the inhibitor is a competitive inhibitor. The theory for this method of representing K_i values is presented below, taken from Segel.⁹²

For competitive inhibition,

$$v = \frac{V_{\max}[S]}{[S] + K_m(1 + [I]/K_i)}$$

The reciprocal of this equation is

$$\frac{1}{v} = \frac{K_m[I]}{V_{\max}[S]K_i} + \frac{1}{V_{\max}} \left(1 + \frac{K_m}{[S]} \right)$$

When $\frac{1}{v} = \frac{1}{V_{\max}}$,

$$\frac{1}{V_{\max}} = \frac{K_m[I]}{V_{\max}[S]K_i} + \frac{1}{V_{\max}} \left(1 + \frac{K_m}{[S]} \right)$$

and

$$1 = \frac{K_m[I]}{[S]K_i} + 1 + \frac{K_m}{[S]}$$

so,

$$-\frac{K_m[I]}{[S]K_i} = \frac{K_m}{[S]}$$

and

$$[I] = -K_i$$